UNIVERSITÀ DELLA CALABRIA

UNIVERSITA' DELLA CALABRIA

Dipartimento di Biologia, Ecologia e Scienze della Terra

Dottorato di Ricerca in

Scienze della vita

XXXI CICLO

INTERFACE RHEOLOGY OF STRUCTURED FOOD

Settore Scientifico Disciplinare ING-IND/24

Coordinatore: Ch.ma Prof.ssa Maria Carmela Cerra

Supervisore: Prof. Domenico Gabriele

Tutor: Prof. Bruno de Cindio

Tutor: Dott. Ing. Noemi Baldino

Dottoranda: Dott.ssa Olga Mileti

Table of contents

O. Mileti (2018), Interface rheology of structured food, Ph.D. Thesis

Introduction

In this work the properties of the interfacial layers covered by vegetable proteins were investigated and interpreted with rheological models. The study of vegetable proteins also concerned their use as stabilizing agents in emulsified systems with low viscosity, having as an idea the product design of vegetable milks produced with vegetable proteins.

Proteins are classically used in the food industry as stabilizing agents thanks to their good stabilizers on the interfacial layers, where the stability conditions are more critical and require surface active agents to be stabilized. They are able to lower the surface/interfacial tension and, thus, improve the process of dispersion of the drops of one phase within the other. The presence of proteins at the interface confers mechanical resistance against phenomena of rupture and coalescence, thanks to the formation of protein layers with a networked and highly resistant structure. Proteins from animal sources are known to perform this task well and for this reason are classically used in the food industry. In particular, vegetable proteins have a good nutritional profile and thanks to a complete amino acid profile, can be used as possible supported animal proteins. Although the literature offers exhaustive information about their nutritional properties, their interfacial properties and, therefore, their ability to stabilize the interface in multiphasic systems, are not as well known in the literature.

The aim of this PhD thesis is an evaluation of the interfacial mechanisms related to the covering of the interfaces by proteins, in particular of vegetable source, as possible alternative to the animal protein classically used in food industry. These systems were analysed by the use of A/W model systems (air-water-protein) with three different proteins obtained by vegetable sources.

The proteins derived by soy, hemp and brown rice sources have been investigated, at the interface and in emulsification process. They are all globular proteins, different in structure, molecular weight, solubility and structuring capacity.

To investigate the several phenomena which occur at the interface, the static measures have been performed in dilatational kinematic, by pendant drop method. These measures have given information about the diffusion, adsorption and rearrangement mechanisms, classically detected for biopolymeric species at the interface.

The mechanical resistance of surface layers covered by vegetable proteins have been investigated by rheological analysis in dilatational and shear kinematic. The former was performed by pendant drop method, as for static measurements. The second was performed by rod magnetic rheometer.

By dilatational rheological analysis have been conducted at critical micellar concentration, previously determined by static measurements at several protein concentrations. The frequency sweep tests and the stress relaxation tests, out of linearity region, have been performed and interpreted by Scott Blair model, which uses a fractional constitutive model and compared with a Maxwell model. The Scott Blair model permitted to correlate the rheological fundamental properties with the technological parameters, as firmness and springiness, two technological value which indicate respectively the consistency and a spring behaviour of a food. Finally an emulsion application were effectuated and correlate with surface analysis. The emulsion, with the three vegetable protein, was optimized to have a vegetable beverage as milk consistency, to formulate a vegetable milk, currently in widespread use with methods known in the literature.

Thus, the thesis is articulated in five chapters. The preliminary chapters 1 is focalized on the vegetable proteins, their chemical-physics characteristics and the information actually present in literature about their interfacial/surface properties and emulsifying/foaming capacities. The chapter 2 is focalized on the analysis of the surface processes under a thermodynamic, a mechanical and a rheological approach. The chapter 3 explains in detail the instrumentation used to characterize the surface with the two kinematics used: dilatational and shear. The former was investigated by the pendant drop and the second with the rod magnetic field rheometer. Thus, these two instrumentations are explained in the chapter 3. The chapter 4 collects all the superficial analysis carried out on the three proteins investigated, including kinetic analysis, rheological analysis and interpretation of the data obtained. Finally in the chapter 5 the product design of a vegetable milk, obtained with vegetable proteins as emulsifier agents, was carried out as application of the information acquired from the surface analysis to a case of very diluted emulsion. The characterization of the systems obtained was carried out by bulk characterization.

Chapter 1

Vegetable proteins: a healthy opportunity

Abstract

Proteins are widely used in the food industry because of their capacity to stabilize emulsions and foams by acting on the interfacial layer of these typical biphasic systems. Nowadays, the most used proteins come from animal sources, even if proteins of vegetable origin are being used successfully due to their healthy properties and the capacity to stabilize some food systems.

The growing request for foods free from ingredients of animal origin has increased the demand for vegetable proteins. Particularly, the interest can be attributed to an increase in the diagnosis of food allergies or intolerances and for ethical reasons.

In this regard, the study of the chemical and physical characteristics of vegetable proteins is essential for their proper use and optimal formulations in food. In this review, the characteristics of three proteins are discussed with particular attention on the surface/interface effect, trying to correlate these to the interfacial properties and to their emulsifying and stabilizing properties.

Keywords: *vegetable proteins, interfacial/surface tension, emulsion, foam, soy protein, hemp protein, rice protein.*

1.1 Introduction

In these last few years lifestyle and the increasing intolerance or allergy diagnosis, as well as religious or ethical problems, have changed the diet of most of the world's population.

All these factors have shifted the food industry's attention away from ingredients of animal to those of vegetable origin.

In the light of the above, vegetable proteins seem to be a potential alternative to animal protein demand, despite some of these appearing deficient in some essential amino acids. In fact, the latter problem can be overcome by using a mixture of vegetable proteins from different sources. In most cases, the nutritional benefits and the limitations in the use of some

new protein sources are still under investigation as well as their behaviour and acceptability with the aim to develop new food products.

Nowadays, the consumption of vegetable drinks and foods with vegetable proteins as an ingredient or a mixture of them has increased and these foods are widely consumed.

Specifically speaking, the proteins in the vegetable drinks are the principal ingredient also used to emulsify the system, thanks to their surface/interfacial properties.

A lot of new products are developing to satisfy the actual exigency and lifestyle and many of these are poor in quality and not stable over time. Therefore, the possibility of finding and developing new stable and high-quality products, with materials guaranteeing nutritional value and highly tolerated, is a very important trend in the food industry (Jnawali et al. 2016).

Food products are in most cases complex and/or multiphasic systems, projected to guarantee the desired shelf-life and organoleptic characteristics. To this purpose, a product must have controlled rheological properties, closely correlated to its texture. In particular, the presence of two or more phases generally involves the control of the superficial/interfacial properties of these multiphasic systems. The formation of foam and emulsion, in fact, involve the formation of several interfaces, generally unstable and stabilized thanks to the control of the interface often carried out by the use of surfactant agents or proteins.

The surfactant species, typically used as emulsifier, is a small molecule of amphiphilic nature able to adsorb at the interface (Bos and van Vliet 2001). Generally, it is preferred to lower the input energy to emulsion/foam formation, facilitating droplets disruption and air bubble formation, because, contrary to its surfactant property, it does not have not a good stabilization effect and the interfacial layers, which can form, do not have a good resistance over time and this is due to its scarce viscoelastic effect (Bos and van Vliet 2001). In the light of the above, to stabilize the interface the emulsifier is often used in presence of macromolecules that have a greater stabilizing effect. The macromolecules principally used are proteins and polysaccharide. In particular, the proteins are more used in the food industry owing to their high versatility. In fact, the proteins are amphiphilic molecules with molecular weight greater then emulsifiers, which anchor themselves to interfacial layers in a reversible or irreversible way, forming a good interfacial viscoelastic layer, giving the required resistance to avoid the coalescence and the rupture of the film (Damodaran 2005, Bos and van Vliet 2001, Bouyer et al. 2012).

In recent years, there has been a great interest in proteins alternative to the animal source and a good alternative is the use of protein extract from vegetable matrices, since they are not very allergenic and are highly versatile.

On vegetable proteins there are several studies attesting their characteristic of forming film for microencapsulation (Nesterenko et al. 2013), also there are studies about their applications in packaging edible films (Lin and Zhao 2007) and fibres for fabrics (Souzandeh et al. 2016), and on their use in emulsion formulation (Xiang, Lyu and Narsimhan 2016, Piazza et al. 2009). Although their use and their marketing are quite widespread, their fundamental properties are little known.

While the interfacial proprieties of animal proteins have been studied, the interfacial properties of vegetable proteins have been less investigated.

Since vegetable proteins may be an interesting alternative to proteins of animal origin, moreover, for use in foams and emulsions, this review aims at giving the essential information and the state of the art on the superficial and interfacial properties of vegetable proteins to evaluate their potential use as stabilizing agents. Particularly, attention is focused on vegetable proteins extracted from soy, hemp and rice.

1.2 Characterization and chemical-physical characteristics

Vegetable proteins are constituted of four main fractions even if they come from different sources: glutenin, globulin, albumin and prolamin.

All of these proteins are classified as simple proteins according to the classification of Osborne (1909), based on their solubility in a several solvents. They have many differences in their chemical-physical characteristics and they are present in varying amounts in the three proteins under analysis. Glutelin and globulin are the principal fractions in all three cases, instead, the remaining fractions are present in smaller quantities.

1.2.1 Soy Protein

Soybean is the most important crop cultivated in the word and it also is an abundant source of proteins. They are a good protein source thanks to their complete aminoacidic profile, suitable for use in lower cholesterol content diets (Nishinari et al. 2014).

Soybean composition is about 40% protein, 35% carbohydrate and 20% oil, as shown in the following Figure 1.1:
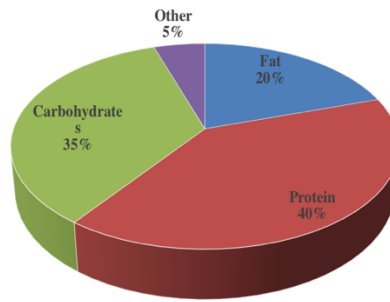
Figure 1.2.1.1 Percentage composition of the soybean

To obtain only the protein fraction, the soybean undergoes purification treatments and the resulting fraction is a mixing of several protein types.

In general, the soybean proteins are produced by aqueous extraction of protein in alkaline conditions with a selective recovery of these made by acid precipitation, followed by several separation steps, like washing, neutralization and drying (Moure et al. 2006, Tang 2017). It is notorious that every single step of the purification and isolation process, as well as the raw material, influences the yield, structure, and the functionalities of the product (Tang 2017). Globulin is the main protein fraction contained in soybean and it is present in four different forms (2S, 7S, 11S, 15S), classified according to their sedimentation coefficient, which is a measure of the sedimentation velocity of a molecular specie and which is classically measured in svedberg (S). In the following Figure 1.2.1.2 this classification is schematically illustrated.
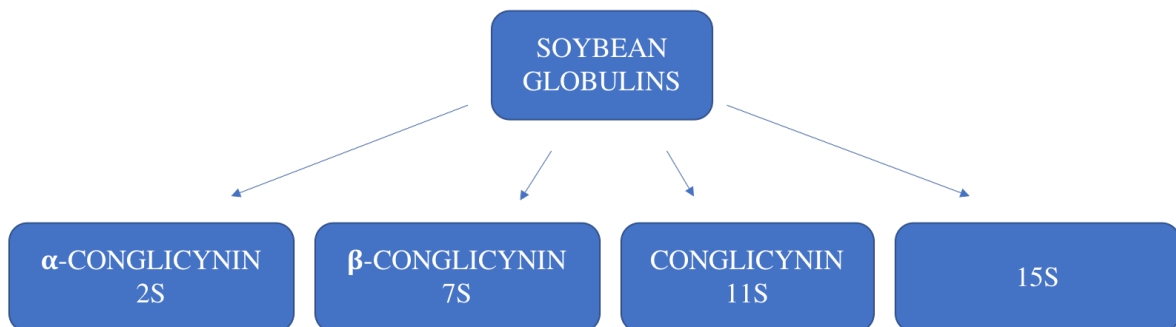
Figure 1.2.1.2 Soybean globulin classification

In particular, the 7S fraction in turn is constituted of three other fractions: β-conglycinin, γ-conglycinin and basic 7S globulin (Barac et al. 2004, Singh et al. 2015, Wagner and Gueguen 1995), of which β-conglycinin is the most abundant.

The 7S fraction is constituted of three fractions: γ-conglycinin, β-conglycinin and basic 7S globulin (Barac et al. 2004, Singh et al. 2015, Wagner and Gueguen 1995), of which β-conglycinin is the most abundant.

The quantity present in soybean of each protein fraction is variable in relation to the native cultivar, but on average the globulins profile is outlined in the scheme reported in Figure 1.2.1.3 (Tang et al. 2006b).
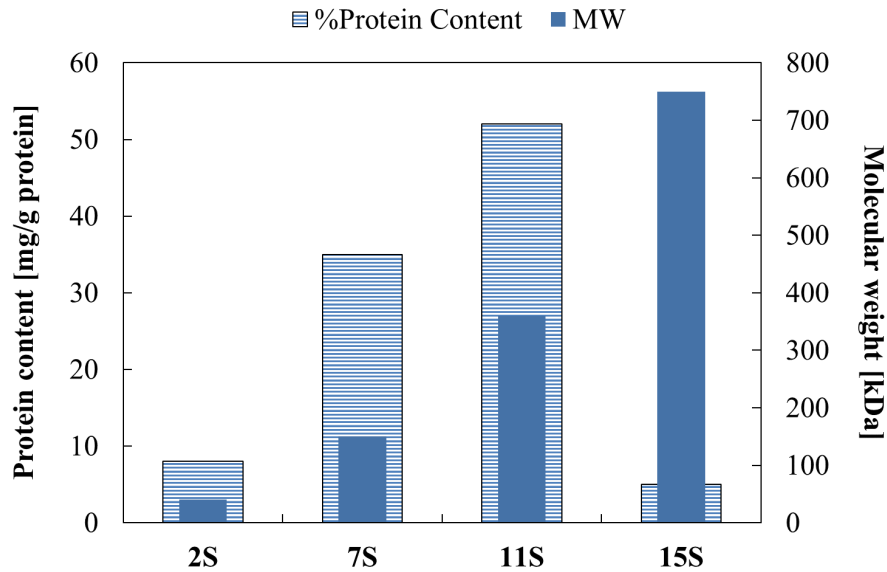
Figure 1.2.1.3 Protein content (on the right axis) and molecular weight (on the left axis) of the three globulins fractions contained in the soy proteins.

Glycinin 11S is the most abundant fraction in soybean proteins and constitutes on average 50% of the total protein. It is characterized by an MW of 360 kDa and has a compact quaternary structure stabilized with disulfide, electrostatic and hydrophobic bonds (Martin, Bos and van Vliet 2002, Barac et al. 2004). The 11S fraction has a hexamer structure, constituted of six monomers AB, where A is an acid polypeptide and B is a basic polypeptide and they are linked by disulfide bond SS (Martin et al. 2002, Barac et al. 2004, Wagner and Gueguen 1995). Its molecular structure is as a cylinder of two rings with a hexagonal form with dimensional length characteristic of 11x11x 7.5 nm (Martin et al. 2002, Barac et al. 2004, Tang 2017), as schematically reported in Figure 1.2.1.4.
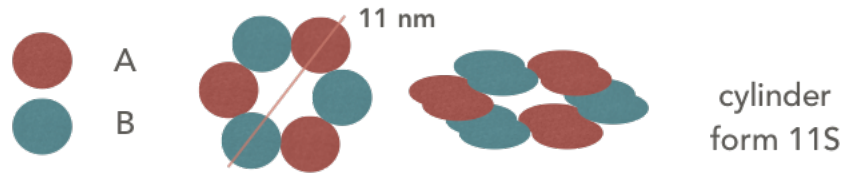
Figure 1.2.1.4 Scheme of 11S fraction of soy globulin

When environmental conditions change (i.e. pH, ionic strength), in particular to electrostatic effects, it is possible to observe a dissociation of the 11S in a simpler form, as 7S and 3S or an association effect that converts 11S in 15S form (Martin et al. 2002, Lakemond et al. 2000). In particular, at pH=6.7 the 11S form is predominant and the 3S is absent, but increasing the environment acidy (so, at the decrease the pH under the isoelectric point), the 7S and 3S forms become more and more present, as a results of the dissociation effect of the 11S, that is completely absent (Lakemond et al. 2000, Martin et al. 2002, Tang 2017). By tryptophan fluorescence (Lakemond et al. 2000) a dependence of glycinin dissociation with ionic strength was not observed.

The 11S/7S ratio is variable with the source cultivar and ranges between 0.5 and 1.7 (Ortiz et al. 2003, Pesic et al. 2005, Tang 2017). This factor influences the physical properties of soybean proteins, giving them more or less emulsifying properties and influencing their stabilization ability (Tang 2017, Pesic et al. 2005).

With reference to their aminoacidic composition, in Figure 1.2.1.5 a complete profile as documented by Tang 2006 has been reported.
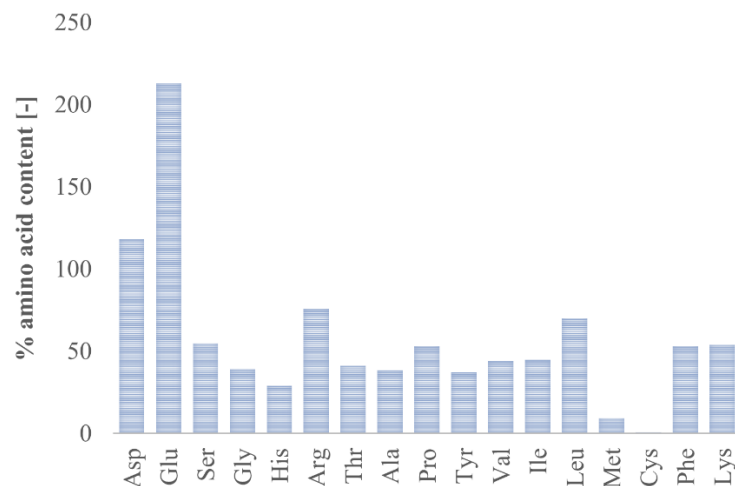
Figure 1.2.1.5 Total amino acids composition of isolate soy protein (Tang et al. 2006a).

In particular, the profile of essential amino acids is shown in Figure 1.2.1.6:
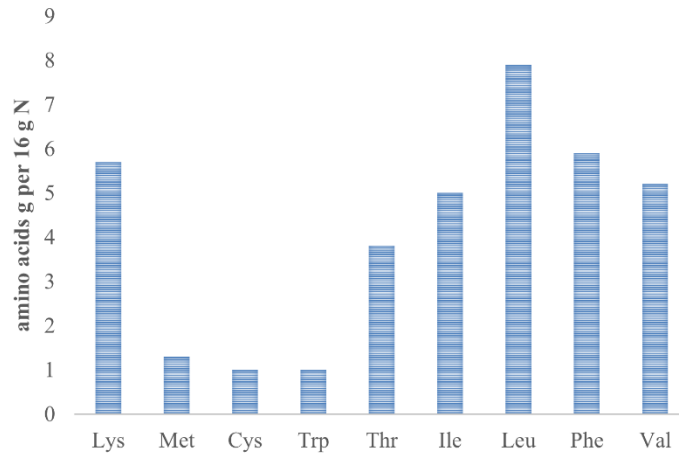
Figure 1.2.1.6 Essential amino acids composition of isolate soy protein.

It should be pointed out that the soy protein aminoacidic profile contains all the essential amino acids (Singh et al. 2008).

One of the most important chemical-physical properties is solubility in aqueous solutions. Therefore, an important point is the solubility of glycinin in the solutions because it can influence the functional properties of the glycinin protein. A complete and detailed analysis of glycinin solubility was carried out by Lankemond and coworkers (Lakemond et al. 2000), who analyzed the effects of pH and ionic strength (I) on the solubility of the protein. In particular, it is important to underline that at neutral condition and I=0.5 the solubility of the glycinin protein is complete, but decreasing the pH, the solubility decreases too, until it reaches 30% for pH=3. Furthermore, in the same pH condition, the ionic strength influences the solubility as reported in Figure 1.2.1.7.
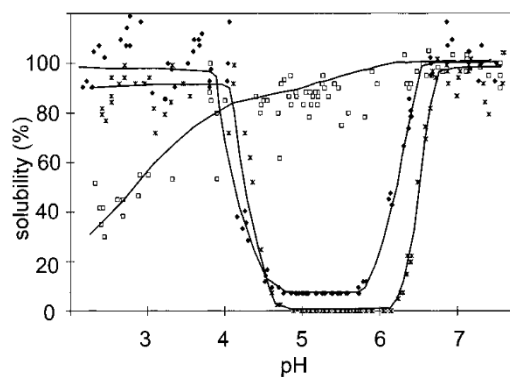
Figure 1.2.1.7 pH and I effect on glycinin protein, pH-dependent solubility profiles of glycinin [I) 0.5 (0), 0.2 (|), 0.03 (/)] determined after incubation of 0.6 mg/mL samples for 16 h at 20 °C (Lakemond et al. 2000)

Moreover, at pH=7, the solubility is independent of ionic strength, but decreasing the pH value up to about 4 and also lowing the ionic strength, the protein solubility decreases drastically. Under pH=4 the trend is reversed and lowering the ionic strength, the protein becomes more soluble.

1.2.2 Hemp Protein

Industrial hemp (*Cannabis sativa L.*) is traditionally processed for its high fibre content in the textile industry (Malomo, He and Aluko 2014, Wang et al. 2008), but in the last few years, there has been a wide use of hemp seeds in the food sector. Hemp seeds, but also seed meal, are rich in proteins (25%) and oil (30%), the latter consisting of 80-90% of unsaturated fatty acid whose composition, with the total seed composition, are reported in Figure 1.2.2.1 (A) and (B) (Callaway 2004, Wang et al. 2008).
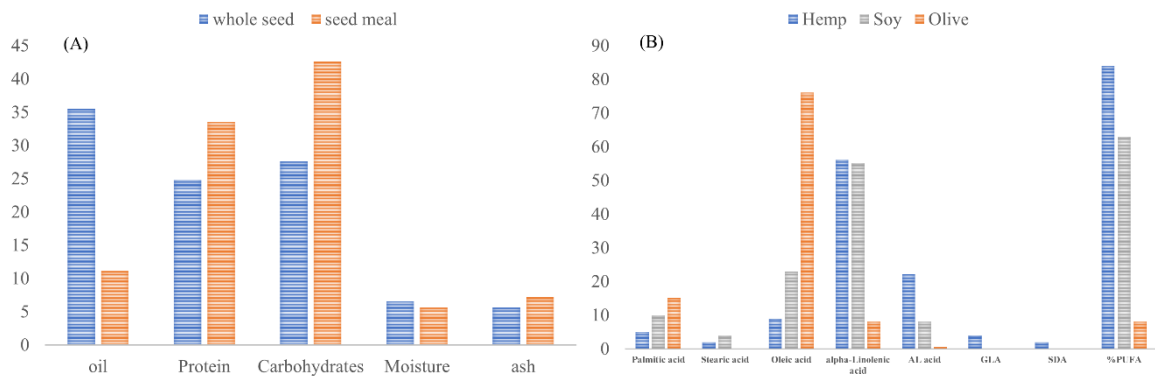
Figure 1.2.2.1 Seed meal and seed whole hemp composition (A) and oil composition comparison of hemp with another different source (soy and olive) (B) (Callaway 2004)

From the oil composition, it is possible to note that hemp oil is rich in linoleic and alpha-linoleic acid, two fatty acids comprised in the EFA classification, Essential Fatty Acids, not synthesizable by the human organism (Callaway 2004, Pojic et al. 2014). A good balance between linoleic and α-linoleic acids is suitable in the diet to prevent coronary heart disease, in particular, the ratio, linoleic/α-linoleic, in hemp seed oil is around 2-3, that is the value suitable to a healthy diet. Furthermore, linoleic acid has several beneficial properties for the organism including LDL cholesterol (Teh and Birch 2013).

Also, WHO/FAO defined guidelines for a balanced diet in which the PUFA/SFA ratio must be above 0.4. In support of what was said about hemp oil benefits to health, the hemp meal fractions have a PUFA/SFA ratio of about 7 (Pojic et al. 2014).

Because of the high quality of hemp oil and proteins, this crop is a good source of nutrients and it can be employed as an ingredient to formulate new food products.

The principal proteins contained in hemp seeds are edestin and albumin and the nutritional value of these are comparable to egg white and soybean proteins (Callaway 2004, Hadnadev et al. 2018). Hemp proteins also have a globular nature. In particular, edestin is a legumin characterized by AS and BS block to form a hexameric structure in which AS and BS are

linked by disulfide bonds (Wang et al. 2008, Tang et al. 2006a, Malomo et al. 2014). In the following Table 1.2.2.1 the molecular weight of hemp proteins is summarized (Tang et al. 2006a):

	Content %	MW [kDa]
Edestin	82	212
Albumin	13	18.4
Glycoprotein	5	48

Table 1.2.2.1 Average values for hemp protein content and respective molecular weights

The molecular weight of edestin is more controversial in the literature and different values are reported ranging between 212 kDa and 290-300 kDa (Wang et al. 2008). Hemp (Cannabis sativa L.) seed proteins are rich in highly digestible amino acids and in accordance with (Callaway 2004), the amino acid profile is complete with all essential amino acids and it is comparable with the soy protein profile. Typical amino acids composition is reported in Figure 1.2.2.2 (Tang et al. 2006a, Callaway 2004, Wang et al. 2008, Malomo et al. 2014).
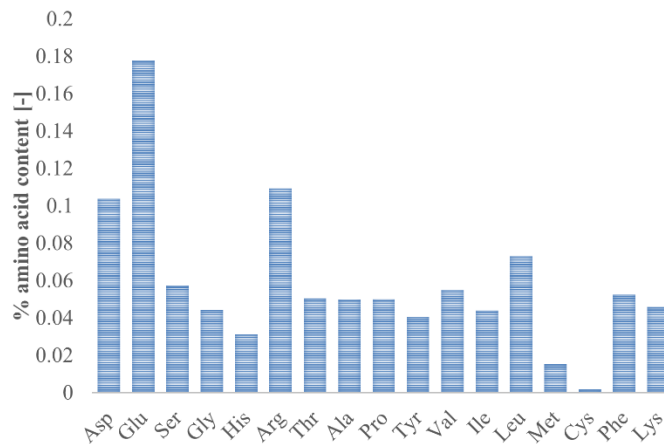
Figure 1.2.2.2 Amino acid composition of hemp protein in accord with several authors (Tang et al. 2006a, Callaway 2004, Wang et al. 2008)

Even if the amino acid profile reported in the literature is very similar, small differences can be attributed to the raw material used, to the extraction method used and to the purification processes adopted to obtain the isolated protein (Malomo et al. 2014). There are several methods to separate the principal fractions of the hemp matrix, like mechanical pressing or a much more evolved technique, like supercritical extraction. As said, a simple and classic

method to obtain different hemp fractions is mechanical pressing and a related simplified scheme is reported in Figure 1.2.2.3.
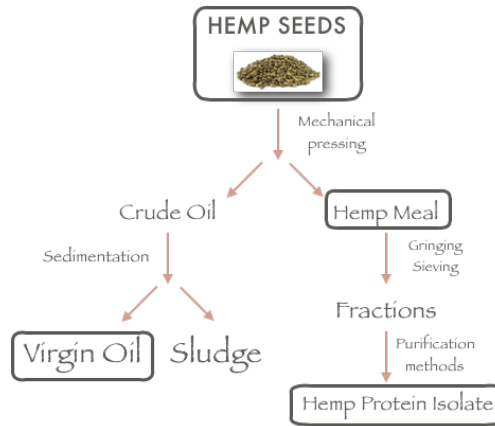
Figure 1.2.2.3 Typical scheme of hemp seeds pressing separation.
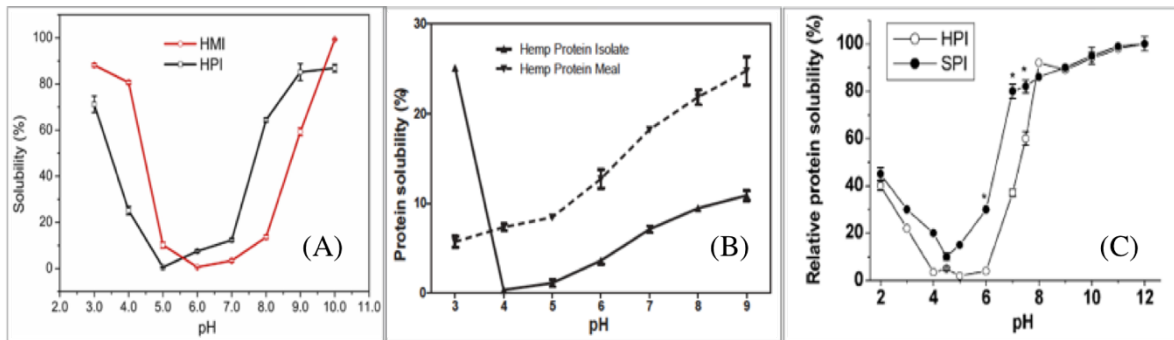
Figure 1.2.2.4 Hemp solubility data from three several literature studies, respectively from (Hadnadev et al. 2018)(A), (Malomo et al. 2014)(B), (Tang et al. 2006a) (C).

Although the overall trend is similar, some discrepancies can be observed among the three plots in Figure . In fact, (Malomo et al. 2014) reports a general trend of hemp protein solubility with the value that is lower than those reported by (Tang et al. 2006a) and (Hadnadev et al. 2018). This discrepancy could be related to the method of treatment of the hemp seeds, more or less degradative for proteins.

(Malomo et al. 2014) in the comparison of solubility of HPM and HPI show a linearity in the increasing of solubility with pH for HPM and general solubility values greater than HPI. This effect can be related to a purified method that could have to impart some structural modifications, strengthening protein-protein interactions in HPI, as suggested also from intrinsic emission fluorescence spectroscopy measurements (Malomo et al. 2014).

From the solubility analysis, hemp proteins showed low solubility in pH condition between 4 and 6. Under pH 4.0 the solubility is better and reaches a value of 40% at pH 2.0. Only

below pH 8.0, the solubility reaches values of 90% (Tang et al. 2006a). This effect probably is related to the edestin solubility that is favored in an alkaline environment.

The composition and structure of the hemp seed protein are strictly linked to the purification method with which they are isolated (Hadnadev et al. 2018, Malomo et al. 2014). The most important methods, which can be used to isolate the hemp protein, are isoelectric precipitation and micellization. The first step is the oil extraction from hemp meal using a hexane extraction, then from the obtained meal, it is possible to isolate the proteins. After the oil extraction, pH changes are used to promote protein precipitation, first raising the pH to basic conditions (about 10.0) and then centrifuging. The use of basic pH allows maximum solubilization and the subsequent centrifugation allows the precipitation of any heavy species remaining in the starting meal. In this way, the supernatant is recovered and acidified to pH 5.0, that is, the isoelectric point and, therefore, to the minimum solubility condition. Therefore, the protein is isolated by hydroelectric precipitation (Malomo et al. 2014, Tang et al. 2006a, Wang et al. 2008, Hadnadev et al. 2018).

The second method, micellization, uses a salt solution to promote the extraction of protein, and an intermediate centrifugation, which deletes the residual insoluble part. The supernatant, in the latter case, is treated through dialysis and with a final centrifugation to recover the precipitated proteins (Hadnadev et al. 2018). By a comparison of the yield obtained in several works, it can be noted that the data are not uniform, but present important differences, probably because affected by the first extractive phase that is quite difficult to control.

Comparing only these two methods, because they are the most used (Hadnadev et al. 2018), it can be observed that micellization permits a higher protein content to be obtained, preventing damage and preserving the native state of the proteins, so the protein obtained is suitable for high-protein food products, designed for sports people. On the contrary, the isoelectric precipitation gives partial desaturated proteins and improves the exposure of polar amino acid side on the molecular chain. The latter factor gives protein obtained by isoelectric precipitation a high capacity to retain water, so it is suitable for its use in the food industry as emulsifier and texture agents.

1.2.3 Brown Rice Protein

Rice production is the second highest in the world after wheat. It is mainly produced for human consumption, but also, although in smaller quantities, for animal feed. The environmental conditions for rice cultivation are very flexible, a characteristic that improves

its production (Cho and Lim 2016). In addition to being colourless, several studies attested its hypoallergenic, anti-oxidative, anti-hypertensive, anticancer and anti-obesity properties (Amagliani et al. 2017a, Agboola, Ng and Mills 2005, Day 2013). Nowadays, rice proteins are widely used for many food applications such as bakery foodstuffs, whipped toppings, drinks etc. due to their high water and oil binding capacities (Cao et al. 2009).

In particular, brown rice is produced from rough rice through a threshing process. It is composed of three fractions: starchy endosperm (which is the predominant fraction, constituting 92% of the total), embryo and bran. Discarding the latter fraction, white rice is obtained (Cho and Lim 2016). The nutritional properties of brown rice are greater than the more diffused white rice, thanks to the presence of the bran, but also thanks to the presence of lipids, amino acids and another nutritional components but because of its roughness, however, BR it is less consumed compared to white rice (Cho and Lim 2016). BR is also a good source of proteins because it contains about 76% of amino acids and the 36% of these are essential (Kalman 2014; Santos et al. 2013).

Albumin, globulin, glutelin and prolamin are the proteins inside the rice (Cao et al. 2009; Amagliani et al. 2017a; Van der Borght et al. 2006; Day 2013). Obviously, the protein content is different, according to the treatment and the raw materials, as well as to the processes to obtain the several fractions and to the cultivar (Amagliani et al. 2017a). In Figure 1.2.3.1 illustrates the total contribution of protein and the singular contribution of each protein in the different fractions:
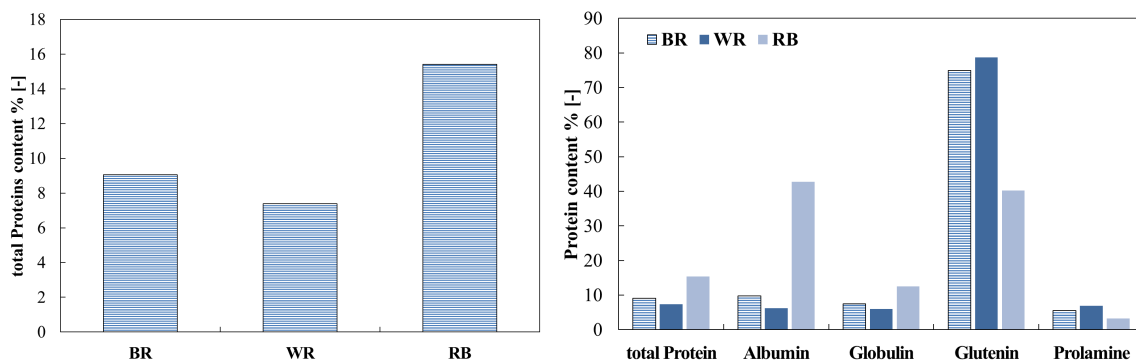
Figure 1.2.3.1 Typology and content of different proteins inside whole rice (Cao et al. 2009, Chandi and Sogi 2007)

The total value of protein content in the different matrixes can vary with the cultivar and ambient factor, so Figure 1.2.3.1 shows the value reported by (Cao et al. 2009), but there are other studies (Zhou et al. 2002; Chandi and Sogi 2007) that show similar but not equal values. The protein ratios of the four fractions present in black rice vary greatly, also

according to the initial cultivars (Chandi and Sogi 2007). As can be seen from Figure 1.2.3.1, the principal fraction of brown rice is still glutelin (Chandi and Sogi 2007; Cao et al. 2009). The amino acidic profile of brown rice has been extensively studied by Kalman (2014) and a summary is shown in Figure 1.2.3.2.
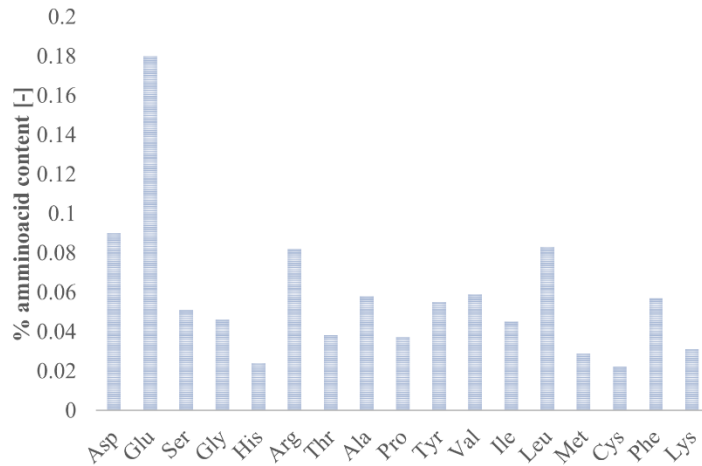
Figure 1.2.3.2 Amino acid profile Brown Rice (Kalman 2014)

The amino acid profile reveals a lower presence of essential amino acids in rice protein with respect to dairy proteins (Amagliani et al. 2017b), which are the proteins most widely used in the food industry to stabilize multiphase systems.

The molecular weight of rice proteins has a wide variability (Amagliani et al. 2017b) and the isoelectric point is at pH 4.5. As is well-known, moving away from the isoelectric point, the solubility of the proteins increases, denaturation is also favored and, so, their solubilization enhanced (Cao et al. 2009). In particular, the higher solubility is reached at pH 10, while the minimum value is achieved at the isoelectric point.

1.3 Interfacial properties of vegetable proteins

The amphiphilic nature of proteins gives them the characteristic of migrating at the interface, so lowering the surface/interfacial tension.

The surface properties of soy proteins are determined by the chemical-physical characteristics of the protein and by the characteristics of the aqueous phase, like pH and ionic strength (Patino et al. 2005; Nino et al. 2005; Martin et al. 2002). Despite their wide uses, knowledge about their surface/interfacial properties is scarce. β-conglycinin has a packed globular structure, low molecular flexibility and an important steric hindrance, which prevents it from migrating at interface easily. To improve its surface/interfacial activity its structure can be modified by reduction, deamidation or dissociation (Wagner and Gueguen 1995). Soy glycinin reduction has been found to have an effect on hydrophobicity, foam

stability and surface elasticity (Martin et al. 2002). Adsorption at interface can induce variations in the structure, particularly, it has been observed that the denatured globulins (heated to temperatures higher than those of denaturation) do not undergo structural variations while the native globulins, in the process of absorption at the interface, modify their structure, varying their conformational state (Tang 2017).

Patino et al.(2005) and (2003) in their works, have studied the dilational properties varying the pH value at pH 2.0, 5.0 and 8.0.

From static measurements, a good surface activity of soy globulins can be noted, with dependence on pH, as said before. At pH 8.0 and 2.0, the surface equilibrium pressure shows high values. Specifically speaking, at pH 2.0 (Patino et al. 2003) and pH 3.0 (Martin et al. 2002), the surface effect is principally given by 7S because at this pH the 11S form tends to dissociate itself in the more simple 2S and 7S forms. Consequently, the 7S form, being smaller than 11S, allows a faster diffusion to interfacial layers (Martin et al. 2002). The interfacial tension decrease is directly related to soy globulins reduction (Martin et al. 2002; Wagner and Gueguen 1995), even if it is important to underline that, waiting for the necessary time to reach the equilibrium conditions, the differences between the different forms of soy glycinin disappear (Martin et al. 2002). This effect can be explained by their complex structure: 11S, being more packed and larger, needs more time to unfold and rearrange to show the same effects as 7S/3S forms (Martin et al. 2002; Bos, Dunnewind and van Vliet 2003).

By analysis of isothermal adsorption, the soy proteins surface pressure increases with their bulk concentration with a sigmoidal trend, typical of macromolecular species and, consequently, of other proteins used in the food industry (Ortiz et al. 2003). The CMC condition is reached at a concentration of 0.1% w/w at pH 5.0 while, at pH 2.0 and 8.0, is reached at a concentration of 1%w/w (Ortiz et al. 2003).

From dilational rheology, a time dependence of the surface dilational moduli can be observed in all pH conditions for soy globulins. In addition, in this case, the observed surface properties are determined also by molecular structure and environment conditions. The decrease of pH implies a structural change, which involves a change of the functional group exposure, which involves also the surface effects change. The surface dilational modulus increases with time, probably because the protein continues to spread at the interface and, in this way, protein-protein interactions are formed, closely packed, which gives elasticity at the interface and that form an elastic gel-like layer. Increasing the bulk protein concentration, this effect is more evident and gives rise to multilayers as found by Brewster angle

microscopy (BAM) (Patino et al. 2003; Ortiz et al. 2003). This layer presents a heterogeneity that, for long times, leads to a collapse of the structure and, consequently, a decreasing of the surface dilational modulus. All globulins form surface layers, but the 11S form seems to create a more compact surface layer with respect to the 3S, which achieves a more flexible structure and a more elastic network (Martin et al. 2002).

If the previous information is analyzed in the light of the Graham & Philips and Ward-Today model ((Patino et al. 2005), it can be seen that the diffusion step at pH 5.0 becomes the unique step of the interfacial mechanisms. In these conditions, in fact, the globulin is in an aggregative form, because near to its electric point, so the migration to the interface is hindered by its aggregation state. The reverse situation is observable at pH 2.0, at which good solubility promotes the diffusion step and the penetration and unfolding mechanisms can be observed.

By analyzing the behavior of the protein in frequency, it becomes evident that the surface layer of soy protein has an elastic behaviour that can be associated with the formation/rupture of the multilayers, for high protein concentrations, induced by the imposed deformation rate at low frequencies (<0,1 Hz).

In addition, the value of the elastic modulus is mainly referred to glycinin, which seems to stabilize the system thanks to its disulfide bonds. Therefore, the glycinin seems to give a good elasticity to the interfacial layer more than β-conglycinin (Patino et al. 2003). From an interfacial shear point of view, in the literature interesting results can be found on soy glycinin viscosity at different pH values, which show comparable interfacial shear viscosity values for glycinin with lysozyme, β-lactoglobulin or ovalbumin (Martin et al. 2002)

In comparison with other proteins (of which vegetable proteins are proposed as a substitute), globulins are sensitive to the globular structure that gives them a low mobility and low performance in the short term, as in the diffusion step. Casein, a typical whey protein, used as stabilizer and emulsifier, is a flexible and random coil protein, its hydrophobicity and small size, gives it good surface properties in the short time analysis (Bos et al. 2003). Also in dynamic measurements, casein does not have a good performance and these are not variable over time. On the contrary, glycinin and gliadin are able to create a good surface layer, with elastic behaviour that increases over time (Bos et al. 2003). In the following Figure 7 the interfacial properties are summarized, such as surface tension, elasticity, tan d and the molecular weight of the three proteins compared.
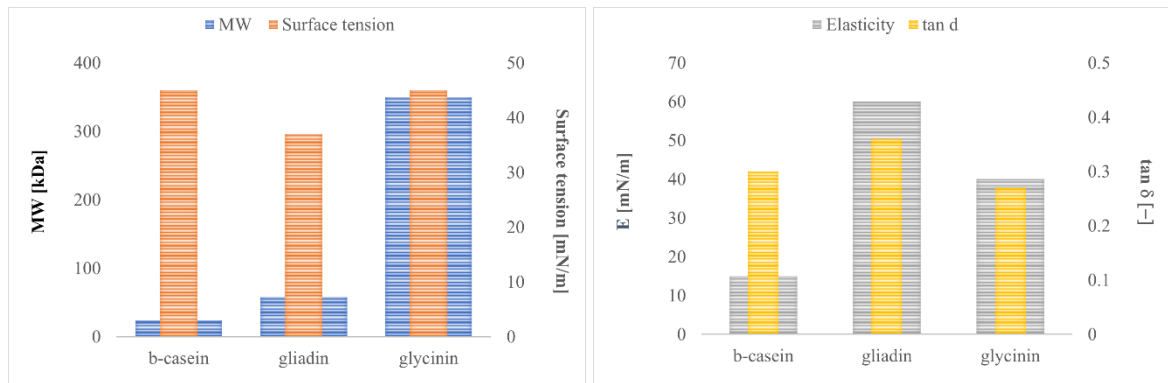
Figure 1.3.1 Comparison between β-casein, gliadin and glycinin about principal surface indicator (Bos et al. 2003)

The surface effects were evaluated taking into account other factors, because complex phenomena give rise to surface/interfacial layers formation and stabilization.

About surface/interfacial properties of hemp proteins, there are no scientific works that give information on their surface activity. Only the work of (Baltazar-Y-Jimenez and Bismarck 2007) has been done on the surface activity of hemp fibre, owing to its wide application field. The surface effect of several fibres sources was tested and from this analysis, hemp fibre shows a good surface activity. Even in the case of brown rice, there are no scientific studies of surface/interface properties.

1.4 Foaming and emulsifying properties

The use of proteins in emulsion and foam formulations is a technique to form and stabilize them. The proteins are able to diffuse rapidly at the interface, adsorb and rearrange their structure, in this way the proteins can lower the surface tension and can form a viscoelastic film, resistant to the destabilization phenomena, such as coalescence (Damodaran 2005; Tang 2017; Bos and van Vliet 2001).

There is a lack of rich literature about the foaming and emulsifying studies of vegetable proteins. A method to quantify the characteristic to form an emulsion is the evaluation of some empirical and qualitative parameters: emulsifying ability (EC) (McClements 2007), emulsifying activity index (EAI) (and emulsion stability index (ESI) (Pearce and Kinsella 1979; McClements 2007). The emulsifying capability of a protein is the quantity of oil that the protein can englobe in an emulsion, the emulsifying activity index is the total interfacial area formed by a specific quantity of protein in an emulsion formulation (Tang et al. 2006a; Tang 2017), the emulsion stability index is an indicator of the characteristic of the emulsion

not to undergo the phenomena of aggregation of the drops dispersed inside it (McClements 2007). Soy proteins are good stabilizers, thanks to their steric hindrance, they can form a viscoelastic layer around the oil droplets with great thickness. This characteristic results in a good performance to prevent coalescence separation (Tang 2017).

The foaming properties of soy globulins are great, particularly in acid conditions, under isoelectric point, soy glycinin can form stable foams, with fine bubbles characterized by unimodal size distribution (Martin et al. 2002), coalescing resistant. With respect to several forms that can be present in solution at different environmental conditions, the opinions are contrasting, (Tang 2017) attests a greater emulsifying ability for 7S form and attributes to it a lower molecular weight of 7S than 11S, but also the better flexibility of 7S than 11S.

Other studies (Pesic et al. 2005) reported an opposite result. More precisely, the emulsification activity decreases when the 7S concentration increases and the 11S/7S ratio increases.

This effect is caused by the hydrophobicity of glycinin and by the exposure of their functional groups. Also, Pesic et al. (2005) show that the glycinin/b-conglycinin ratio does not influence the emulsifying stability.

Furthermore, if at low protein concentration, the conformational state, the hydrophobicity, the solubility, the flexibility of the structure, are all important factors that can change the emulsifying effect, at high protein concentration, the processes involved to form the surface/interfacial layers are very fast and the previously-stated factors become irrelevant (Tang 2017).
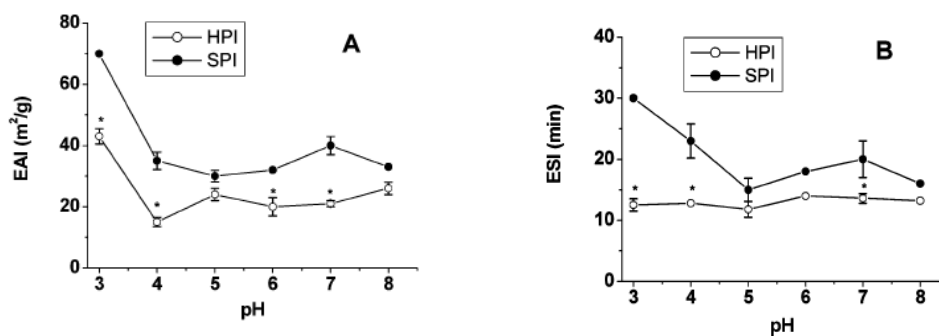
Figure 1.4.1 Index of emulsification activity (A) and index of emulsification stability (B), for hemp and soy isolate proteins, to varying pH (Tang et al. 2006a)

It can be noted that the soy EAI and ESI are always greater than hemp protein, but in particular, pH condition, also that the value of both proteins is very similar. At pH 4.0 it seems that EAI is determined by solubility, for both proteins, in fact decreasing the pH, the hemp and soy solubility increase, and, in the same way, also the EAI index increases (Tang et al. 2006a). Concerning emulsifying activity, there is no marked dependence of hemp

protein ESI on pH and, in all pH range, the ESI values are lower than soy proteins. The latter shows more variability from pH and under pH 5.0 show an increasing emulsifying activity (Tang et al. 2006a). In the work of (Malomo et al. 2014), the emulsion stability value is greater than the emulsion stability value of (Tang et al. 2006a) study, throughout the pH range. Furthermore, the emulsion stability does not have a strong dependence on pH (Malomo et al. 2014).

Moreover, there are no great differences in the stability of the foams created by using HPM and in the stability of the foams created by using HPI.

Malomo et al. (2014) studied the foaming capacity of HPM and HPI. His study shows that decreasing the pH, the foam capacity decreases and reaches a minimum value at pH=5. At pH 3.0, and only for the HPI sample, the foaming capacity reaches greater value, probably in accordance with the solubility trend. Malomo et al. (2014) studied also the stability of the hemp protein foam and reported the foams created by using HPI are more stable than the same formed by using HPM. The foaming stability of HPI is independent of pH conditions, while the foaming stability of HPM presents a variation in function of pH and protein concentration.

Cao et al. (2009) studied the foaming properties of rice proteins, in particular varying several environmental factors, like salt and sugar concentration and also ionic strength and pH. Closely related to their solubility, the foaming and emulsifying proprieties (capacity and stability) of rice proteins improve in environmental conditions that are away from the isoelectric pH value (Cao et al. 2009; Pinciroli et al. 2009). Away from this condition, their effect is more significant. (Pinciroli et al. 2009) investigated the foaming and emulsifying properties of brown rice at pH 3 and pH 9, also in this experiments it could be noted that always increasing the solubilization of the proteins, the foaming properties improve, but the emulsifying properties are not related to solubility effects. (Cao et al. 2009) also showed that sugar addiction decreases the foam/emulsion capacity and improves the foam/emulsion stability. The salt concentration also influences the foaming and emulsifying properties, in particular, the salt concentration increase improves the foaming capacity and stability, but, in the case of emulsion, the increase of NaCl concentration decreases both the emulsifying capacity and stability (Cao et al. 2009).

1.5 Conclusion

Vegetable proteins are a good alternative to the classical proteins used in the food industry as stabilizer and emulsifier. The introduction of vegetable proteins in food formulation can

increase the target of the consumer, involving intolerants, allergic people, sportsmen and those, for ethical reasons, who do not consume food with animal derivatives.

The implementing of vegetable proteins in food formulation required the knowledge of their rheological properties in both bulk and surface/interface. There is a great gap in the knowledge of the surfactant properties of these proteins and about their conferring viscoelasticity to interfaces, so a more detailed analysis of surface properties of all vegetable protein is suitable.

From literature data, hemp proteins are a good ingredient usable in the food industry as a source of nutrition but, their functional properties are lower than soy protein (Wang et al. 2008; Tang et al. 2006a; Malomo et al. 2014), so, the hypothesis of their use after structural modification could improve this factor and give it a more extended field of applications.

The amino acid comparison between hemp and soy profile shows that hemp protein is lower in the content of some essential amino acids than soy protein, but, the ratio of essential amino acid to total amino acids is greater for hemp protein than soy protein (Wang et al. 2008). In general, the vegetable proteins analyzed are all rich in amino acid, enough to compete with animal proteins.

The environment conditions of the protein solution are fundamental to give the best performance to the proteins, such as pH, ionic strength or co-solute. So a good matching of all of these parameters can give good applicative results. The use of other species, such as polysaccharides, with the function of the stabilizer of multiphasic systems, can be a good resource to improve the protein effect, both for interfacial layers and for the bulk phase.

As proteins are used in foams and emulsions because of their characteristic of stabilizing the two-step interface, and as the use of plant proteins in food formulations is increasingly taking hold, the need to know their surface and interface properties is then a necessity for the optimization of new food products.

REFERENCES

Agboola, S., D. Ng & D. Mills (2005) Characterisation and functional properties of Australian rice protein isolates. *Journal of Cereal Science,* 41**,** 283-290.

Amagliani, L., J. O'Regan, A. L. Kelly & J. A. O'Mahony (2017a) The composition, extraction, functionality and applications of rice proteins: A review. *Trends in Food Science & Technology,* 64**,** 1-12.

Amagliani, L., J. O'Regan, A. L. Keny & J. A. O'Mahony (2017b) Composition and protein profile analysis of rice protein ingredients. *Journal of Food Composition and Analysis*, 59**,** 18-26.

Barac, M. B., Stanojevic, S., P., Jonanovic, S., T., & Pesic, M., P. (2004) - Soy protein modification: A review. APTEFF, 35, 1-280

Baltazar-Y-Jimenez, A. & A. Bismarck (2007) Surface modification of lignocellulosic fibres in atmospheric air pressure plasma. *Green Chemistry,* 9**,** 1057-1066.

Bos, M. A., B. Dunnewind & T. van Vliet (2003) Foams and surface rheological properties of beta-casein, gliadin and glycinin. *Colloids and Surfaces B-Biointerfaces,* 31**,** 95-105.

Bos, M. A. & T. van Vliet (2001) Interfacial rheological properties of adsorbed protein layers and surfactants: a review. *Advances in Colloid and Interface Science,* 91**,** 437-471.

Bouyer, E., G. Mekhloufi, V. Rosilio, J. L. Grossiord & F. Agnely (2012) Proteins, polysaccharides, and their complexes used as stabilizers for emulsions: Alternatives to synthetic surfactants in the pharmaceutical field? *International Journal of Pharmaceutics,* 436**,** 359-378.

Callaway, J. C. (2004) Hempseed as a nutritional resource: An overview. *Euphytica,* 140**,** 65-72.

Cao, X. H., H. B. Wen, C. J. Li & Z. X. Gu (2009) Differences in functional properties and biochemical characteristics of congenetic rice proteins. *Journal of Cereal Science,* 50**,** 184-189.

Chandi, G. K. & D. S. Sogi (2007) Biochemical characterisation of rice protein fractions. *International Journal of Food Science and Technology,* 42**,** 1357-1362.

Cho, D. H. & S. T. Lim (2016) Germinated brown rice and its bio-functional compounds. *Food Chemistry,* 196**,** 259-271.

Damodaran, S. (2005) Protein stabilization of emulsions and foams. *Journal of Food Science,* 70**,** R54-R66.

Day, L. (2013) Proteins from land plants - Potential resources for human nutrition and food security. *Trends in Food Science & Technology,* 32**,** 25-42.

Hadnadev, M., T. Dapcevic-Hadnadev, A. Lazaridou, T. Moschakis, A. M. Michaelidou, S. Popovic & C. G. Biliaderis (2018) Hempseed meal protein isolates prepared by different isolation techniques. Part I. physicochemical properties. *Food Hydrocolloids,* 79**,** 526-533.

Jnawali P., Kumar V., Tanwar B. (2016), Celiac disease: Overview and considerations for development of gluten-freefoods, *Food Science and Human Wellness,* 5, 169–176.

Kalman D. S. (2014), Amino Acid Composition of an Organic Brown Rice Protein Concentrate and Isolate Compared to Soy and Whey Concentrates and Isolates, *Foods,* 3, 394-402.

Lakemond, C. M. M., H. H. J. de Jongh, M. Hessing, H. Gruppen & A. G. J. Voragen (2000) Soy glycinin: Influence of pH and ionic strength on solubility and molecular structure at ambient temperatures. *Journal of Agricultural and Food Chemistry,* 48**,** 1985-1990.

Lin, D. & Y. Y. Zhao (2007) Innovations in the development and application of edible coatings for fresh and minimally processed fruits and vegetables. *Comprehensive Reviews in Food Science and Food Safety,* 6**,** 60-75.

Malomo, S. A., R. He & R. E. Aluko (2014) Structural and Functional Properties of Hemp Seed Protein Products. *Journal of Food Science,* 79**,** C1512-C1521.

Martin, A. H., M. A. Bos & T. van Vliet (2002) Interfacial rheological properties and conformational aspects of soy glycinin at the air/water interface. *Food Hydrocolloids,* 16**,** 63-71.

McClements, D. J. (2007) Critical review of techniques and methodologies for characterization of emulsion stability. *Critical Reviews in Food Science and Nutrition,* 47**,** 611-649.

Moure, A., J. Sineiro, H. Dominguez & J. C. Parajo (2006) Functionality of oilseed protein products: A review. *Food Research International,* 39**,** 945-963.

Nesterenko, A., I. Alric, F. Silvestre & V. Durrieu (2013) Vegetable proteins in microencapsulation: A review of recent interventions and their effectiveness. *Industrial Crops and Products,* 42**,** 469-479.

Nino, M. R. R., C. C. Sanchez, V. P. Ruiz-Henestrosa & J. M. R. Patino (2005) Milk and soy protein films at the air-water interface. *Food Hydrocolloids,* 19**,** 417-428.

Nishinari, K., Y. Fang, S. Guo & G. O. Phillips (2014) Soy proteins: A review on composition, aggregation and emulsification. *Food Hydrocolloids,* 39**,** 301-318.

Ortiz, S. E. M., C. C. Sanchez, M. R. R. Nino, M. C. Anon & J. M. R. Patino (2003) Structural characterization and surface activity of spread and adsorbed soy globulin films at equilibrium. *Colloids and Surfaces B-Biointerfaces,* 32**,** 57-67.

Osborne, T.B., (1909), The Vegetable Proteins. Longmans, Green and Co., London.

Patino, J. M. R., R. R. Nino, C. C. Sanchez, S. E. M. Ortiz & C. Anon (2005) Dilatational properties of soy globulin adsorbed films at the air-water interface from acidic solutions. *Journal of Food Engineering,* 68**,** 429-437.

Patino, J. M. R., S. E. M. Ortiz, C. C. Sanchez, M. R. R. Nino & M. C. Anon (2003) Dynamic properties of soy globulin adsorbed films at the air-water interface. *Journal of Colloid and Interface Science,* 268**,** 50-57.

Pearce and Kinsella (1979), Functional Properties of Soy Proteins, J. AM. OIL CHEMISTS' SOC., (VOL. 56)

Pesic, M. B., B. V. Vucelic-Radovic, M. B. Barac & S. P. Stanojevic (2005) The influence of genotypic variation in protein composition on emulsifying properties of soy proteins. *Journal of the American Oil Chemists Society,* 82**,** 667-672.

Piazza, L., N. Durr-Auster, J. Gigli, E. J. Windhab & P. Fischer (2009) Interfacial rheology of soy proteins - High methoxyl pectin films. *Food Hydrocolloids,* 23**,** 2125-2131.

Pinciroli, M., A. A. Vidal, M. C. Anon & E. N. Martinez (2009) Comparison between protein functional properties of two rice cultivars. *Lwt-Food Science and Technology,* 42**,** 1605-1610.

Pojic, M., A. Misan, M. Sakac, T. D. Hadnadev, B. Saric, I. Milovanovic & M. Hadnadev (2014) Characterization of Byproducts Originating from Hemp Oil Processing. *Journal of Agricultural and Food Chemistry,* 62**,** 12436-12442.

Santos, K., R. D. D. Silveira, C. C. G. Martin-Didonet & C. Brondani (2013) Storage protein profile and amino acid content in wild rice Oryza glumaepatula. *Pesquisa Agropecuaria Brasileira,* 48**,** 66-72.

Singh, A., M. Meena, D. Kumar, A. K. Dubey & M. I. Hassan (2015) Structural and Functional Analysis of Various Globulin Proteins from Soy Seed. *Critical Reviews in Food Science and Nutrition,* 55**,** 1491-1502.

Singh, P., R. Kumar, S. N. Sabapathy & A. S. Bawa (2008) Functional and edible uses of soy protein products. *Comprehensive Reviews in Food Science and Food Safety,* 7**,** 14-28.

Souzandeh, H., K. S. Johnson, Y. Wang, K. Bhamidipaty & W. H. Zhong (2016) Soy-Protein-Based Nanofabrics for Highly Efficient and Multifunctional Air Filtration. *Acs Applied Materials & Interfaces*, 8**,** 20023-20031.

Tang, C. H. (2017) Emulsifying properties of soy proteins: A critical review with emphasis on the role of conformational flexibility. *Critical Reviews in Food Science and Nutrition*, 57**,** 2636-2679.

Tang, C. H., Z. Ten, X. S. Wang & X. Q. Yang (2006a) Physicochemical and functional properties of hemp (Cannabis sativa L.) protein isolate. *Journal of Agricultural and Food Chemistry*, 54**,** 8945-8950.

Tang, C. H., H. Wu, H. P. Yu, L. Li, Z. Chen & X. Q. Yang (2006b) Coagulation and gelation of soy protein isolates induced by microbial transglutaminase. *Journal of Food Biochemistry,* 30**,** 35-55.

Teh, S. S. & J. Birch (2013) Physicochemical and quality characteristics of cold-pressed hemp, flax and canola seed oils. *Journal of Food Composition and Analysis,* 30**,** 26-31.

Van der Borght, A., G. E. Vandeputte, V. Derycke, K. Brijs, G. Daenen & J. A. Delcour (2006) Extractability and chromatographic separation of rice endosperm proteins. *Journal of Cereal Science,* 44**,** 68-74.

Wagner, J. R. & J. Gueguen (1995) EFFECTS OF DISSOCIATION, DEAMIDATION, AND REDUCING TREATMENT ON STRUCTURAL AND SURFACE-ACTIVE PROPERTIES OF SOY GLYCININ. *Journal of Agricultural and Food Chemistry,* 43**,** 1993-2000.

Wang, X. S., C. H. Tang, X. Q. Yang & W. R. Gao (2008) Characterization, amino acid composition and in vitro digestibility of hemp (Cannabis sativa L.) proteins. *Food Chemistry,* 107**,** 11-18.

Xiang, N., Y. Lyu & G. Narsimhan (2016) Characterization of fish oil in water emulsion produced by layer by layer deposition of soy beta-conglycinin and high methoxyl pectin. *Food Hydrocolloids,* 52**,** 678-689.

Zhou, Z. K., K. Robards, S. Helliwell & C. Blanchard (2002) Composition and functional properties of rice. *International Journal of Food Science and Technology,* 37**,** 849-868.

Chapter 2

Interface and surface tension (state of the art)

Abstract

Food products are typically multiphasic systems, characterized by two or more phases in contact with each other. The formation and the stability of these systems are more complex and depend from several factors, related either to continuous phase phenomena or interfacial phase phenomena. In particular, interfaces are zones of strong instability, because their disadvantageous thermodynamic state. The use of the surfactant agents give stability to these systems mainly at interfacial level. Furthermore, the surfactant agents allow to realize the defined rheological properties characteristics of the interfacial layer. The study of the interface can be done with several techniques, but, about its analysis, there are significant gaps in the scientific literature. In this paper, the interfacial layer will be analysed using thermodynamic, mechanical and rheological approaches to describe the current state of art on this matter and to define the rheological constitutive relationship able to describe the interfacial behaviour.

Keywords: surface tension, interfacial rheology, emulsion, foam, fractional model

2.1 Introduction

Many industrial products are multiphase systems, consisting of two or more immiscible phases in contact with each other. For their preparation to get a homogeneous system it is necessary to disperse finely one phase inside the other. This results in a large increase in the contact area between the phases due to the creation of drops or bubbles or, in other words, interfaces. Interface increase may cause instability leading to phase separation. The interface is defined as the zone of separation between the two phases, where a direct contact occurs between them, with the onset of a zone of great instability. In fact, when a multiphase system is created, it is necessary to supply energy needed to break the bonds of the continuous phase to force it to stay in contact with the phase that is immiscible in it. The energy supplied to the system implies an increase in the energy of the system, with the consequence of putting it in an energetically disadvantaged condition. Of course, the system will tend to evolve towards a more favored energy condition, i.e. an energetic minimum corresponding to the separation of the phases. To avoid this and to stabilize the system, some components are

added. In this way, it is possible to stabilize kinetically these systems, making them stable for a well-defined time that corresponds to their shelf life. These components are the **surf**ace **act**ive **agen**ts (surfactants), so called because of their ability to act directly at the interface changing their properties (Rosen). Their main characteristic is to lower the energy needed for the formation of the system and thus to lower the driving force leading to the separation of phases. In addition to this, they are able to form viscoelastic films at the interface that make these thin layers resistant to collision and breakage. There are two large classes of surface active agents: emulsifiers and biopolymers. They differ mainly in their size but not only. Emulsifiers are characterized by a low molecular weight and they show a high mobility and affinity to reach the surface layers. Biopolymers have high molecular weight and they show a slower migration at the interface but, compared to emulsifiers, they are able to create more stable and resistant interface films. Surfactants with low molecular weight (LMW) include detergents, emulsifiers and lipids. They may be water or oil soluble, and usually form a compact adsorbed layer with a low interfacial tension. Biopolymers are amphiphilic macromolecules, and the most commonly used are proteins that typically form viscoelastic, irreversibly adsorbed layers.

In many cases, the use of both species, in conditions of favorable interaction between the two, is suggested to have both effects at the same time, i.e.: they have to reach the interface quickly but also to ensure a high mechanical strength (Wilde 2000; Bos and van Vliet 2001). All this suggests that such a small region is crucial for several asp ects such as the stability and texture of the products, this means that the study of interface properties is very important and a deeper knowledge is needed, although less considered by the scientific community.

Despite the importance of the interface for the product and process design, there are many critical issues in tackling this matter. The scientific literature, often, treats interfaces in too approximate a fashion, assuming that the surface is an area that can be characterized by the properties of the two adjacent bulk phases. But, it is obvious that, the presence of stabilizing agents, suggests the layer region should be considered as a specific volume, more than a surface, which cannot be neglected. Thus, it is wise to consider an "interfacial bulk" with properties that are unique and different from the two adjacent phases. Furthermore, an interface volume means admitting that there is no longer discontinuity between the continuous phases at the interface, and the properties vary continuously passing from one to the other in that volume. All these problems can be analyzed by studying interfaces from different points of view, focused on thermodynamic and mechanical aspects. This implies

that the rheological analysis should provide details about the constitutive equation of the interface, linking stress and deformation in that interfacial region.

It should be noticed that there is a problem of dimensions also for the interfacial stress, because it should have, generally, all the six components and not only one, as often appears in the current literature. If the state is static, the tensor stress reduces to an isotropic stress with the consequence that there is only the normal component and it assumes the meaning of a pressure.

To investigate the characteristics of interfacial layers, it is possible to use several methods and techniques: ellipsometry, to determine the adsorbed amount and layer thickness, spectroscopy, to determine lateral mobility and conformational changes, tensiometry, to evaluate the surface activity, i.e. the mechanisms and the rate of the adsorption of the molecules at the interfaces, and, finally, interfacial rheology techniques, to study the response of the interfacial film to any specific deformation (Bos and van Vliet 2001; Wilde 2000).

In this chapter, an overview will be given of the nature of the interfacial region, and its analysis using both a mechanical, thermodynamic and rheological approach.

2.2 Interface definition and surface tension

'The world of neglected dimensions' said Wolfgang Ostwald in 1915, referring to surface science as unique properties of interfaces, but also referring to the low value that frequently sciences give to the latter. But, in the reality surface and interface properties strongly influence the formation, stabilization and texture of multiphasic systems, in which the interfaces presence is important and not negligible. So, now the question is: what is really an interface? An interface is the transition region separating two or more immiscible phases, in particular it is possible to discern between interface and surface, indicating with the first the separation zone between two liquid (or a solid and a liquid) phases, whilst, with surface, it is possible to indicate the separation zone between a liquid (or solid) and a gas phase (McClements D.J., 2016). Typically, a surface of every material should be considered as the last layer that is directly in contact with the air.

Referring to the classical definition of a surface, the surface tension (gas/liquid or gas/solid) or interfacial tension (liquid/liquid or solid/liquid), can be imagined as the force needed to maintain the surface shape. This definition is ambiguous and the definition of surface tension is difficult if does not represent a physical reality.

Let us analyze the simple case of a drop of water suspended in air, as depicted in the following figure 2.2.1:
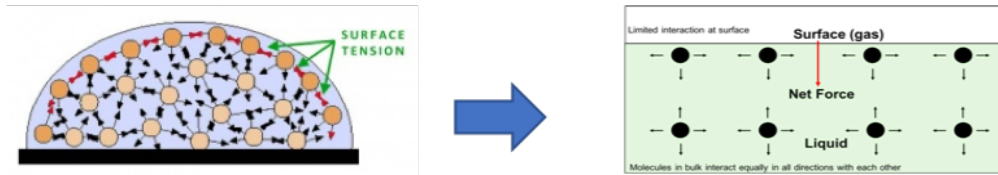
Figure 2.2.1 Scheme of surface effect

The water molecules in the water bulk are surrounded by other water molecules, that interact between them, building a sort of protective state where all the molecules are balanced by the neighbors (Bush). On the contrary, the surface water molecules are surrounded by fewer water molecules with the consequence that they stay in an energetically unfavorable state. To maintain their shape, the molecules exhibit a supplementary negative force, necessary to retain the interface in a curved shape. The result is the presence of an interfacial energy per area capable of resisting the creation of a new interfacial area. The same happens between two fluids, therefore, if the interfacial tension does not arise, they are miscible (Bush). According to this approach, it is possible to define the surface tension as:

$$\Delta G = \gamma \Delta A \qquad (2.2.1)$$

Namely, the surface tension is the proportional constant defining the energy ΔG to be supplied to increase the surface area of ΔA. Surface tension γ has the units of force/length, or equivalently energy/area, and so may be thought of as a negative pressure. Pressure is generally defined as an isotropic force per unit of area that acts throughout the bulk of a fluid: a small surface element dA will undergo a total force p(x)dA, owing to the local pressure field p(x). If the surface A is closed, and the pressure uniform, the net pressure force acting on S is zero and the fluid remains static (Bush).

The creation of new surface requires an energetic input linked to the contact area increase and a fluid system will act to minimize surface areas (McClements D.J., 2016). So, the surface tension appear as a proportional factor linking the energy to be given to the system when a new area is formed *(e.g. this property is important also to link this quantity with the wetting and spreading effect. This evaluation is very important in coating sciences, where the ability to cover a material and to achieve a good adhesion with the support is fundamental to give a good result. The effect is related to the physical characteristics of the interface in terms of composition, polarity, hydrophilic or hydrophobic balance, and surface irregularity).*

The interface is a particular zone in which, although it is a zone between two separated phases, the properties are not equal to these two phases, but in this small region the properties

are variable from those of a pure phase to those ones of the other phase. According to this statement, there are different way to tackle this problem and in the following sections attention will be focused on mechanical, thermodynamic and rheological points of view.

2.3 Thermodynamic approach to define a surface

The interface that separates two phases is often assumed to be a planar surface, thereby neglecting the highly dynamic nature of the interfacial region in which different mechanisms occur, related to the possible presence of molecules added to stabilize it. All this makes the interface region variable both in terms of thickness and energy contribution of the binding forces among the different components, and of mechanical resistance of this small layer. Recently, McClements D.J. (2016) proposed a scheme of the oil/water interface through continuum theory and molecular theory, as shown in the following picture:
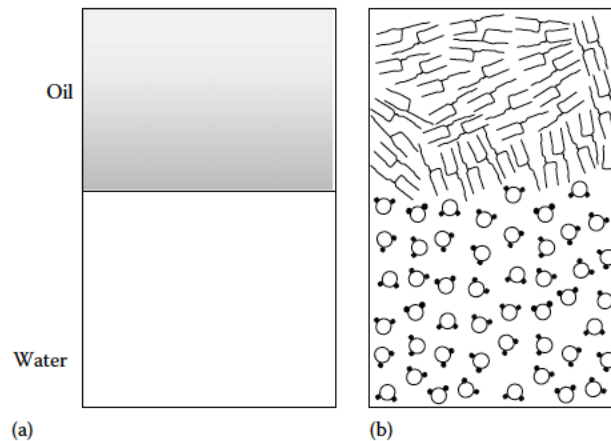
Figure 2.3.1. Scheme of Oil/Water interface according to the Continuum (a) and Molecular theories (b), taken from McClements D.J. (2016)

The interface is generated by a net separation between the two phases, assuming that the two phases are insoluble with each other. For this reason, in order to disperse one phase into the other, it is necessary to supply energy and overcome the interface potential to increase the interface area. The amount of energy that must be supplied is assumed to be proportional to the increase of the contact area between the oil and water molecules (McClements D.J. (2016)):

$$\Delta G = \gamma \Delta A \qquad (2.3.1)$$

where ΔG is the free energy required to increase the contact area between the two immiscible liquids by ΔA (at constant temperature and pressure), and γ is a constant of proportionality called the i*nterfacial tension*, which, for air/water interface, it is known as the surface tension. The interfacial tension is defined by McClements D.J. (2016) as a contractile force exhibited to minimize the contact area between two phases.

To lower the input energy necessary to form a new interfacial area, specific agents possessing surface activity capable of lowering the surface/interface tension can be introduced into the system, consequently, decreasing the energy necessary to homogenize the two phases. These molecules are known as surface active agents or surfactants, and they are molecules with the good characteristic of migrating at interface and lowering the surface/interfacial tension. It is worth noticing that a molecule tends to be accumulated at an interface when the free energy of the adsorbed state is significantly lower than that of the unadsorbed state (McClements D.J., 2016). The difference between the adsorbed and unadsorbed states free energy (ΔG_{ads}) is determined by the change of the interaction energies of the molecules involved, as well as by entropic effects. The surfactant agent is a molecule characterized by a typical configuration with a polar part (head) and an apolar part (tail), this give an amphiphilic property that is the fundamental requirement to perform its function at the interface.
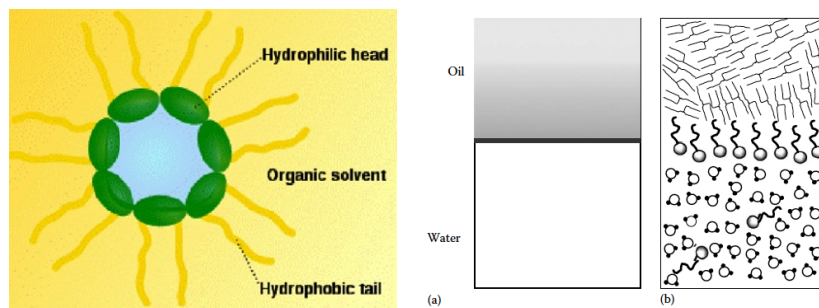
Figure 2.3.2 A surfactant at the interface oil/water and a scheme of Oil/Water interface with adsorbed emulsifiers, according to the Continuum (a) and Molecular theories (b), taken from McClements D.J. (2016),(Lal, O'Connor and Eyres, 2006)

The surfactant agent arrives at the interface and exposes the polar segment towards the water and the nonpolar segments towards the other phase. When they are dispersed in bulk water, some of the nonpolar segments come into contact with water, which is energetically unfavorable because of the hydrophobic effect. On the contrary, when they are adsorbed at an interface, they are able to maximize the number of energetically favorable interactions between the polar segments and water, while minimizing the number of unfavorable interactions between the nonpolar segments and water. The hydrophobicity of the surfactants is the main driving force of the adsorption at interface, but there are other phenomena that may take place such as: electrostatic interactions, steric interactions/repulsion and hydrogen bonding.

There are several entropic effects associated with adsorption, mainly due to the fact that, when molecules are adsorbed at an interface, they are confined to stay in a region much smaller than the volume it would occupy inside a liquid bulk, with the consequence that its

molecular rotation is restricted. Furthermore, the number of different conformations that it can show may either increase or decrease, e.g. the possible conformations exhibited by flexible random coil biopolymers, usually decreases after adsorption, whereas the possible conformations, shown by globular biopolymers, usually increases. Finally, also an entropic effect can be achieved because of a new organization of molecules resulting from adsorption (McClements D.J., 2016).

The characteristic of surfactant molecules to lower the surface/interfacial tension is governed by their packing ability at an interface, which is determined by their molecular geometry, by their hydrophobicity, their interactions with other molecules at interface (McClements D.J.; 2016). The rate at which the conformation of a surfactant changes at an oil–water interface depends on its molecular structure. Flexible random-coil molecules can change their conformations rapidly, whereas rigid globular molecules are less sensitive to changes. Immediately after adsorption to an interface, a globular protein has a conformation that is similar to that shown inside the bulk aqueous phase. Thereafter, when time elapses, it alters its conformation so that it can optimize the number of favorable interactions between the nonpolar amino acids and the oil molecules. The configuration of surfactants at an interface can play an important role on the bulk physicochemical properties of food emulsions. The coalescence stability of many oil-in-water emulsions is determined by the unfolding and the interaction of proteins at the droplet surface. When globular proteins unfold, they expose more reactive amino acids that can form hydrophobic and disulfide bonds with their neighbors, thus generating a highly viscoelastic membrane that is resistant to coalescence.

The reduction of the surface/interfacial tension, following the addition of surfactants, can be evaluated as the surface pressure, which is the difference between the interfacial tension γ_0 of a pure oil/water (or gas/water) interface, and the interfacial tension γ in the presence of the emulsifier:

$$\pi = \gamma_0 - \gamma \qquad\qquad (2.3.2)$$

When increasing surfactant concentration, the surface pressure increases, until the surface pressure reaches a constant value and does not change anymore with further surfactant addition: in this state the surface layer is saturated with the surfactant.

In the following Figure 2.3.3, a plot of both surface tension and surface pressure are shown when changing concentration in the case of a protein surfactant:
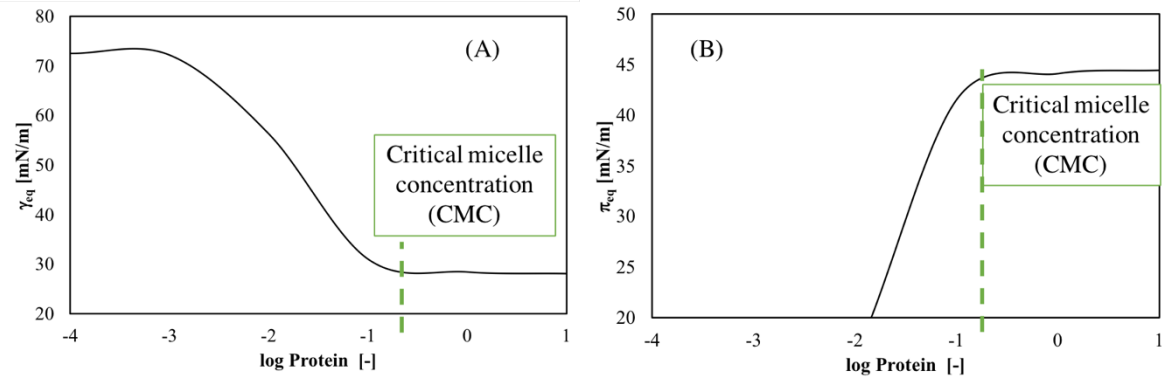
Figure 2.3.3 Example of sigmoidal trend of surface tension (A) for a protein and respective surface pressure (B) trend

The decreasing of surface tension and the increasing of the surface pressure, corresponds to the saturation of the surface layers and the minimum value of surfactant necessary to cover all the surface is called critical micelle concentration (CMC). When the surfactant concentration values overcome CMC, the surface tension remains constant.

Thus, it can be stated that lowering the interface tension (and increasing the surface pressure), means lowering the work necessary to create a new interface area or to deform the interface. Referring to a free interface, the deformation power must be related to a surface leading to the following equation:

$$W = \gamma \dot{\tilde{\alpha}} \tag{2.3.3}$$

As a consequence the first and second thermodynamic principles assume the following form:

$$\dot{\tilde{U}} = q + \gamma \dot{\tilde{\alpha}} \tag{2.3.4}$$

$$\dot{\tilde{S}} \geq \frac{q}{T} \tag{2.3.5}$$

If these two are combined, by eliminating q it is obtained:

$$\dot{\tilde{U}} \leq T\dot{\tilde{S}} + \gamma \dot{\tilde{\alpha}} \tag{2.3.6}$$

The Helmotz free energy in this case is a continuous and differentiable function of the state variable T, $\tilde{\alpha}$, then $\tilde{A} = \tilde{A}(T, \tilde{\alpha})$.

Performing the time derivate, it is obtained:

$$\dot{\tilde{A}} = \frac{\delta A}{\delta T}\bigg|_{\tilde{V},\tilde{\alpha}} \dot{T} + \frac{\delta A}{\delta \alpha}\bigg|_{\tilde{V},T} \dot{\tilde{\alpha}} \tag{2.3.7}$$

Considering the Helmotz free energy definition:

$$\dot{\tilde{U}} = \dot{\tilde{A}} + T\dot{\tilde{S}} + \tilde{S}\dot{T} \tag{2.3.8}$$

By using equation 2.3.7, equation 2.3.8 becomes

$$\dot{\tilde{U}} = \frac{\delta \tilde{A}}{\delta T}\bigg|_{\tilde{V},\tilde{\alpha}} \dot{T} + \frac{\delta \tilde{A}}{\delta \tilde{\alpha}}\bigg|_{\tilde{V},T} \dot{\tilde{\alpha}} + T\dot{\tilde{S}} + \tilde{S}\dot{T} \leq T\dot{\tilde{S}} + \gamma \dot{\tilde{\alpha}} \tag{2.3.9}$$

$$\left(\frac{\delta \tilde{A}}{\delta T}\bigg|_{\tilde{V},\tilde{\alpha}} + \tilde{S}\right) \dot{T} + \left(\frac{\delta \tilde{A}}{\delta \tilde{\alpha}}\bigg|_{\tilde{V},T} - \gamma\right) \dot{\tilde{\alpha}} \leq 0 \tag{2.3.10}$$

This relationship must hold for any given transformation, thus it results:

$$\tilde{S} = \frac{\delta \tilde{A}}{\delta T}\bigg|_{\tilde{V},\tilde{\alpha}}, \gamma = \frac{\delta \tilde{A}}{\delta \tilde{\alpha}}\bigg|_{\tilde{V},T} \tag{2.3.11}$$

Thus the following four Maxwell equations are obtained:

$$\dot{\tilde{U}} = T\dot{\tilde{S}} + \gamma \dot{\tilde{\alpha}}$$

$$\dot{\tilde{H}} = T\dot{\tilde{S}} - \dot{\gamma}\tilde{\alpha}$$

$$\dot{\tilde{A}} = -\tilde{S}\dot{T} + \gamma \dot{\tilde{\alpha}}$$

$$\dot{\tilde{G}} = -\tilde{S}\dot{T} - \dot{\gamma}\tilde{\alpha} \tag{2.3.12}$$

The use of the state function, which is defined as an additive being referred to a given mass, links the surface tension to the bulk of the material, with the consequence that the surface is not physically identified. In fact, the current literature tends to identify the properties at the interface referring to those of the bulk. This generates a strong problem of discontinuity at the interface separating two phases, in which the properties are typically neither of the one nor of the other phase, and appear to be different at the same identical point. This problem can be overcome by using the above-mentioned static solution for the surface tension, and by assuming the mechanical equilibrium between the two phases, but, in this way, this seems to undermine the identity of the interface zone.

In the presence of superficially active agents, the problem becomes more important, since the interface is characterized by their presence due to their size, which becomes no longer negligible, but also to their concentration that is different from that of the bulk.

An interphase volume can be considered within which the properties vary from those of pure phase α to pure phase β.
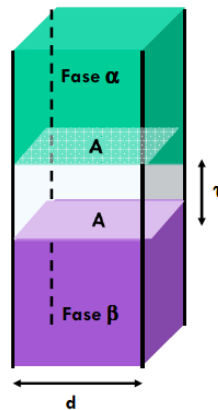
Figure 2.3.4 Interphase scheme

Outside the interphase volume the properties are constant, thus the state function additivity is maintained and the thermodynamic balance becomes:

$$U = U^\alpha + U^\beta + U^\sigma \tag{2.3.13}$$

$$U^\alpha = TS^\alpha - PV^\alpha + \sum_i \mu_i n_i{}^\alpha \qquad (2.3.14)$$

$$U^\beta = TS^\beta - PV^\beta + \sum_i \mu_i n_i{}^\beta \qquad (2.3.15)$$

$$U^\sigma = TS^\sigma - PV^\sigma + \gamma A + \sum_i \mu_i n_i{}^\sigma \qquad (2.3.16)$$

By making the derivative respect to time U^σ the latter becomes:

$$\dot{U}^\sigma = T\dot{S}^\sigma + \dot{T}S^\sigma - P\dot{V}^\sigma - \dot{P}V^\sigma + \gamma\dot{A} + \dot{\gamma}A + \sum_i \mu_i \dot{n}_i{}^\sigma + \sum_i \dot{\mu}_i n_i{}^\sigma \quad (2.3.17)$$

That for small, isobaric, isothermal and reversible change and according to Gibbs-Duhem constraint, is obtained:

$$\dot{U}^\sigma = T\dot{S}^\sigma - \dot{P}V^\sigma + \dot{\gamma}A + \sum_i \mu_i \dot{n}_i{}^\sigma \qquad (2.3.18)$$

By making the difference between eq. 2.3.16 and eq. 2.3.17, the state equation of the interphase is obtained:

$$S^\sigma \dot{T} - V^\sigma \dot{P} + A\dot{\gamma} + \sum_i n_i{}^\sigma \dot{\mu}_i = 0 \qquad (2.3.19)$$

The difficulty is still to identify which is the planar interface where to define interface properties that seem to require a surface and not a volume. Therefore, inside the interphase volume, where the extensive variables are continuous and vary along the thickness τ, it is necessary to identify a surface.
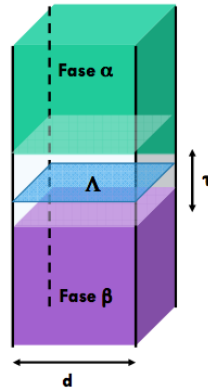
Figure 2.3.5 Interphase scheme with Gibbs dividing surface

Following Gibbs approach, the interphase is a region with a thickness τ along which the properties of the system vary from values specific for the phase α to those characteristic of phase β (Eastoe J., 2010). Inside this region Gibbs identifies a surface Λ, the interface surface, on which surface properties should be evaluated, which is defined as the Gibbs dividing surface (McClements, D.J., 2016). The thermodynamic balance, according to the Gibbs multicomponent system theory, will take account of the three different contributions: phase α, phase β and interphase σ. Therefore, equation 2.3.19 can be applied, that for P and T constant, becomes:

$$A\dot{\gamma} + \sum_i n_i{}^\sigma \dot{\mu}_i = 0 \qquad (2.3.20)$$

Dividing for the area:

$$\dot{\gamma} = -\sum_i \dot{\mu}_i \frac{n_i^\sigma}{A} \tag{2.3.21}$$

$$\dot{\gamma} = -\sum_i \Gamma_i^\sigma \dot{\mu}_i \tag{2.3.22}$$

The latter equation is called the Gibbs-Duhem equation for the surface, and:

$$\Gamma_i^\sigma = \frac{n_i^\sigma}{A} \tag{2.3.23}$$

Γ_i^σ, is the surface excess of component i, which is the difference between the quantity of a component actually present at the interface, and the quantity of a bulk component, as if there were no migration effects at the interface and the concentration remains constant.

Area A is referred to Λ and its location is effectuated evaluating the position where the reference concentration is greatest.
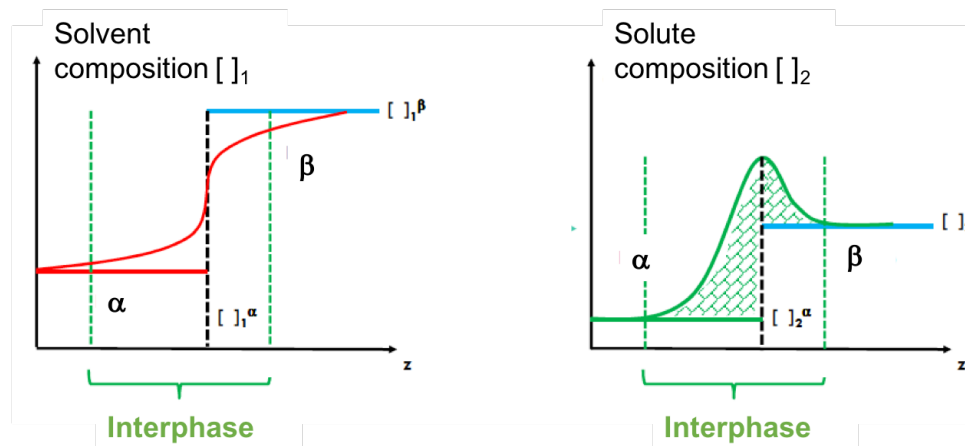
Figure 2.3.6 Idealized system for the definition of the Gibbs dividing surface

The definition of the Gibbs dividing surface is, obviously arbitrary and is chosen in such a way that the surface excess adsorption of the solvent is zero. An important approximation associated with Gibbs adsorption equation is the 'exact' location of the interface.

The surface excess concentration is an important information for formulating food emulsions because it determines the emulsifier amount necessary to create an emulsion with a defined characteristic of drop size distribution. The smaller the value of Γ, the greater the area of the interface that can be covered with the same quantity of surfactant, and, therefore, the smaller the droplets which can be stabilized by the emulsifier. Plots of surface tension versus surfactant concentration are very useful because they indicate the maximum surface pressure (π_{max}) that can be achieved when the surface is saturated by an emulsifier, which leads to important consequences for the formation and stability of food emulsions and foams.

2.4 Mechanical approach to define a surface

Surface tension has been defined (up to now) as a scalar, without taking into account its tensorial character. This has been possible because it was considered only a static state, but

when a dynamic condition is considered, a proper definition is needed. Following the mechanical analysis of a body, an attempt can be made to apply the continuous mechanics approach also to the interface layers. So a surface tension tensor can be defined:

$$\boldsymbol{\Gamma} = \left\| \begin{matrix} \gamma_{11} & \gamma_{12} & \gamma_{13} \\ \gamma_{21} & \gamma_{22} & \gamma_{23} \\ \gamma_{31} & \gamma_{32} & \gamma_{33} \end{matrix} \right\| \tag{2.4.1}$$

As in bulk analysis, the stress tensor can be divided in two contributions, an isotropic part $(\boldsymbol{\Gamma} = -\gamma_0 \boldsymbol{I}_0)$ and a deviatoric part $(\boldsymbol{\Gamma}_{dev})$:

$$\boldsymbol{\Gamma} = -\gamma_0 \boldsymbol{I} + \boldsymbol{\Gamma}_{dev} \tag{2.4.2}$$

$$\boldsymbol{\Gamma}_0 = \gamma_0 \left\| \begin{matrix} 1 & 0 & 0 \\ 0 & 1 & 0 \\ 0 & 0 & 1 \end{matrix} \right\| \tag{2.4.3}$$

$$\boldsymbol{\Gamma}_{dev} = \left\| \begin{matrix} \gamma_{11} + \gamma_0 & \gamma_{12} & \gamma_{13} \\ \gamma_{21} & \gamma_{22} + \gamma_0 & \gamma_{23} \\ \gamma_{31} & \gamma_{32} & \gamma_{33} + \gamma_0 \end{matrix} \right\| \tag{2.4.4}$$

To carry out a mechanical balance, the superficial stress tensor should be inserted in this form.

In the scientific literature Bush analyzes the mechanical behavior of the interface, considering the surface stress (the surface tension) only as a scalar quantity γ_0, without considering that the surface tension, being a tensor, has, theoretically, nine components, of which six are independent. The Bush analysis considers the interface S between two fluids of different density and he assumes that the surface is bounded by a closed contour C, as shown in the following figure:
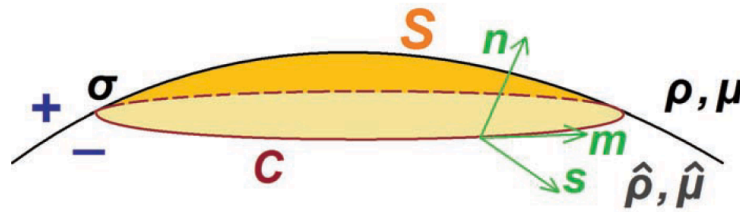
Figure 2.4.1 Scheme of a surface S with contour C, dividing two fluid. n, m and s are respectively the normal to S, the tangent to the contour C and the normal to C and tangent to S.

At this point, a control volume may be assumed as the region V that includes this area and has a thickness ε, as shown in the following picture:
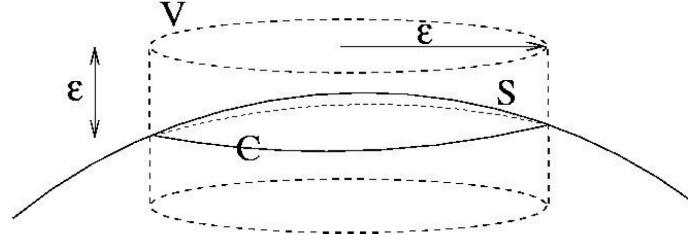
Figure 2.4.2 Scheme of an interfacial layer with a control volume ε to mechanical balance

The force balance on this element reads:

$$\int_V \rho \frac{Du}{Dt} dV = \int_V \boldsymbol{f} dV + \int_S [\boldsymbol{t}(\boldsymbol{n}) + \hat{\boldsymbol{t}}(\hat{\boldsymbol{n}})] dS + \int_C \gamma s dl \qquad (2.4.5)$$

The term on the left side of the force balance represents the inertial force associated with acceleration of fluid, while on the right side the first term represents the body forces on fluid, Both these terms are referred to volume V, since they are body forces. The second term in the right side of eq. 2.4.5 stands for the superficial forces that the fluid exerts on the upper and lower surfaces of volume V. Finally, the last term is the surface tension acting along the contour C. According to this physical model, when the thickness value is $\epsilon \rightarrow 0$, the body terms go more rapidly to zero and, so, the surface balance becomes:

$$\int_S [\boldsymbol{t}(\boldsymbol{n}) + \hat{\boldsymbol{t}}(\hat{\boldsymbol{n}})] dS + \int_C \gamma s dl = 0 \qquad (2.4.6)$$

From the continuum mechanics, by indicating with $\boldsymbol{n}$ the surface vector and with $\mathbf{T}$ the bulk stress tensor, it is found that:

$$\boldsymbol{t}(\boldsymbol{n}) = \boldsymbol{n} \cdot \mathbf{T} \qquad (2.4.7)$$

The same can be done on the lower surface with a surface vector $\hat{\boldsymbol{n}}$ and a bulk stress tensor $\hat{\mathbf{T}}$ referred to the other material, obtaining:

$$\hat{\boldsymbol{t}}(\hat{\boldsymbol{n}}) = \hat{\boldsymbol{n}} \cdot \hat{\mathbf{T}} = -\boldsymbol{n} \cdot \hat{\mathbf{T}} \qquad (2.4.8)$$

The mathematical manipulation of the balance equation allows reversal of the contour integral into surface integral by Stokes Theorem, giving homogeneity to the equation:

$$\int_C \gamma s dl = \int_S [\nabla \gamma - \gamma \boldsymbol{n}(\nabla \cdot \boldsymbol{n})] dS \qquad (2.4.9)$$

Thus the balance equation assumes the following form:

$$\int_S [\boldsymbol{n} \cdot \mathbf{T} - \boldsymbol{n} \cdot \hat{\mathbf{T}}] dS = \int_S [\gamma \boldsymbol{n}(\nabla \cdot \boldsymbol{n}) - \nabla \gamma] dS \qquad (2.4.10)$$

Since the volume control is arbitrary, as well as the surface, the two integrating terms must be equal, and, therefore, the final form of surface force balance is:

$$\boldsymbol{n} \cdot \mathbf{T} - \boldsymbol{n} \cdot \hat{\mathbf{T}} = \gamma \boldsymbol{n}(\nabla \cdot \boldsymbol{n}) - \nabla \gamma \qquad (2.4.11)$$

It can be noted, however, that the assumption of a unique value of the surface tension, the same the force balance gives to two terms referred to the surface tension: a normal element

and a tangential stress related to the surface tension gradient. By separating normal force and tangential force balances, the normal component is:

$$\boldsymbol{n} \cdot \mathbf{T} \cdot \boldsymbol{n} - \boldsymbol{n} \cdot \widehat{\mathbf{T}} \cdot \boldsymbol{n} = \gamma(\nabla \cdot \boldsymbol{n}) \qquad (2.4.12)$$

and the tangential component is:

$$\boldsymbol{n} \cdot \mathbf{T} \cdot \boldsymbol{t} - \boldsymbol{n} \cdot \widehat{\mathbf{T}} \cdot \boldsymbol{t} = \nabla\gamma \cdot \boldsymbol{t} \qquad (2.4.13)$$

If a free surface such as air-water is considered, the air phase can be assumed dynamically of no significative, and therefore the normal stress balance becomes:

$$\boldsymbol{n} \cdot \mathbf{T} \cdot \boldsymbol{n} = \gamma(\nabla \cdot \boldsymbol{n}) \qquad (2.4.14)$$

and the tangential balance is:

$$\boldsymbol{n} \cdot \mathbf{T} \cdot \boldsymbol{t} = \nabla\gamma \cdot \boldsymbol{t} \qquad (2.4.15)$$

where $\boldsymbol{n}$ and $\boldsymbol{t}$ are respectively, the normal and the tangent unit vector to the surface and $\boldsymbol{T}$ is the bulk stress tensor. It is worth noticing that the tangential stress is balanced by a surface tension gradient.

If the case of fluids in a static configuration is considered, for the bulk it holds:

$$\boldsymbol{T} = -p\boldsymbol{I} \qquad (2.4.16)$$

Thus the stress tensor is isotropic and the forces reduce to pressure forces:

$$\boldsymbol{n} \cdot \mathbf{T} \cdot \boldsymbol{n} - \boldsymbol{n} \cdot \widehat{\mathbf{T}} \cdot \boldsymbol{n} = \hat{p} - p \qquad (2.4.17)$$

And consequently

$$\hat{p} - p = \gamma(\nabla \cdot \boldsymbol{n}) \qquad (2.4.18)$$

Therefore, the pressure gap is balanced by the curvature forces. This is the classic Laplace equation. In this static configuration, as expected, the tangential stresses are absents:

$$\boldsymbol{n} \cdot \mathbf{T} \cdot \boldsymbol{t} = \nabla\gamma \cdot \boldsymbol{t} = 0 \qquad (2.4.19)$$

So it can be observed that in an isostatic system (bulk and interface) to obtain a surface tension it is necessary to impart a curvature at interface, and, conversely, if the surface is flat there is no surface tension. Consequently, it should be admitted that if a surface tension gradient is present a system cannot be static. The pressure difference between two fluids across the interface can produce a curvature at interface, but the presence of motion of the fluid will be balanced only by an interfacial tension gradient (Marangoni stresses).

The results described so far are a good starting point for the force balance point of view, and a good upgrading, with respect to actual scientific literature, will be the insertion of a surface tension tensor $\boldsymbol{\Gamma}$, instead of a single scalar. In this way, a complete analysis can be done of the interfacial region overcoming the superficial isostaticity.

If the surface tension stress tensor $\boldsymbol{\Gamma}$ is inserted in the force balance, it is found:

$$n \cdot \mathbf{T} - n \cdot \widehat{\mathbf{T}} = \mathbf{\Gamma} \cdot n (\nabla \cdot n) - \nabla \cdot \mathbf{\Gamma} \qquad (2.4.20)$$

The components with respect to a reference frame (*n, s, m*) become:

$$n \cdot \mathbf{T} \cdot n - n \cdot \widehat{\mathbf{T}} \cdot n = n \cdot \mathbf{\Gamma} \cdot n (\nabla \cdot n) - n \cdot \nabla \cdot \mathbf{\Gamma} \qquad (2.4.21)$$

$$n \cdot \mathbf{T} \cdot s - n \cdot \widehat{\mathbf{T}} \cdot s = -s \cdot \nabla \cdot \mathbf{\Gamma} \qquad (2.4.22)$$

$$n \cdot \mathbf{T} \cdot m - n \cdot \widehat{\mathbf{T}} \cdot m = -m \cdot \nabla \cdot \mathbf{\Gamma} \qquad (2.4.23)$$

In conclusion, to solve any deformation problem it is needed to know the state equations for the two bulks and that for the separation surface.

2.5 Rheological approach

To know the mechanical behavior of the interface, interfacial rheology has been widely studied with the aim to find a correlation between interfacial stress and deformation. As already stated, the interfacial behavior is important for both texture and stability of foams and emulsions, which are systems characterized by the presence of several interfacial areas (Murray 2002; Bos and van Vliet, 2001). While the most apparent outcome of surfactant adsorption is the reduction of interfacial tension, the response to deformation of a surfactant covering the interface, is more relevant for understanding emulsion/foam functional properties than the equilibrium behavior (Murray 2002; Bos and van Vliet, 2001), because it allows a specific constitutive equation for the interface to be built.

Interfacial rheology is usually subdivided according to the kinematics of the deformation: shear or dilatational. The first one involves shearing deformations of an interfacial area element while its area is maintained constant; on the contrary, dilational rheology describes the mechanical response to changes in size of an interfacial area element while retaining its shape (McClements D.J., 2016; Bos and van Vliet, 2001; Erni P., 2011). In the following Figure 2.5.1. is shown a scheme of these two deformation fields:
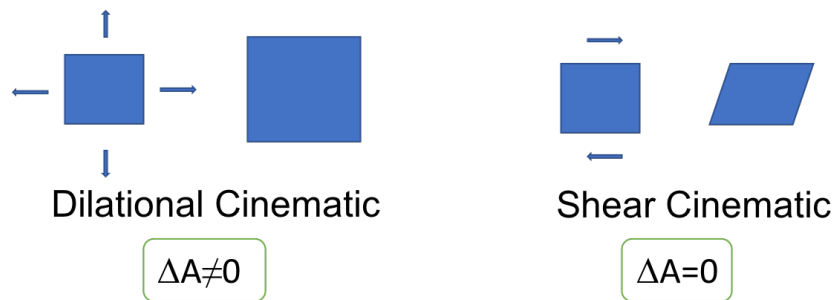

Figure 2.5.1. Example of a two-dimensional dilational and shear deformation of an interface

Shear involves perturbing a 2-dimensional interface in any direction parallel to the interfacial plane. On the contrary, in dilatational rheology, the interfacial area changes while the

interfacial tension, γ, is measured. Let us recall that γ is the surface stress tensor component that tends to react to any increase in the area (Bos and van Vliet, 2001). It is well accepted that, while shear viscosity can contribute appreciably to the long-term stability of dispersions, dilatational rheological properties play an important role in short-term stability. Practically, in many applications, such as emulsion and foam stability study, both deformation modes are expected to be important and, if the interfacial shear rheology has been dominated strongly by the continuum mechanics approach, the interfacial dilatational rheology often follows the thermodynamic/physical chemistry approach (Erni P., 2011). Although measurement techniques tend to isolate effects by studying them separately.

From a rheological point of view, an interface can be treated as a separate phase, with its own rheological properties, viscous and elastic, well distinguished from those characteristics of continuous phases. In the rheological interfacial literature the interface is a planar surface on which the surface tension is often written as a 2D tensor. Even if questionable from the thermodynamic point of view, following this approach (Krotov et al. 2009) the surface tensor assumes this form:

$$\boldsymbol{\gamma} = \left\| \begin{matrix} \gamma_{xx} & \gamma_{xy} \\ \gamma_{yx} & \gamma_{yy} \end{matrix} \right\| \equiv \left\| \begin{matrix} \gamma_{11} & \gamma_{12} \\ \gamma_{21} & \gamma_{22} \end{matrix} \right\| \quad (2.5.1)$$

where the component γ_{xy} determines the forces in the x direction per unit length of the contact line perpendicular to the y direction. Only three of these values are independent, because the matrix must be symmetric, therefore γ_{xy} is equal to γ_{yx}.

In the field of small perturbations the superposition principle can be applied, therefore, the 2D tensor $\hat{\gamma}$ can be represented as the sum of the non-perturbed ($\gamma_0 \cdot \hat{\mathbf{1}}$) and a perturbed contribution ($\boldsymbol{\Delta\hat{\gamma}}$) (Krotov et al. 2009):

$$\gamma_0 \cdot \hat{\mathbf{1}} = \left\| \begin{matrix} \gamma_0 & 0 \\ 0 & \gamma_0 \end{matrix} \right\| \equiv \gamma_0 \cdot \left\| \begin{matrix} 1 & 0 \\ 0 & 1 \end{matrix} \right\| \quad (2.5.2)$$

$$\boldsymbol{\Delta\hat{\gamma}} = \left\| \begin{matrix} \gamma_{11} - \gamma_0 & \gamma_{12} \\ \gamma_{21} & \gamma_{22} - \gamma_0 \end{matrix} \right\| \quad (2.5.3)$$

Moreover, $\Delta\hat{\gamma}$ can be decomposed in an isotropic part $\Delta\hat{\gamma}_i$ and a deviatoric part $\Delta\hat{\gamma}_d$, corresponding to the non-isotropic residual of the tensor $\Delta\hat{\gamma}$. The following expression is found:

$$\Delta\hat{\gamma} = \Delta\hat{\gamma}_i + \Delta\hat{\gamma}_d \quad (2.5.4)$$

$$\Delta\hat{\gamma}_i = \left\| \begin{matrix} (\Delta\hat{\gamma}_{xx} + \Delta\hat{\gamma}_{yy})/2 & 0 \\ 0 & (\Delta\hat{\gamma}_{xx} + \Delta\hat{\gamma}_{yy})/2 \end{matrix} \right\| \quad (2.5.5)$$

$$\Delta\hat{\gamma}_d = \left\| \begin{matrix} (\Delta\hat{\gamma}_{xx} - \Delta\hat{\gamma}_{yy})/2 & \gamma_{xy} \\ \gamma_{yx} & (\Delta\hat{\gamma}_{yy} - \Delta\hat{\gamma}_{xx})/2 \end{matrix} \right\| \quad (2.5.6)$$

$$\Delta\hat{\gamma} = \left\|\begin{matrix} (\Delta\hat{\gamma}_{xx} + \Delta\hat{\gamma}_{yy})/2 & 0 \\ 0 & (\Delta\hat{\gamma}_{xx} + \Delta\hat{\gamma}_{yy})/2 \end{matrix}\right\| + \left\|\begin{matrix} (\Delta\hat{\gamma}_{xx} - \Delta\hat{\gamma}_{yy})/2 & \gamma_{xy} \\ \gamma_{yx} & (\Delta\hat{\gamma}_{yy} - \Delta\hat{\gamma}_{xx})/2 \end{matrix}\right\| \quad (2.5.7)$$

In a similar way the deformation tensor $\hat{e}$ may be decomposed into two contributions, isotropic $\hat{e}_i$ and deviatoric $\hat{e}_d$. The displacement vector $u(x_1, x_2)$ can be defined as:

$$\hat{e} = \hat{e}_i + \hat{e}_d \quad (2.5.8)$$

$$\hat{e}_i = \left\|\begin{matrix} \left(\frac{\partial u_x}{\partial x} + \frac{\partial u_y}{\partial y}\right)/2 & 0 \\ 0 & \left(\frac{\partial u_x}{\partial x} + \frac{\partial u_y}{\partial y}\right)/2 \end{matrix}\right\| \quad (2.5.9)$$

$$\hat{e}_d = \left\|\begin{matrix} \left(\frac{\partial u_x}{\partial x} - \frac{\partial u_y}{\partial y}\right)/2 & \left(\frac{\partial u_x}{\partial y} + \frac{\partial u_y}{\partial x}\right)/2 \\ \left(\frac{\partial u_x}{\partial y} + \frac{\partial u_y}{\partial x}\right)/2 & \left(\frac{\partial u_y}{\partial y} - \frac{\partial u_x}{\partial x}\right)/2 \end{matrix}\right\| \quad (2.5.10)$$

If they are considered purely elastic interfaces, the correlation between stress and deformation is linear and the proportionality coefficient is the specific elastic modulus:

$$\Delta\hat{\gamma}_i = k_i\hat{e}_i \quad (2.5.11)$$

$$\Delta\hat{\gamma}_d = k_d\hat{e}_d \quad (2.5.12)$$

Thus, k_i and k_d are two elastic constants referred to a two-dimensional continuum, under small perturbations deformation field, which can be correlated to the surface properties.

By considering a small square element of the interfacial layer, where the surfactant is located to form a sort of monolayer, if the side of the square is indicated with L, the isotropic deformation is ΔL. This implies that the square area is $A = L^2$ and varies as $\Delta A = 2L\Delta L$, thus the isotropic deformation is $\Delta L/L = \Delta A/2A$.

Then, the deformation tensor becomes:

$$\hat{e} = \hat{e}_i = \left\|\begin{matrix} \Delta A/2A & 0 \\ 0 & \Delta A/2A \end{matrix}\right\| = \frac{\Delta A}{2A} \cdot \hat{1} \quad (2.5.13)$$

and consequently:

$$\Delta\hat{\gamma} = \Delta\hat{\gamma}_i = \left\|\begin{matrix} \Delta\gamma & 0 \\ 0 & \Delta\gamma \end{matrix}\right\| = \Delta\gamma \cdot \hat{1} \quad (2.5.14)$$

By substituting eq.2.5.11 and taking into account eq.2.5.13, it is found:

$$\Delta\hat{\gamma} = k_i\frac{\Delta A}{2A} \quad (2.5.15)$$

Because the modulus is defined in terms of engineering deformation:

$$E \equiv \frac{\Delta\gamma}{\Delta A/A} \quad (2.5.16)$$

Thus for a pure isotropic deformation it holds:

$$k_i = 2E \quad (2.5.17)$$

When considering a pure shear deformation of a surface monolayer, the deformation and the stress tensor are:

$$\hat{e} = \hat{e}_d = \left\| \begin{matrix} 0 & \frac{\partial u_x}{2\partial y} \\ \frac{\partial u_x}{2\partial y} & 0 \end{matrix} \right\| = \frac{\partial u_x}{2\partial y} \cdot \left\| \begin{matrix} 0 & 1 \\ 1 & 0 \end{matrix} \right\| \tag{2.5.18}$$

$$\Delta\hat{\gamma} = \Delta\hat{\gamma}_d = \left\| \begin{matrix} 0 & \Delta\gamma_{xy} \\ \Delta\gamma_{yx} & 0 \end{matrix} \right\| = \Delta\gamma_{xy} \cdot \left\| \begin{matrix} 0 & 1 \\ 1 & 0 \end{matrix} \right\| \tag{2.5.19}$$

Owing to the symmetry of the stress tensor it holds $\Delta\gamma_{xy} = \Delta\gamma_{yx}$, and therefore it is possible to relate the stress tension variation to its shear deformation:

$$\Delta\gamma_{xy} = \frac{k_d \partial u_x}{2\partial y} = G\frac{\partial u_x}{\partial y} \tag{2.5.20}$$

From eq.2.5.12 it is found:

$$k_d = 2G \tag{2.5.21}$$

where G is the shear stress modulus.

Finally, for a surface showing a purely elastic Hookian mechanical behavior, the rheological constitutive equation for isotropic and deviatoric tensions, become:

$$\Delta\hat{\gamma}_i = 2E\hat{e}_i \tag{2.5.22}$$

$$\Delta\hat{\gamma}_d = 2G\hat{e}_d \tag{2.5.23}$$

We can now turn to the tensorial formulation of rheological equations for a two-dimensional purely viscous liquid, in which the stress depends on the deformation velocities. In this case, it is necessary to consider the velocities v_x and v_y and define the two-dimensional deformation velocity tensor:

$$\hat{\dot{e}} = \left\| \begin{matrix} \frac{\partial v_x}{\partial x} & \left(\frac{\partial v_x}{\partial y} + \frac{\partial v_y}{\partial x}\right)/2 \\ \left(\frac{\partial v_x}{\partial y} + \frac{\partial v_y}{\partial x}\right)/2 & \frac{\partial v_y}{\partial y} \end{matrix} \right\| \tag{2.5.24}$$

that can be split again into isotropic and deviatoric components:

$$\hat{\dot{e}} = \hat{\dot{e}}_i + \hat{\dot{e}}_d \tag{2.5.25}$$

$$\hat{\dot{e}}_i = \left\| \begin{matrix} \left(\frac{\partial v_x}{\partial x} + \frac{\partial v_y}{\partial y}\right)/2 & 0 \\ 0 & \left(\frac{\partial v_x}{\partial x} + \frac{\partial v_y}{\partial y}\right)/2 \end{matrix} \right\| \tag{2.5.26}$$

$$\hat{\dot{e}}_d = \left\| \begin{matrix} \left(\frac{\partial v_x}{\partial x} - \frac{\partial v_y}{\partial y}\right)/2 & \left(\frac{\partial v_x}{\partial y} + \frac{\partial v_y}{\partial x}\right)/2 \\ \left(\frac{\partial v_x}{\partial y} + \frac{\partial v_y}{\partial x}\right)/2 & -\left(\frac{\partial v_x}{\partial x} - \frac{\partial v_y}{\partial y}\right)/2 \end{matrix} \right\| \tag{2.5.27}$$

Following the above same procedure used for the purely elastic case, if an interface with a purely Newtonian viscous behavior is considered, it holds:

$$\Delta\hat{\gamma}_i = m_i\hat{\dot{e}}_i \tag{2.5.28}$$

$$\Delta\hat{\gamma}_d = m_d \hat{e}_d \tag{2.5.29}$$

where m_i and m_d are material constants that can be correlated to physical parameters, namely, shear and dilatational viscosity (η and η_d respectively), called also, respectively, the first and the second viscosity.

The shear (first) viscosity is:

$$\eta = \Delta\gamma_{xy} / \frac{\partial v_x}{\partial y} \tag{2.5.30}$$

and the dilatational (second) viscosity is:

$$\eta_d = \Delta\gamma / \frac{\dot{A}}{A} \tag{2.5.31}$$

If a pure dilatation is considered, it may be assumed:

$$\frac{\partial v_x}{\partial y} = \frac{\partial v_y}{\partial x} = 0 \tag{2.5.32}$$

$$\frac{\partial v_x}{\partial x} = \frac{\partial v_y}{\partial y} = \frac{\dot{L}}{L} = \frac{\dot{A}}{A} \tag{2.5.33}$$

Thus, in this case, the rate of deformation has only the isotropic component not zero:

$$\hat{e} = \hat{e}_i = \left\|\begin{matrix} \frac{\partial v_x}{\partial x} & 0 \\ 0 & \frac{\partial v_y}{\partial y} \end{matrix}\right\| = \left\|\begin{matrix} \frac{\dot{A}}{2A} & 0 \\ 0 & \frac{\dot{A}}{2A} \end{matrix}\right\| = \frac{\dot{A}}{2A}\hat{\mathbf{1}} \tag{2.5.34}$$

Consequently, it holds:

$$m_i = 2\eta_d \tag{2.5.35}$$

In the case of a pure shear deformation, the deformation rate becomes:

$$\hat{e} = \hat{e}_d = \left\|\begin{matrix} 0 & \frac{1}{2}\frac{\partial v_x}{\partial y} \\ \frac{1}{2}\frac{\partial v_x}{\partial y} & 0 \end{matrix}\right\| = \frac{1}{2}\frac{\partial v_x}{\partial y}\left\|\begin{matrix} 0 & 1 \\ 1 & 0 \end{matrix}\right\| \tag{2.5.36}$$

and it holds

$$m_d = 2\eta \tag{2.5.37}$$

Finally, if these results are coupled, in the case of a purely viscous interface, it is possible to write:

$$\Delta\hat{\gamma}_i = m_i \hat{e}_i = 2\eta_d \hat{e}_i \tag{2.5.38}$$

$$\Delta\hat{\gamma}_d = m_d \hat{e}_d = 2\eta \hat{e}_d \tag{2.5.39}$$

In general, an interface may show both contributions, elastic and viscous. In the small perturbation regime, superposition principle of effects may be applied and the two deformations may be added. Taking into account eqs.2.5.22 and 2.5.38, and eqs. 2.5.23 and 2.5.39, it is found:

$$\Delta\hat{\gamma}_i = 2E\hat{e}_i + 2\eta_d \hat{e}_i \tag{2.5.40}$$

$$\Delta\hat{\gamma}_d = 2G\hat{e}_d + 2\eta \hat{e}_d \tag{2.5.41}$$

These equations are a mathematical representation of the viscoelastic Kelvin-Voigt model, which assumes that the mechanical behavior of a body is the combination of a purely viscous dashpot and a purely elastic spring, connected in a parallel fashion, (fig.2.5.2):
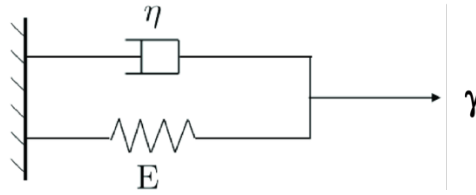
Figure 2.5.2. Schematic representation of Kelvin-Voigt model

To obtain the deformation from the imposed stress, it is possible to start from isotropic and deviatoric tensors, by integration over the actual time t:

$$\hat{e}_i = \frac{1}{2\eta_d} \int_0^t \Delta\hat{\gamma}_i dt \qquad (2.5.42)$$

$$\hat{e}_d = \frac{1}{2\eta} \int_0^t \Delta\hat{\gamma}_d dt \qquad (2.5.43)$$

By adding the elastic contribution, it is obtained:

$$\hat{e}_i = \frac{\Delta\hat{\gamma}_i}{2E} + \frac{1}{2\eta_d} \int_0^t \Delta\hat{\gamma}_i dt \qquad (2.5.44)$$

$$\hat{e}_d = \frac{\Delta\hat{\gamma}_d}{2G} + \frac{1}{2\eta} \int_0^t \Delta\hat{\gamma}_d dt \qquad (2.5.45)$$

By differentiating respect to time, a differential form of the viscoelasticity may be found:

$$\Delta\dot{\hat{\gamma}}_i + \left(\frac{E}{\eta_d}\right) \Delta\hat{\gamma}_i = 2E\dot{\hat{e}}_i \qquad (2.5.46)$$

$$\Delta\dot{\hat{\gamma}}_d + \left(\frac{G}{\eta}\right) \Delta\hat{\gamma}_d = 2G\dot{\hat{e}}_d \qquad (2.5.47)$$

These are the interfacial rheological Maxwell model, which interprets the mechanical behavior of the interface as a dashpot and elastic element combined as a series (fig. 2.5.3):
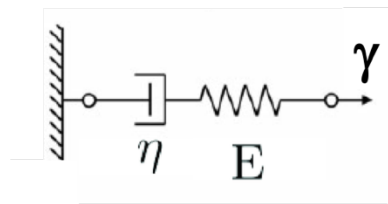
Figure 2.5.3 Schematic representation of Maxwell model

Starting from the same initial expressions for the isotropic and deviation tensors, which characterize the elastic and viscous properties of the continuum, different constitutive equations can be developed for several rheological properties.

In the case of an oscillatory dilatational kinematics, a oscillatory strain is imposed:

$$e = e_0 sin(\omega t) \qquad (2.5.48)$$

$$\gamma = \gamma_0 sin(\omega t + \delta) = \gamma_0 \left(E^{'} sin\omega t + E^{''}(\omega)cos\omega t \right) \qquad (2.5.49)$$

it is found that for an interface whose behavior is described by a Maxwell model:

$$E'(\omega) = E_0 \frac{\omega^2 \tau^2}{1+\omega^2 \tau^2} \qquad (2.5.50)$$

$$E''(\omega) = E_0 \frac{\omega \tau}{1+\omega^2 \tau^2} \qquad (2.5.51)$$

$$E^*(\omega) = E_0 \left(\frac{\omega^2 \tau^2}{1+\omega^2 \tau^2} + i \frac{\omega \tau}{1+\omega^2 \tau^2} \right) \qquad (2.5.52)$$

A constitutive model, developed only for Newtonian interface that is widely used, is the Boussinesq-Scriven model that describes the surface stress tensor $\boldsymbol{T}^s$ as a linear function of the surface rate of deformation tensor $\boldsymbol{D}^s$ (Lopez and Hirsa 1998):

$$\boldsymbol{T}^s = \gamma \boldsymbol{I}_s + \boldsymbol{S}^s = (\gamma + (\kappa^s - \mu^s)\nabla_s \boldsymbol{u})\boldsymbol{I}_s + 2\mu^s \boldsymbol{D}^s \qquad (2.5.53)$$

where κ^s is the surface dilational viscosity, μ^s is the surface shear viscosity, γ is the surface tension considered as a scalar quantity, $\boldsymbol{u}$ is the surface velocity vector, and ,finally, $\boldsymbol{S}^s$ is the excess contribution. The viscous contribution to the surface stress tensor can be described as a linear function of the surface rate of deformation tensor:

$$2\boldsymbol{D}^s = \nabla_s \boldsymbol{u} \cdot \boldsymbol{I}_s + \boldsymbol{I}_s \cdot (\nabla_s \boldsymbol{u})^T \qquad (2.5.54)$$

It is worth noting that the surface viscosities, κ^s and μ^s, are assumed to be independent of the deformation rate in the Boussinesq-Scriven constitutive law.

Finally, all these above-described models, are valid only for systems that can be linearized around an equilibrium state and where only the first order effect of the surface viscosities have to be accounted for.

2.6 The novel quasi-properties approach

The complex rheological behavior of food materials, as well as that of many others materials, often is interpreted by power-law models either during transient measurement (shear flow, creep or relaxation) and at dynamic equilibrium (oscillatory measurements). In fact, structured materials and their combination show a linear behavior in a log-log diagram. This holds not only when concerning with the bulk properties, but, also, when analyzing superficial ones. To interpret the experimental data, the power law models can be put in the form of either the Maxwell or Kelvin-Voight models, using different combination of elasticity and viscosity properties, in particular, to characterize the interfacial properties. But, they are based on the axiomatic assumption that elastic and viscous effects are separate and can be summed.

There is the possibility of approaching the problem from another point of view, consisting in assuming that the mechanical effect of the interface can be interpreted through an unusual model, based on the fractional derivatives. The pioneer of this method was Scott-Blair who introduced the theory of "quasi-properties" to study and understand the "physical rheology of complex materials", focusing his attention on the bulk properties (Rogosin and Mainardi, 2015). On the basis of the equation of Nutting, who considered the power-law model to interpret the materials "anomalous" behavior, and recalling some results obtained by some other authors, as Germant, in the first half of the last century, Scott-Blair proposed the introduction of the fractional calculus to interpret the rheological behavior of complex materials (Rogosin and Mainardi, 2015). He was forced to do that when studying foods, because he noticed that, the firmness, an organoleptic property noticed by consumers, is judged neither by deformation, nor by rate of deformation, nor by any mixture of these two parameters. The aim of Scott-Blair was to determine the firmness of various materials, thinking that the firmness is not a simple addition of viscous and elastic contributes, but something in between these two (Rogosin and Mainardi 2015; Jaishankar and McKinley, 2013; Valerio, Machado and Kiryakova 2014; Faber, Jaishankar and McKinley 2017a; Wagner et al. 2017). This suggests that it should be some intermediate entity, namely a fractional derivative $\frac{d^{\alpha}\gamma(t)}{dt^{\alpha}}$, that corresponds to say that the firmness can have elastic and viscous contribute (Rogosin and Mainardi 2015; Jaishankar and McKinley, 2014). The simplest constitutive equation in fractional derivative, based on the Caputo derivative, is:

$$\sigma(t) = \mathbb{V}\frac{d^{\alpha}\gamma(t)}{dt^{\alpha}} \tag{2.6.1}$$

where α, a numeric parameter that should be a rational number, ranges between *0* and *1*, and its numerical value indicates the mechanical behavior of the materials changing from solid ($\alpha=0$) and liquid ($\alpha=1$). $\mathbb{V}$ is defined quasi-property, not being neither an elastic modulus nor a viscosity, and its measure units are *Pa·s$^{\alpha}$*, corresponding to the solid modulus in the case of $\alpha=0$, or to the viscous modulus in the case of $\alpha=1$. The mechanical meaning of $\mathbb{V}$, in general, can be seen as an indicator of the stiffness of the system (Wagner et al. 2017). The model of the Scott-Blair element, also called the spring-pot element (Jaishankar and McKinley 2013; Rogosin and Mainardi 2015; Faber et al. 2017a), is a compact way to describe the firmness of a material, compensating, in such a way, for the gap between classic spring and a dashpot elements. This model was applied to bulk properties, but recently there has been trend to apply it also to interfaces (Jaishankar and McKinley, 2013). It was found that fractional stress–strain relationships is a good approach for viscoelastic interfaces and

is a simple constitutive model that can be used to describe, quantitatively, the power-law rheological behavior exhibited by those interfaces. The spring-pot element has only two material parameters and can be used to build more complex models. In the Figure is shown a representation of the spring-pot element as a state between the two extreme cases, on the left the purely viscous and on the right the purely solid:

$$\sigma_{dashpot} = \eta \dot{\gamma} \qquad \sigma_{spring-pot} = \frac{\mathbb{V} d^{\alpha} \gamma}{dt^{\alpha}} \qquad \sigma_{spring} = G\gamma$$
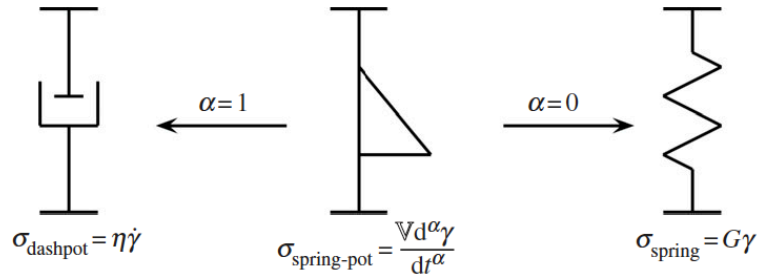
Figure 2.6.1. Schematic of a spring-pot as an element that interpolates between a spring (α =0) and a dashpot (α =1) (Jaishankar and McKinley 2013).

On this basis, other models have been built combining several Scott Blair elements, for instance according to a Maxwell fashion scheme, it is possible to build a model called fractional Maxwell model (FMM), characterized by two spring-pot element (fig.2.6.2):
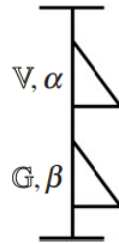
Figure 7. Schematic of a Fractional Maxwell model (FMM) (Jaishankar and McKinley 2013)

The equation of FMM is straightforward to obtain and reads:

$$\sigma(t) + \frac{\mathbb{V}}{\mathbb{G}} \frac{d^{\alpha-\beta}\sigma(t)}{dt^{\alpha-\beta}} = \mathbb{V}\frac{d^{\alpha}\gamma(t)}{dt^{\alpha}} \qquad (2.6.2)$$

When $\alpha > \beta$, the term $(\mathbb{V}/\mathbb{G})^{1/(\alpha-\beta)}$ represents the relaxation time of the fractional model. Referring to Fig.2.6.2, the SB element with parameters $\mathbb{G}$ and β represents the mechanical spectrum of reversible viscoelastic processes of the material, while the SB element with parameters $\mathbb{V}$ and α should take into account, empirically, any additional irreversible plastic part. It is worthy to note that the arranging of the elements in series corresponds to sum the elastic and plastic strains, and this allows every physical process to be modelled (Faber, Jaishankar and McKinley, 2017b).

This approach may be extended to interfacial behavior, thus it is possible to define the surface quasi-property $\mathbb{V}_s$ and $\mathbb{G}_s$, having units of (Pa·m·s$^{\alpha}$) and (Pa·m·s$^{\beta}$). The interfacial constitutive equation in fractional terms can be written as eq. 2.6.2.

The fractional constitutive models with the concept of material quasi-properties, enables the quantitative description of complex time-dependent interfacial phenomena (Jaishankar and McKinley, 2013). It has been shown that this model is consistent with the principles of thermodynamics (Jaishankar and McKinley, 2013). When subjecting the material to a dynamic test, by the Fourier transform, the elastic and loss moduli G', G'' and G* for the SB element are:

$$G^*_s(\omega) = \mathbb{G}(i\omega)^\alpha \tag{2.6.3}$$

$$G'_s(\omega) = \mathbb{G}\omega^\alpha cos(\pi\alpha/2) \tag{2.6.4}$$

$$G''_s(\omega) = \mathbb{G}\omega^\alpha sin(\pi\alpha/2) \tag{2.6.5}$$

Analogously for the FMM, the complex, the storage and the loss moduli assume the following form as a function of the applied oscillation frequency (Jaishankar and McKinley, 2013; Jaishankar and McKinley, 2014):

$$G^*_s(\omega) = \frac{\mathbb{V}_s(i\omega)^\alpha \cdot \mathbb{G}_s(i\omega)^\beta}{\mathbb{G}_s(i\omega)^\alpha + \mathbb{V}_s(i\omega)^\beta} \tag{2.6.6}$$

$$G'_s(\omega) = \frac{\left(\mathbb{G}_s\omega^\beta\right)^2 \mathbb{V}_s\omega^\alpha \cos(\pi\alpha/2) + (\mathbb{V}_s\omega^\alpha)^2 \mathbb{G}_s\omega^\beta \cos(\pi\beta/2)}{(\mathbb{V}_s\omega^\alpha)^2 + \left(\mathbb{G}_s\omega^\beta\right)^2 + 2\mathbb{V}_s\omega^\alpha\mathbb{G}_s\omega^\beta \cos(\pi(\alpha-\beta)/2)} \tag{2.6.7}$$

$$G''_s(\omega) = \frac{\left(\mathbb{G}_s\omega^\beta\right)^2 \mathbb{V}_s\omega^\alpha \sin(\pi\alpha/2) + (\mathbb{V}_s\omega^\alpha)^2 \mathbb{G}_s\omega^\beta \sin(\pi\beta/2)}{(\mathbb{V}_s\omega^\alpha)^2 + \left(\mathbb{G}_s\omega^\beta\right)^2 + 2\mathbb{V}_s\omega^\alpha\mathbb{G}_s\omega^\beta \cos(\pi(\alpha-\beta)/2)} \tag{2.6.8}$$

The interface behavior can also be interpreted by arranging two spring-pot elements in parallel obtaining the Fractional Kelvin-Voigt Model (FKVM). While the FMM is good to describe the rheological properties of multiscale materials that exhibit sol-like flow over long timescales, the FKVM seems to be more preferable to describe a gel-like response in the long-time scale (Jaishankar and McKinley, 2014). Both the FMM and the FKVM are characterized by only four parameters (the two power-law exponents) which control the scaling for the transient and frequency response, and the two quasi-properties, which set the intensity of the stresses in these multiscale materials (Jaishankar and McKinley, 2014).

2.7 Technological properties

The introduction of fractional models to interpret interface rheological behavior, but also the results for bulk properties of the materials, can give an important tool to estimate e.g. food consistency linking this attribute to the physical perceptions of a food.

It should be recalled, for instance, that the consistency assessment has no mathematical framework defining it and is linked to the subjectivity of individual assessment.

Recently, it has appeared that, using this approach, it is possible to try to find a relationship between the Scott-Blair analysis and the sensory parameters perceived (Faber et al. 2017a).

Up to now, they have been considered bulk characteristics as firmness F, springiness S, and rubberiness R, which are 'technological properties' rather than true material properties. The evaluation of these parameters is effectuated by pressing (firmness) and depressing (springiness) by hands, so by a strongly subjective method. During the assessment to evaluate these properties, the panelist chooses the method to use as a function of the firmness itself. In rheological terms the firmness, springiness, and rubberiness of food gels can be considered as viscoelastic texture attributes but there is not a unique consensus on a definition of these three parameters (Faber et al. 2017a). The aim of Scott Blair was to give a unique sense to these parameters and, through the fractional calculus, he gives the expression of F, S and R in terms of quasi-properties and power law exponent (Faber et al. 2017a). In linear viscoelastic regime, Scott Blair defined the firmness as the time-dependent parameter characterizing the resistance of the material to creep. It can be expressed by the inverse of the maximum compliance *J(t)* measured at the end of the creep phase, referred to the time of observation (t_f):

$$F \equiv \frac{1}{max\{J(t)\}} = \frac{1}{J(t_f)} \tag{2.7.1}$$

F is expressed in Pa.

Springiness is defined as "the rate at which a deformed material goes back to its undeformed condition after the deforming force has been removed" (Faber et al. 2017a):

$$S \equiv \frac{|J(t_s)-J(t_f)|}{t_s-t_f} = \frac{|J(t_f+\Delta t_s)-J(t_f)|}{\Delta t_s} \tag{2.7.2}$$

S is expressed in [Pa*s]$^{-1}$ and t_s is the time of observation. In this way, the springiness can be evaluated by analyzing the materials after stress removal, also reported as the rate at which the materials springs back (Faber et al. 2017a).

Finally, the rubberiness may be expressed as:

$$R \equiv \frac{|J(t_f)-J(t_r)|}{J(t_f)} = 1 - \frac{J(t_f+\Delta t_r)}{J(t_f)} \tag{2.7.3}$$

R is dimensionless and can be associated with how much a material returns to its initial condition, representing the relative amount of strain recovered. If the material recovers all the strain within t_r, R=1; on the contrary, if the material does not recover anything within t_r, R=0.

These three parameters can be determined from a creep/recovery experiment, as shown in Figure 2.7.3, illustrating the correspondence between characteristic times of each evaluations.
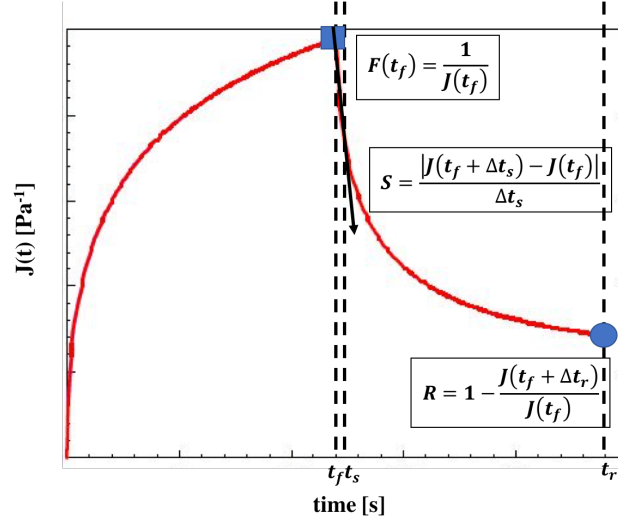
Figure 2.6.3. Creep test with technological parameters determination

The use of the fractional model of Scott Blair, makes it possible to correlate the three parameters to creep/recovery measurements (FSR model). According to the compliance definition, in the simple case of a single spring-pot element, it is obtained:

$$J(t) \equiv \frac{\gamma(t)}{\sigma_0} = \frac{1}{\mathbb{G}} \frac{t^\beta}{\Gamma(1+\beta)} \qquad (2.6.9)$$

Thus the three parameters are found:

$$F(t_f) = \frac{1}{J(t_f)} = \mathbb{G}\Gamma(1+\beta)t_f^{-\beta} \qquad (2.6.10)$$

$$S = \frac{\left|(1+\Delta t_s/t_f)^\beta - (\Delta t_s/t_f)^\beta - 1\right|}{F(t_f)\Delta t_s} \qquad (2.6.11)$$

$$R = 1 - t_f^{-\beta}\left(\left(t_f + \Delta t_r\right)^\beta - \Delta t_r^\beta\right) \qquad (2.6.12)$$

It should be noted that these three parameters are time dependent, *F* and *S* are determined by both fractional parameters, whilst *R* is determined only by the β exponent.

In this way, the technological properties can be correlated to the quasi-properties of the fractional model. It is obvious that the FSR model is very simple, being a single spring-pot model, but it is possible to extend this approach to the FMM model or even more complex combinations of fractional elements (Faber et al. 2017b). In a similar way, it will be auspicious to extend the methodology to interfacial layers finding these parameters, because of their capability to give a direct evaluation of technological parameters of the surfaces.

The relationship between interfacial rheological analysis and the technological parameters is not yet available, but, thanks to a new generation of rheometer, this area of study can be explored, with the aim to create a connection from surface measurements and surface parameters.

Even if not unique, tensiometry and interfacial rheology are two valid techniques to investigate the interfacial properties. Dilatational and shear kinematics are complementary and focus on different aspects of the interfacial layer, and their combination is useful to interpret better the composition, interactions and mechanical behavior of a deformed film. Surface shear rheology is more sensitive to predict the long-term stability to coalescence and disproportion, dilatational rheology plays an important role in the short-term stability to formation of bubbles or droplets (Bos and van Vliet, 2001; Wilde 2000).

2.8 Interfacial rheology and emulsion/foam stability

The term stability, referred to emulsion and foam systems, is mainly used to describe their capability to resist the changes occurring in their properties with time. There are a variety of physico-chemical mechanisms that may be responsible for alterations in the properties of foams and emulsions. The most important instability phenomenon that can occur in a multiphasic systems are illustrated in the following Figure :
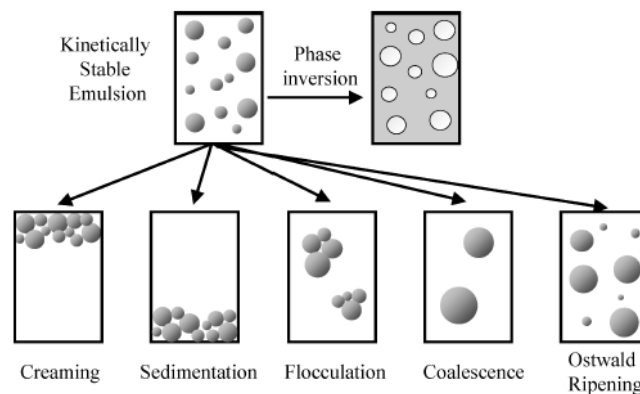
Figure 8 Schematic diagram of most common instability mechanisms that occur in food emulsions (McClements 2007)

Creaming and *sedimentation* are both forms of *gravitational separation.* Creaming describes the upward movement of droplets due to the fact that they have a lower density than the continuous phase, whereas sedimentation describes the downward movement of droplets due to the fact that they could have a higher density than the continuous phase. *Flocculation* and *coalescence* are both types of droplet aggregation. The first occurs when two or more droplets come together to form an aggregate, whereas coalescence is the process where two or more droplets merge to form a single larger droplet. *Phase inversion* is the process whereby a disperse phase becomes a continuous phase and vice versa. Similar mechanisms are responsible for the foam instability (McClements D. J., 2007). It could be thought that there is no direct relationship between interfacial rheological measurements and emulsion and or foam formation capability, but the results obtained by tensiometry and interfacial

rheology have demonstrated that these techniques are valid tools to improve the product design of food systems and not only. It should be remarked that an increase of interfacial properties is not always positively correlated with emulsion/foam stability (Bos and van Vliet 2001). Moreover, there is an interest in how interfacial rheology can affect the bulk viscosity of emulsions. The viscosity of emulsions is highly dependent on the interactions between emulsion droplets, and those interactions could well depend on the rheology of the interface. Despite all these considerations, it is important to emphasize that, so far, there is no reliable theory for the relationship between interfacial rheological properties and stability phenomena, particularly for protein stabilized emulsions and foams. Ideas and hypotheses are mainly based on circumstantial evidence.

2.9 Conclusion

Food systems are classified as "soft matter systems" because they are heterogeneous products with complex matrices. Their formation and control involve a rather wide range of time scale: from the sub-millisecond regime, during the formation of foam bubbles or emulsion drops, up to months or even years, associated with the long-term shelf life of canned food products (Fischer et al. 2009). Many ingredients are used to control the desired textural properties because of their influence on some important characteristics of the final food. Many characteristics of food materials often need the use of very specific measurement techniques, such as squeeze flow, extensional rheometry, interfacial rheometry or rheo-optics. The study of the rheology of food materials is essential for quite a lot of aspects of food science and technology.

Interfacial rheology is an important tool to study the mechanical behaviour of surfaces and interfaces. Although surface/interfacial rheometry has been developed, the understanding and study of interfaces is still underdeveloped and presents inconsistencies between its real nature and the mathematical simplification that actually is used in scientifically analysing it. The bidimensional approach of the stress tensor does not consider and neglects the thickness and, therefore, the volume that is part of the interface. Furthermore, the surface/interfacial tension is always evaluated as an isotropic contribute, instead of a tensor with all component as in the bulk case.

The matching between the development of a theory, that takes into account the complete interfacial tensor, and a constitutive model, which links the surface tensor with several types of deformation, considering, particularly, the time dependency of the interface and all relaxation phenomena, can give rise to a full interpretation and analysis of the

surfaces/interfaces phenomena, proposing also a relationship with texture and technological properties. Furthermore, although both interface rheology and emulsions/foam studies are the subjects of the literature studies, the connections between these fields is less known, although the possibility of establishing a closer link between bulk and interface properties is desirable.

REFERENCES

Bos, M. A. & T. van Vliet (2001) Interfacial rheological properties of adsorbed protein layers and surfactants: a review. *Advances in Colloid and Interface Science,* 91**,** 437-471.

Bush J. W.M., Surface Tension Module, Department of Mathematics, MIT.

Erni, P. (2011) Deformation modes of complex fluid interfaces. *Soft Matter,* 7**,** 7586-7600.

Eastoe J. (2010), Surfactant Aggregation and Adsorption at Interfaces in T. Cosgrove Colloid Science Principle, Methods and Applications. Second Edition Wiley, U.K., chapter 4

Faber, T. J., A. Jaishankar & G. H. McKinley (2017a) Describing the firmness, springiness and rubberiness of food gels using fractional calculus. Part I: Theoretical framework. *Food Hydrocolloids,* 62**,** 311-324.

Faber, T. J., A. Jaishankar & G. H. McKinley (2017b) Describing the firmness, springiness and rubberiness of food gels using fractional calculus. Part II: Measurements on semi-hard cheese. *Food Hydrocolloids,* 62**,** 325-339.

Fischer, P., M. Pollard, P. Erni, I. Marti & S. Padar (2009) Rheological approaches to food systems. *Comptes Rendus Physique,* 10**,** 740-750.

Jaishankar, A. & G. H. McKinley (2013) Power-law rheology in the bulk and at the interface: quasi-properties and fractional constitutive equations. *Proceedings of the Royal Society a-Mathematical Physical and Engineering Sciences,* 469.

Jaishankar, A. & G. H. McKinley (2014) A fractional K-BKZ constitutive formulation for describing the nonlinear rheology of multiscale complex fluids. *Journal of Rheology,* 58**,** 1751-1788.

Krotov V. V., Basics of interfacial rheology, In: R. Miller, L. Liggieri Interfacial Rheology Volume 1 , Brill Academic Pub, Leiden Boston 2009, 1-37

Lal, S. N. D., C. J. O'Connor & L. Eyres (2006) Application of emulsifiers/stabilizers in dairy products of high rheology. *Advances in Colloid and Interface Science,* 123**,** 433-437.

Lopez, J. M. & A. Hirsa (1998) Direct determination of the dependence of the surface shear and dilatational viscosities on the thermodynamic state of the interface: Theoretical foundations. *Journal of Colloid and Interface Science,* 206**,** 231-239.

McClements D.J. (2016), Food emulsion: Principles, Practice and Techniques. Third Edition, CRC Press: Boca Raton, FL., chapter 5

McClements, D. J. (2007) Critical review of techniques and methodologies for characterization of emulsion stability. *Critical Reviews in Food Science and Nutrition,* 47**,** 611-649.

Murray, B. S. (2002) Interfacial rheology of food emulsifiers and proteins. *Current Opinion in Colloid & Interface Science,* 7**,** 426-431.

Rogosin, S. & F. Mainardi (2015) George William Scott Blair - the pioneer of fractional calculus in rheology. *Communications in Applied and Industrial Mathematics,* 6.

Rosen M.J., Surfactants and interfacial phenomena, Fourth Edition, John Wiley & Sons, New Jersey (U.S.A) 2012, 208-238

Valerio, D., J. T. Machado & V. Kiryakova (2014) Some pioneers of the applications of fractional calculus. *Fractional Calculus and Applied Analysis,* 17**,** 552-578.

Wagner, C. E., A. C. Barbati, J. Engmann, A. S. Burbidge & G. H. McKinley (2017) Quantifying the consistency and rheology of liquid foods using fractional calculus. *Food Hydrocolloids,* 69**,** 242-254.

Wilde, P. J. (2000) Interfaces: their role in foam and emulsion behaviour. *Current Opinion in Colloid & Interface Science,* 5**,** 176-181.

Chapter 3

Interfacial tensiometers and rheometers

Abstract

The formation and stabilisation of emulsions and foams are strongly determined by the properties of the interfaces. The study of interfacial rheology plays a key role in understanding the processes and structures present at the interface. The investigation of interface properties can be effectuated by measuring the interfacial tension under interface deformations. The deformations can be purely shear or dilational, giving different information respectively. The response of a film of molecules at an interface to expansion or compression is important to determine the formation and stability of colloidal systems, such as emulsions and foams. Shear analysis, indeed, can give important information about long-term stability. There are different types of interfacial rheometers and, according to suitable uses, they are able to give deformations about the mechanical resistance of the interfaces to the imparted deformation. They are classified according to the method by which the information is obtained and according to the imposed deformation kinematics, they can be subdivided into direct and indirect and into dilation and shear. The aim of this chapter is to give an overview on the interfacial measurement techniques, in particular describing the pendant drop method and the magnetic needle shear rheometer.

3.1. Introduction

There are several methods to measure surface/interfacial tension and they can be direct or indirect. The direct methods can evaluate the interfacial tension by direct measure of the force generating at the interface, the indirect method calculates the interfacial tension by acquisition of the imagine or the displacement under an imposed stress field (Drelich et al. 2002). Direct measurement can be effectuated using a microbalance, a plate, a ring, a rod or other probes brought into contact with the interface. The resistance of the fluid is directly related to the interfacial tension. A microbalance measures the force (F) acting along the three-phase contact line through the weight of the liquid meniscus standing

above the plane of the fluid-fluid interface and translates this into a force. The force is exactly equal to the weight of the liquid meniscus standing above the plane of the fluid-fluid interface. The interfacial tension can be calculated by using the following eq. 3.1.1:

$$\gamma = \frac{F}{p \cos \theta}$$

(3.1.1)

where F is the force, p is the wetted perimeter and θ is the contact angle measured for the liquid meniscus in contact with the object surface. The two principal techniques which use this principle to measure the interface tension are the Wilhelmy plate and the du Nouy ring methods. The Wilhelmy plate technique consists in a vertical plate puts in a fixed position relative to the horizontal surface of the liquid as schematically reported in Figure 3.1.1.
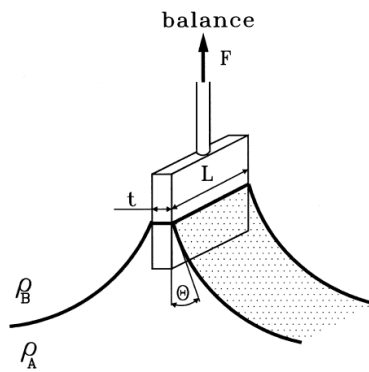
Figure 3.1.1 Schematic function of Wilhelmy plate method (Drelich et al. 2002)

The plate can be of roughened platinum-iridium alloy or platinum, but also glass, mica, or steel. The vertical force (F), imposed by the underlying liquid, acts on the plate from the liquid meniscus and it is measured by using a microbalance (Drelich et al. 2002). The force applied to the plate is equal to the weight of the liquid meniscus uplifted over the horizontal surface and it is possible to calculate the interfacial tension using equation 3.1.1 where p, the perimeter, can be evaluated as $p = 2(L + t)$ in reference to Figure 3.1.1. With the du Nouy ring method, the interfacial tension can be evaluated relating it to the force required to pull a wire ring off the interface. The method is schematically represented in Figure 3.1.2:
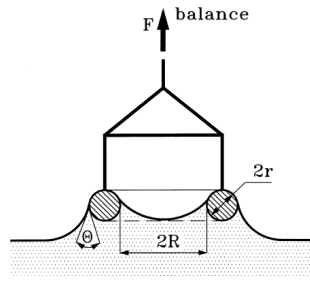
Figure 3.1.2 du Nouy ring scheme (Drelich et al. 2002)

For the du Nouy method, the equation used is:

$$\gamma = \frac{F}{p \cos \theta} f \tag{3.1.2}$$

In equation 3.1.2, there is an additional factor f which is a correction factor to consider an additional volume of liquid that is lifted during the detachment of the ring from the interface. f can vary with the dimension of the ring, with the wettability and with the difference of the fluids density. Furthermore, the perimeter (p) of the three-phase contact line is equal to twice the ring circumference: $p = 4\pi R$. It is always important to verify the perfect wettability of the ring and also that deformation ring phenomena do not occur, these could interfere with the measure (Drelich et al. 2002). The interfacial tension can also evaluated by pressure measure, this is an evident consequence of the pressure difference between the fluids on either side of a curved interface, with the higher pressure on the concave side of the interface. The pressure difference across the interfaces can be evaluated with the Young-Laplace equation as:

$$\Delta P = \gamma \left(\frac{1}{R_1} + \frac{1}{R_2} \right) \tag{3.1.3}$$

where the R_1 and R_2 are the two curvature radii. The more common method that uses this approach to measure the interfacial tension is the maximum bubble pressure method, which consists in measuring the maximum pressure necessary to form a gas bubble into a liquid. The measured pressure will be the sum of two contributions: the capillary pressure caused by the interfacial tension and the hydrostatic pressure imposed by the liquid and which can be written in the following equation 3.1.4:

$$\Delta P = p^* - p_A g h_A \tag{3.1.4}$$

An expression was derived to relate h with the Laplace capillary constant and the bubble meniscus, so the information of height and curvature radii of the bubble can be used to evaluate the interfacial tension. The older methods to determine the interfacial tension are the capillary rise method and drop volume (or weight), reported in Figure 3.1.1.
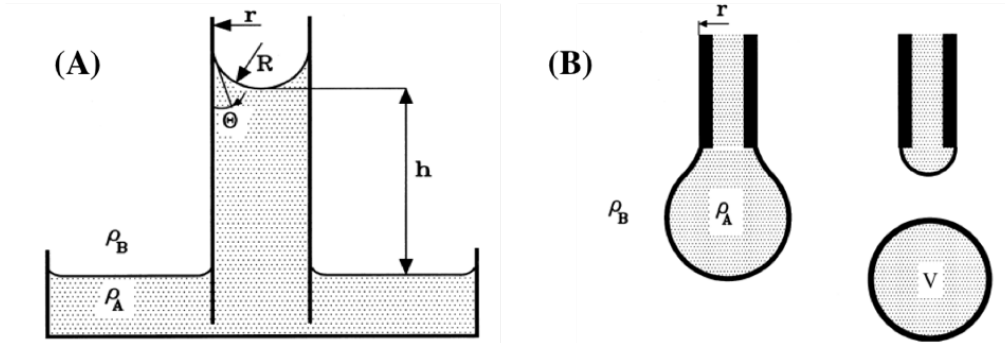
Figure 3.1.1 Scheme of capillarity rice method (A) and drop volume (B)

In the capillary rise method, the height h of the meniscus is measured in a round glass tube having the known inner radius r and for small-diameter tubes (i.e., $r << h$), the shape of the meniscus is spherical and the interfacial tension can be evaluated by the following equation:

$$\gamma = \frac{\Delta\rho g h r}{2\cos\theta} \tag{3.1.5}$$

With the drop volume method it is possible evaluate the weight, W (of volume V), of a falling drop and, consequently, the interfacial tension to weight of falling drop can be correlated:

$$W = V\Delta\rho g = 2\pi r\gamma f \frac{r}{\sqrt[3]{V}} \tag{3.1.6}$$

In the previous equation, r is the radius of the capillary, f is the correction factor required because only a portion of the drop volume is released from the capillary during detachment and it is a function of $\frac{r}{\sqrt[3]{V}}$, through an empirically determined correlation (Drelich et al. 2002).

3.2. The interfacial rheology measurements

From the interfacial tension measurements it is possible to study the rheology of the interfacial layers and to know their mechanical resistance, studying also the correlations between stresses and deformations.

The measurements of interfacial rheology can be effectuated under two different cinematic conditions, dilational and shear (Bos and van Vliet, 2001), as shown in the following picture:
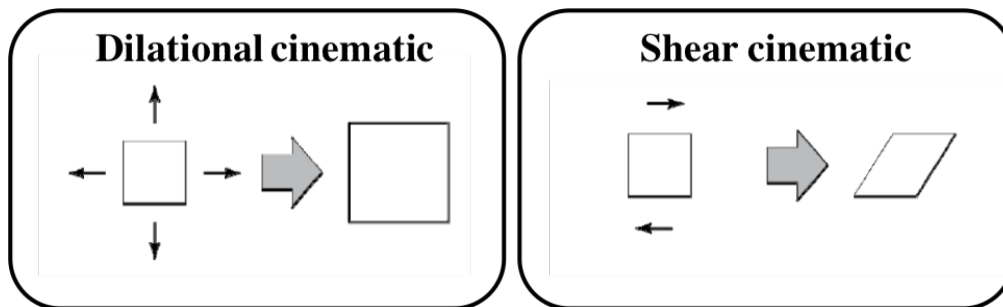
Figure 3.5.1 Dilational and shear cinematics schematization

In dilatational cinematic the interfacial area is increased or decreased giving rise to expansion or compression of the interface, but the form of the area remaining constant. In shear cinematic the interfacial area form is changed, but the area value remains constant (Bos and van Vliet, 2001). The other classification is about the equilibrium condition and the technique of measurements can be differentiated in: close to equilibrium condition or far from equilibrium condition. In both cinematic conditions, close to equilibrium small variations (the area value in dilatational case, the area form in the shear case) are applied and the viscoelastic moduli are returned (E' and E'' in dilatational and G' and G'' in shear). Analogously, far from the equilibrium condition the interfacial area is increased or compressed instantly with an wide amplitude in dilatational, or the wide area form deformation is imposed in shear cinematic. These methods allow the evaluation of the viscosity in shear and dilatational deformation. The shear viscosity has received greater attention than the dilatational case (Bos and van Vliet, 2001). In general, interfacial dilation rheology gives information about a short time stability of foams and emulsions; interfacial shear rheology gives information about the long-term stability. Both types of deformation in reality are present in the dispersion mechanism.

3.2.1   *Interfacial dilatational rheology*

Dilatational rheology involves the variation of the interfacial area with the expansion and compression, during which the interfacial tension is recorded. There are many methods and instruments to evaluate the dilation rheological properties of interfacial layers.

The classical method used is the Langmuir trough, as shown in Figure . Normally, the barriers are used to gradually compress or expand the interface varying the surface concentration. A small modification to this method allows the barriers to be oscillated sinusoidally, producing small changes in the surface area.
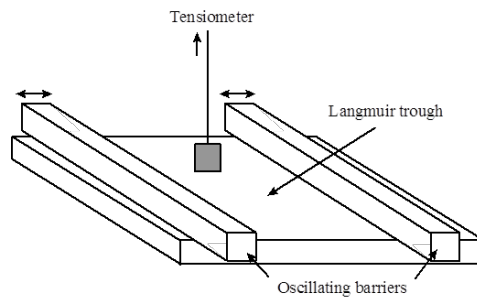
Figure 3.2.1.1 Scheme of a Langmuir trough with oscillating barriers to change the surface area A, whilst simultaneously monitoring surface tension.

Assuming no exchange of surfactants between the surface and the bulk during the compression/expansion cycle, there will be a change in the surface tension. Compressing the interface, the surface surfactant concentration increases and, consequently, the interfacial tension decreases. Conversely, expanding the surface, the surface tension increases. The relationship between surface area and surface tension is shown in the following Figure 3.2.1.2.
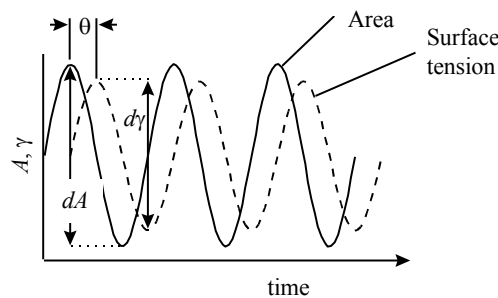
Figure 3.2.1.2 Time dependent relationship between area and surface tension during a typical dilatational rheology experiment

The surface dilatational modulus $|E|$ can be expressed with the following equation:

$$|E| = A\frac{dy}{dA}$$
(3.2.1.1)

$|E|$, the complex dynamic modulus, can be divided in two components, E' and E'', the elastic and the viscous component respectively. If the surface is purely elastic, then the phase angle (θ) will be zero, if it is viscous then θ=90°. In general, the behaviour is usually intermediate between the two extremes, and the two components can be calculated as follows:

$$E' = |E|cos\theta \qquad\qquad (3.2.1.2)$$

$$E'' = |E|sin\theta \qquad\qquad (3.2.1.3)$$

Normally, the experiments should be conducted in the linear region.

Another instrument to evaluate the dilatational rheological properties is a ring trough, shown in the following Figure :
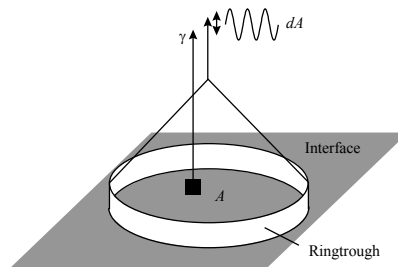
Figure 3.3.1.3 Schematic setup for the Ringtrough method

The instrument setup is widely explained by (Kokelaar, Prins and Degee, 1991). The area *A* is located within a ring, held in the interface. The ring is oscillated up and down through the interface, effectively stretching and compressing the area within the ring. The surface tension is measured to the center of the ring, to ensure the dilatational strain, rather than having a shear component, as in the Langmuir trough setup (Kokelaar et al. 1991).

The pendant drop method is particularly useful in which the interfacial tension is calculated by measuring the size and the shape of a liquid drop suspended from a capillary, in a less dense fluid. Also in this case, the interfacial area is expanded or compressed, but in this case by controlling the liquid flow through the capillary and changing the drop volume thank to an automated pump. This is a very useful technique for looking at a small sample volume, and it avoids the hydrodynamic problems encountered when trying to expand/compress oil/water interfaces. Since the pendant drop technique is more versatile, it can be applied to both liquid–liquid and liquid–air interfaces, it is a technique widely employed for dilatational rheology studies.

3.2.2 *Interfacial shear rheology*

In contrast to the dilatational technique, the surface shear rheology involves shearing deformations of an interfacial area element, retaining its area. For shear rheometry, existing flow geometries and instrument designs have been improved and made more readily available and many of these may be classified as indirect shear rheometer and direct shear rheometers (Erni et al. 2003; Miller et al. 2010). The former provides mechanical information about the interface through image analysis, while the latter permits a direct measurement of the torque or the displacement of a probe located at the interface. The direct surface rheometry is characterized by a drag flow type or a surface pressure driven flow. The best-known viscometers in this category are the canal surface viscometer, the deep-channel surface viscometer, the rotating wall knife-edge surface viscometer and the transient rotating cylinder device. In Figure 3.2.2.1 there is a scheme of a deep-channel surface viscometer.
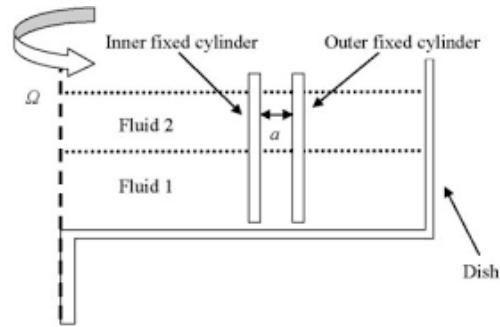
Figure 3.2.2.1 Deep-channel surface viscometer scheme

This rheometer consists of two concentric, stationary vertical cylinders with smooth walls (Miller et al. 2010). This instrument applies a shear deformation by rotating the fluid inside the channel with a known angular velocity, Ω. By using the tracer particles at the fluid interface, the flow and the deformation can easily be monitored by a camera. In this way the surface viscosity can then be calculated using the following correlation (Masschaele et al.):

$$\eta_{surface} = \frac{\eta_{subphase} a}{\pi} \left(\frac{V^*}{V} - 1 \right) \qquad (3.2.2.1)$$

Where a is the channel width, V^* is the reference centerline surface velocity in the absence of a surface film and V the surface velocity in the presence of a monolayer.

The instruments, which realize the direct measure of interfacial rheology, are typically rotating disk geometries, knife-edge, biconical disk rheometer the double gap ring geometry:
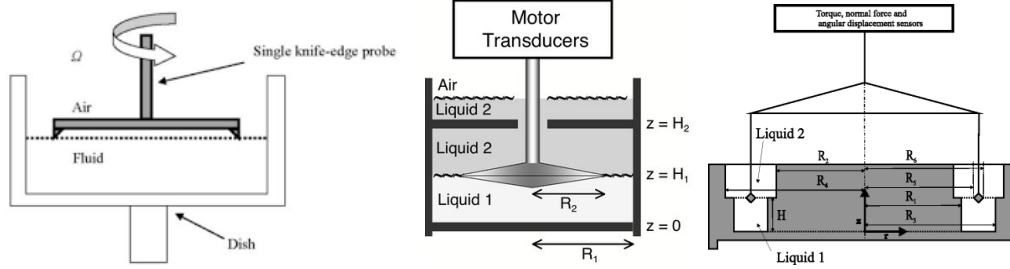
Figure 3.2.2.2 Shear interfacial rheometers

In a class of the direct shear rheometers, the Fuller research group (Reynaert et al. 2008) developed a stress controlled rheometer that uses a needle moving by a magnetic field at the interface, this will be discussed in detail below.

The behaviour of an interface can be influenced or covered by the subphase bulk rheological properties. So, it is important to discriminate whether the measure gives information about the interface in analysis or not. There is a dimensionless number that compares these two contributions, the surface and the subphase bulk effects. The Boussnesq number, Bo, which is the ratio of between the two components of the drag experienced by a rheological probe can be written as a dimensionless group:

$$Bo = \frac{surface\ drag}{subphase\ drag} = \frac{\eta_{surface}}{\eta_{subphase}G} \tag{3.2.2.2}$$

Where $\eta_{surface}$ is the viscosity of the interface, $\eta_{subphase}$ is the viscosity of the subphase bulk and G is a geometrical factor which takes into account the probe perimeter in contact with the interface. If the Bo number is larger than 1, the surface properties are dominant effects; when the Bo number is much smaller than 1, the measured properties are related to the surrounding phases. So, it is important, in surface rheometry, that the measuring system is able to detect the interface properties, also in the presence of these lower and upper fluids. So, to scale the subphase contribution, it is suitable to use small values of G.

For the air water interface, a circular knife-edge geometry is commonly used, as the component from the gas phase can be neglected, and the knife edge does not penetrate into the aqueous phase, thus maximising the response from the interface itself. For fluid interfaces such as the oil-water interface, a very shallow biconical geometry is often used.

As contact has to be made with both phases, the components from those phases need to be subtracted to reveal the contribution from the interface. The final geometry is a Du Nouy ring, commonly used for measuring interfacial tension, but here it has been specifically designed to measure the surface shear viscoelasticity using the method developed by Sherriff and Warburton. The light construction of this geometry makes it very sensitive to interfaces with very low rheological properties.

In these techniques, an oscillatory motion (strain) is applied and the resultant oscillating stress is measured. The strain should be small enough not to break any structures formed at the interface.
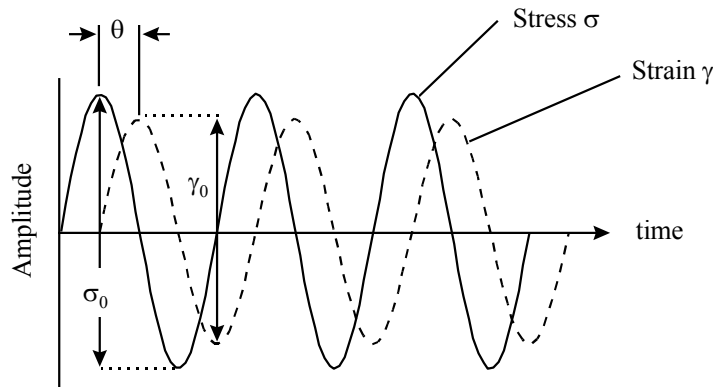
Figure 3.2.2.3 Stress - strain relationship for a typical oscillatory surface shear viscoelasticity measurement.

The total viscoelastic modulus G* is given as:

$$G^* = \frac{\sigma_0}{\gamma_0} \qquad\qquad (3.2.2.3)$$

σ_0 and γ_0 are the amplitudes of the stress and the strain respectively. The stresses and strains are the effective two-dimensional equivalents of the three-dimensional standard viscosity measurements. So the stress here is the applied force per unit distance, and the strain is the distance moved relative to the gap between the geometry and the outer vessel. Similar to the dilatational method, if the phase lag θ is 0 or 90° , then G^* is either totally elastic or viscous respectively. The elastic (G') and viscous (G'') moduli can be calculated as follows:

$$G' = G^* cos\theta \qquad\qquad (3.2.2.4)$$

$$G'' = G^* sin\theta \qquad\qquad (3.2.2.5)$$

3.3 Pendant Drop/Bubble Method

The pendant drop method consists in the evaluation of the surface tension by profile drop analysis in equilibrium mechanical conditions (Ravera, Loglio and Kovalchuk, 2010). Over a century ago, Worthington was the first to propose the evaluation of the interfacial tension from the shape of a pendant liquid drop deformed by gravity. Bashford and Adams, in 1883, defined a first equation to give a numerical solution to the Young-Laplace equation. A typical pendant drop tensiometer is characterized by several parts, schematically reported in the following Figure 3.3.1:
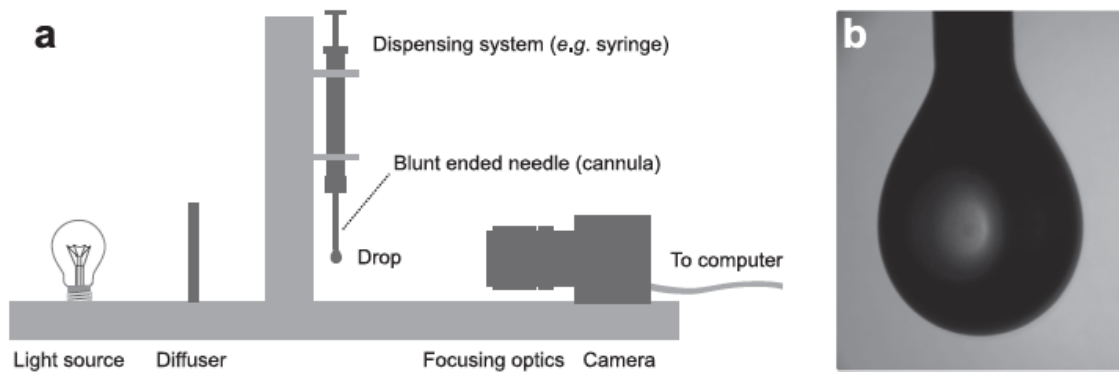
Figure 3.3.1 Pendant drop tensiometer (a) and the drop profile visualization (b) (Berry et al. 2015)

In reference to Figure (a), the apparatus consists of a light source to illumine the cell, a digital camera for images acquisition, which is connected to a computer to analyse the data, a syringe with a needle from which is formed the drop, an automated pump that control the fluid release and the drop formation. The drop is formed in a cuvette in which is present the second phase.

Figure 3.3.2 Syringe cuvette system schematization

The cuvette is important to achieve contact between the two phases, but also to preserve the drop from each environmental disturbance. According to the density differences between the two phases, it is possible to use the configuration of pendant or buoyant drop. When the analysing system is the water/air interface, the cuvette is partially filled of water, so to saturate the system and to decrease the evaporation rate of the drop. The camera continuously captures the image of the drop and calculates the value of the interface tension by means of a numerical fitting procedure. It is more important that there are no optical aberrations around the drop profile, that there are no distortions of the image caused by the lens, that the drop must be axialsymmetric, that the apparatus is on an antivibration table to avoid external disturbances, in particular, external disturbances are less significant at the liquid-liquid interface, because of the protection of the immersion phase, and, finally, that the deformation of the drop from their sphericity is guaranteed (Berry et al. 2015). Indeed, the drop has to be of such dimensions as to ensure a balance between the gravitational, surface and drag forces: if the gravitational contribution is not such as to deform the drop with respect to the sphericity, it happens that the shape factor (Bond number) is close to zero and the measurement is not very accurate (Berry et al. 2015). Furthermore, $Bo \sim R_0^2$, so with the smaller drop, the Bond decreases to very low values that are not suitable to a good instrumental performance. In the following Figure 3.3.3 there is reported a schematic profile of the drop:
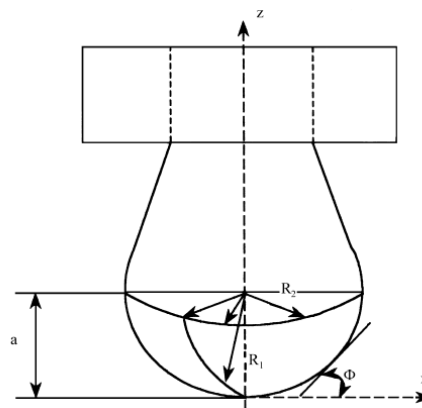
Figure 3.3.3 Pendant drop scheme (Arashiro and Demarquette (1998))

Under mechanical equilibrium condition, the relation between the pressure difference across the interface, the surface tension and the surface curvature is provided by the Laplace equation (Berry et al. 2015, Ravera et al. 2010, Saad and Neumann 2016):

$$\Delta P = \gamma \left(\frac{1}{R_1} + \frac{1}{R_2} \right) \tag{3.3.1}$$

where R_1 and R_2 are the principal radii of curvature; $\Delta P = P_{in} - P_{out}$ is the Laplace pressure across the interface. If there are present no forces other than gravitational, the pressure difference across the interface can be evaluated as the reference ΔP_0 and an hydrostatic pressure contribution, where h is the height of the drop, normally measured from the its apex (Chen 1998; Berry et al. 2015):

$$\Delta P = \Delta P_0 + \Delta \rho g h \tag{3.3.2}$$

So, for a specific γ value, the drop profile is related to the physical properties of the two phases and to the geometric parameters. In this way, from the surface tension it is possible to know the profile of the drop, but vice versa it is difficult because of the difficult calculation. In fact, the integration of the Laplace equation is simple in the cylindrical menisci cases, but owing to the irregular shape it is difficult. For axis-symmetric menisci, the Laplace equation together with the pressure dependence on the drop height, due to the gravity field, lead to a set of three first-order differential equations, the equation of Bashforth–Adams in terms of geometrical parameters of the drop/bubble:

$$\Delta \rho g h = \gamma \left[\frac{d^2 z/dx^2}{[1+(dz/dx)^2]^{3/2}} + \frac{dz/dx}{x[1+(dz/dx)^2]^{1/2}} \right] \tag{3.3.3}$$

This equation does not have an analytical solution, so there are only numerical solutions. Bashforth–Adams were the first to propose a numerical solution, in the form of a nonlinear differential equation:

$$\frac{1}{\frac{R_1}{a}} + \frac{\sin \varphi}{\frac{x}{a}} = -B \frac{z}{a} + 2 \tag{3.3.4}$$

Where a is the curvature radius at drop apex, and R_1 and $\sin \varphi$ are defined as in following:

$$R_1 = \frac{[1+(dz/dx)^2]^{3/2}}{d^2 z/dx^2} \tag{3.3.5}$$

$$\sin \varphi = \frac{dz/dx}{[1+(dz/dx)^2]^{1/2}} \tag{3.3.6}$$

B is the factor form already mentioned above or the Bond number:

$$B = \frac{a^2 g \Delta \rho}{\gamma} \tag{3.3.7}$$

B compares the gravitational force to superficial force, which is the geometrical factor and that corresponds to the Bond number. It is important that $Bo > 0,1$ to have a good measurement accuracy. The Bo determination is the principal step: the fitting of the experimentally measured drop/bubble contour to the theoretical curve gives the *Bo* number and subsequently allows finding the interfacial tension (Ravera et al. 2010; Arashiro and Demarquette, 1998; Chen et al. 1998).

The direct measure of the interfacial tension using a pendant drop system consists of simple steps: 1) capture and digitalization of the image of the pendant drop; 2) extraction of the drop contour, determination of the radius of curvature at the apex necessary for the calculation of interfacial tension; 3) smoothing of the extracted contour of the drop using polynomial regression; 4) shape comparison between the theoretical and experimental drop, inferring the interfacial tension value (Arashiro and Demarquette, 1998). With the pendant drop method several types of measure can be done. By monitoring the static evolution of the drop profile over time, the surface activity of a surfactant species can be evaluated and the typical evolution of the surface tension over time is reported in the following Figure :
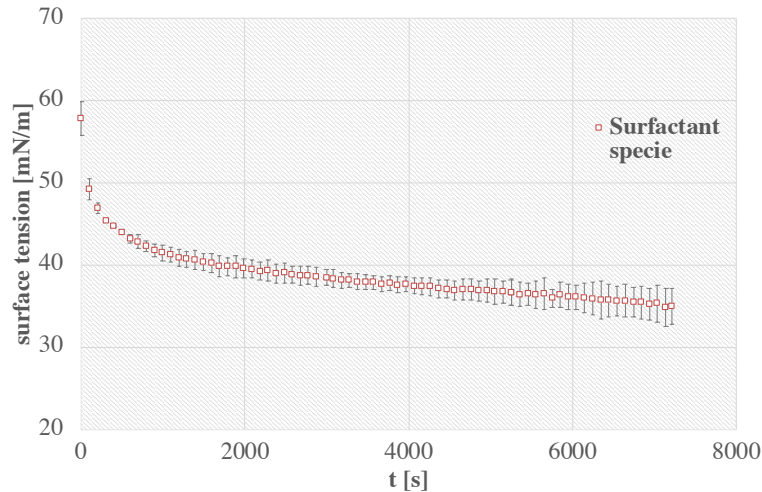
Figure 3.3.4 Typical trend of a surfactant specie

These measurements allow evaluation of the surface activity of the species in analysis in terms of equilibrium value, testing the possible dependence on environmental variables, as concentration, pH, ionic strength, cosolute, temperature, but also the rate of surface tension decrease can be related to the kinetic effect. Indeed, using the adapted interpretation, the rate characteristics of the several interfacial processes can be evaluated. The adsorption rate is determined by many factors such as the molecular characteristics of the surfactant (e.g., size, conformation, and interactions). The main features of the adsorption kinetics of surfactants can include: the diffusion of the molecules from the bulk into the interface; the adsorption and penetration of molecules at the interface; the interfacial aggregation, rearrangement of molecules adsorbed within the interfacial layer, multilayer formation and even interfacial gelation (Seta et al. 2012; Camino et al. 2009; Beverung, Radke and Blanch, 1999, Baeza et al. 2006). In the following picture these typical steps are summarized (Baeza et al. 2006):
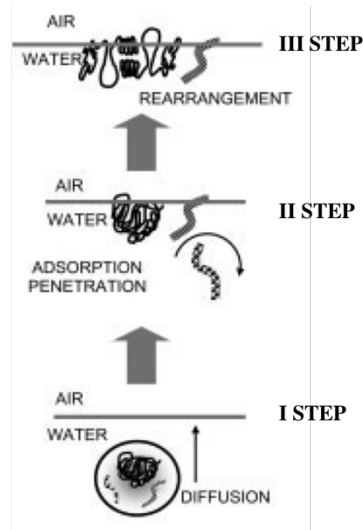
Figure 3.4.5 Interfacial step of surfactant species (Baeza et al. 2006)

3.3.1 Oscillating pendant drop mode

The pendant drop tensiometer is able to study the mechanical resistance of the interfacial layers in dilatational cinematic. In fact, by analysing the harmonic variations of the interfacial area, the dilatational rheology of surface/interfacial layers can be investigated. To study the rheology of interfacial layers it is necessary to study the relationship between the surface modification and the related dilatational stress (Ravera et al. 2010). The dilatational stress of an interface is the interfacial tension variation imposed because the volume of the drop is increased or decreased. By expansion/contraction of the drop (shown in Figure) the interface undergoes a respective variation which implies an interfacial tension variation.
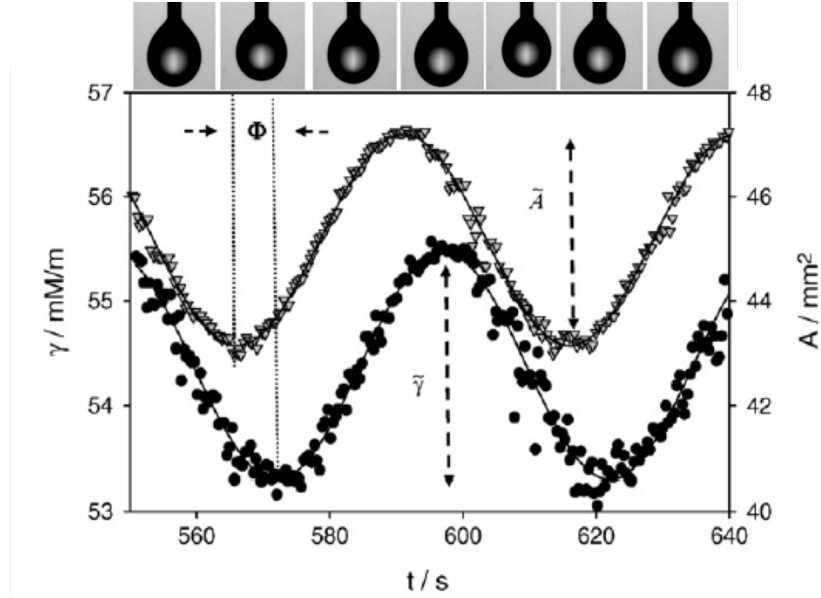
This effect is the response of the system to the deformation imparted. In particular, the interfacial tension variation, referred to the initial undeformed state γ_0 is:

$$\Delta\gamma = \gamma(t) - \gamma_0 \qquad (3.3.1.1)$$

If the interfacial behaviour is purely elastic, the surface stress is proportional to the relative area variation, $\alpha = \Delta A/A0 = (A(t) - A0)/A0$. If the interfacial behaviour is viscous the surface stress is proportional to the relative area variation rate, $\dot\alpha = d\alpha/dt$ (Bouyer et al. 2012; Ravera et al. 2010). In general, the interfaces can show both an elastic and viscous behaviour, so the dilatational stress can be written as in the following equation 3.3.1.2:

$$\Delta\gamma = E_0\alpha + \eta\dot\alpha \qquad (3.3.1.2)$$

E_0 and η are defined dilatational interfacial elasticity and dilatational interfacial viscosity respectively. For low amplitude harmonic perturbation of frequency ω, in fact, the interfacial area variation can be expressed as:

$$\Delta A = \tilde{A}t^{i\omega t} \qquad (3.3.1.3)$$

So, reworking the equation 3.3.1.3, it is possible to obtain:

$$E = \frac{\Delta\gamma}{\Delta A/A_0} = E_0 + i\omega\eta \qquad (3.3.1.4)$$

Where E is visco-elastic modulus, it is a complex variable, frequency dependent, where E_0 is the real part and corresponds to the elastic contribute, $\omega\eta$ is the imaginary part and correspond to the viscous contribute. In small amplitude regime, it is possible to assume the linearity of the system, so for purely harmonic perturbation the interfacial layer properties vary according also to a harmonic variation at the same frequency. In linear regime, the time dependent variables can be written as a superposition of harmonic functions, using a Fourier analysis. Thereby, the interfacial tension variation can be written as:

$$\Delta\gamma = \int_0^t \hat{\varepsilon}(\tau)\alpha(t-\tau)d\tau \qquad (3.3.1.5)$$

$\hat{\varepsilon}$ is the inverse Fourier transform of E, and $E(\omega)$ is the transfer function that characterizes the interface. Practically, the previous equation can be used in the interpretation of experiments of stress-relaxation in which are involved non-harmonic perturbations of the interfacial area, but there are imposed trapezoidal or rectangular volume deformations (Ravera et al. 2010). The oscillating drop/bubble method uses the harmonic oscillations of the drop volume that corresponds to periodic expansion and compression of the interfacial layers area. In response also the interfacial tension varies periodically with the same frequency and with a certain delay with respect to the perturbation. The link between stress and deformation is the dilatational viscoelasticity. So, if a sinusoidal variation of the interfacial area is set:

$$A = A_0 + \tilde{A}\sin(\omega t) \qquad (3.3.1.6)$$

where A_0 is the surface area before the perturbation and $\tilde{A}$ is the amplitude of the area perturbation. Consequently, the interfacial tension exhibits a harmonic response as:

$$\gamma = \gamma_0 + \tilde{\gamma}\sin(\omega t + \phi) \qquad (3.3.1.7)$$

where γ_0 is the equilibrium interfacial tension and $\tilde{\gamma}$ is the interfacial tension variation following the interfacial area disturb. ϕ is the shift phase between the area perturbation and the response of the interfacial tension and corresponds to the viscous contribute of

the interfacial rheological behavior. The dilatational interfacial viscoelasticity can be written as:

$$E(\omega) = A_0 \frac{\tilde{\gamma}}{\tilde{A}} cos\phi + iA_0 \frac{\tilde{\gamma}}{\tilde{A}} sin\phi \qquad (3.3.1.8)$$

In a pendant drop tensiometer, using the oscillating drop/bubble method, the interfacial tension is acquired continuously over time, while a controlled harmonic perturbation is applied to the drop. The analysis of the experimental signal is effectuated via DFT (Discrete Fourier Transform) algorithms. Under a linear regime, the output signal detected can contain harmonics with frequencies different from that imposed due to some external disturbances or to a weak nonlinearity of the system. For this reason it is preferable to adopt a procedure of harmonics extraction based on the Discrete Fourier analysis. The component at frequency ω of a generic experimental signal $g(t)$ presenting a phase δ is:

$$g = g_0 + \tilde{g} \, sin\,(\omega t + \delta) \qquad (3.3.1.9)$$

By discretization of this experimental signal, at the generic time t_j, using the Fourier series expansion, it is possible obtain:

$$\Delta g_j = A \, cos\,(\omega t_j) + B sin\,(\omega t_j) \qquad (3.3.1.10)$$

With

$$A = \frac{1}{N \sum_{K=1}^{N} g_K 2cos\,(\omega t_K)} \qquad (3.3.1.11)$$

$$B = \frac{1}{N \sum_{K=1}^{N} g_K 2sin\,(\omega t_K)} \qquad (3.3.1.12)$$

Where N is the experimental points number and g_K is the measured value at t_K time. One obtains:

$$\tilde{g} = \sqrt{A^2 + B^2} \qquad (3.3.1.13)$$

$$\delta = arctan\left(\frac{B}{A}\right) \qquad (3.3.1.14)$$

The number of oscillations must be such as to allow stationary status to be reached. To evaluate the validity of linearity hypothesis, the THD parameter can be evaluated. The THD is the total harmonic distortion parameter and it is defined as:

$$THD = \frac{\sqrt{a_2{}^2 + a_3{}^2 + \cdots + a_n{}^2}}{a_1} \qquad (3.3.1.15)$$

a_n are the higher harmonic amplitude values, a_1 is the value of fundamental frequency amplitude. For periodic oscillations with different amplitudes at the same frequency, the THD suggests a linear regime in the relationship between an imposed interfacial area variation and the resulting interfacial tension response.

3.4. The magnetic rod interfacial stress rheometer

The magnetic interfacial needle stress rheometer is a device able to impose the shear deformation on an interface and to give information about the mechanical resistance of this region.
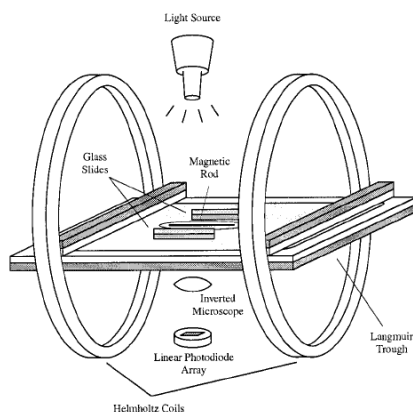
Figure 3.4.1 Magnetic rod rheometer scheme (Brooks et al. 1999)

The instrument is constituted of a Langmuir trough containing the sample and of a Wilhelmy balance used for the control of the surface pressure. If the surface pressure measure is not required, a smaller Petri dish can be used to contain the sample so as to reduce the sample quantity to analyse. A magnetized rod with radius "a" is placed at the interface between the two phases, supported by surface or interfacial tension. The needle is positioned in a rectangular channel with a variable width. All the Petri dish containing the magnetic needle is placed between the two coils in Helmholtz condition that provide

a magnetic field gradient balancing the current through the coils (Brooks et al. 1999, Verwijlen et al. 2011). The current is controlled by two dc power supplies controlled with a function generator interfaced with a PC through. The magnetic field applies a force on the magnetized rod to move the needle and shear the interfacial film. The position of the needle is captured by a camera and the resulting image is projected onto a photodiode array thus defining the strain rate. By applying a perturbation to the current in one of the coils, a force able to move the needle can be generated. The force and position signals are digitized using a data acquisition system. The ratio of the displacement amplitude (z) to the force amplitude (F), as well as the signals angle phase difference is determined from the frequency spectrum obtained by taking the fast Fourier transform of the two signals:

$$\frac{z}{F} = \frac{1}{(k-m\omega^2)^2+(\omega d)^2} \tag{3.4.1}$$

$$\delta = arctan\left(\frac{-\omega d}{k-m\omega^2}\right) \tag{3.4.2}$$

k is a spring constant, d is a drag coefficient and m is the inertial mass. In relation to the *Bo* number, it is possible to improve the sensitivity of the instrument by varying the k, m and d parameters. This effect can be realized using particularized needles. In fact, the needle is characterized by a magnetic part contained in a larger teflon part as shown in the following picture:
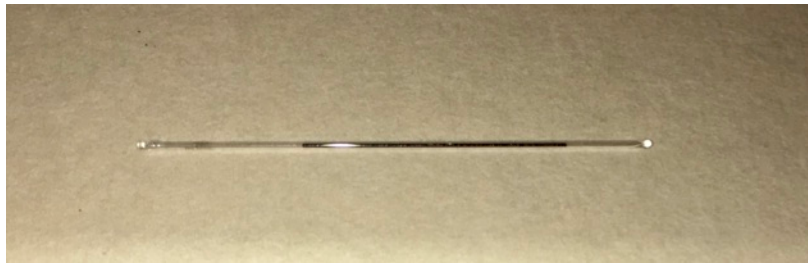
Figure 3.4. 2 Magnetic needle of interfacial shear rheometer

With this constitution it is possible utilize more or less long or more or less heavy needles, varying the force balance impressed on the interface and consequently the sensitivity offered by the instrument, without scaling the Helmhotz coils. The use of the small needle favours a greater sensitivity, thanks to an increase of interfacial contribute with respect to the bulk. It is possible, furthermore, to modify the wettability of the needle, by silanization

of the needle material that gives it a more hydrophobicity. The sensitivity limits of the needle can be calculated by a Bond evaluation:

$$B = \frac{g(\rho_{needle} - \rho_{subphase})\pi a^2}{2\gamma}$$ (3.4.3)

According to the surface tension of the interface and the contact angle made by the needle with the interface, the needle will be supported or sink through the interface.

The needle position is time dependent and by a camera it can be recorded and can give the interfacial strain measure (Verwijlen et al. 2011). By analysing the data, it is necessary to correlate the imposed current with the applied force.

It is possible to evaluate the interfacial properties imposing an oscillatory current on Helmhotz coils and detecting the speed at which the rod moves. The geometry of the system is schematized in the following picture:
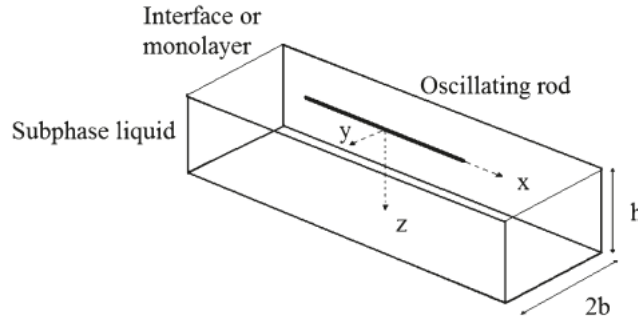
Figure 3.4.3 Oscillating rod schematization

The needle is located at the center of the channel and its flow is independent of x direction, because it is possible to neglect the end effects. Considering the air as a light phase and a Newtonian fluid as a subphase, the force that acting on the needle is:

$$f = f_0 \cos(\omega t)$$ (3.4.5)

The velocity field has a sole component in the x-direction, which is variable in the y-direction and time dependent:

$$\boldsymbol{u} = u_x(y, t)$$ (3.4.6)

Hence, it is possible to write the velocity variation using the Stokes equation for the time-dependent system:

$$\rho \frac{\partial u}{\partial t} = \eta \left(\frac{\partial^2 u}{\partial y^2} + \frac{\partial^2 u}{\partial z^2} \right)$$ (3.4.7)

Considering a symmetry condition at y = 0:

$$\left.\frac{\partial u}{\partial y}\right|_{(0,z,t)} = 0 \tag{3.4.8}$$

And, referring to Figure and considering the no-slip boundary conditions at the side walls (y=b; y=-b) and at the bottom (z=h):

$$u(b, z, t) = 0 \tag{3.4.9}$$

$$u(y, h, t) = 0 \tag{3.4.10}$$

It is convenient to define and to use the dimensionless variables in the previous equations:

$$\tau = \omega t, \ Y = \frac{y}{a}, \ Z = \frac{z}{a}, \ U = \frac{u}{u_c},$$

In this way equation 3.4.7 became:

$$Re \frac{\partial U}{\partial t} = \left(\frac{\partial^2 U}{\partial Y^2} + \frac{\partial^2 U}{\partial Z^2}\right) \tag{3.4.11}$$

$$Re = \frac{\rho \omega a^2}{\eta} \tag{3.4.12}$$

In which the boundary conditions became:

$$\left.\frac{\partial U}{\partial t}\right|_{(0,Z,\tau)} = 0$$

$$\tag{3.4.13}$$

$$U\left(\frac{b}{a}, Z, \tau\right) = 0 \tag{3.4.14}$$

$$U\left(Y, \frac{h}{a}, \tau\right) = 0 \tag{3.4.15}$$

The solution to the velocity profile is the real part of

$$U(Y, Z, \tau) = \Re\{e^{it}V(Y, Z)\} \tag{3.4.16}$$

Where V satisfies the equation:

$$i \cdot Re \cdot V = \left(\frac{\partial^2 V}{\partial Y^2} + \frac{\partial^2 V}{\partial Z^2}\right) \tag{3.4.17}$$

To complete the solution it is necessary to consider the motion equation at the interface. So, to interface with a Newtonian behaviour, considering a surface as a planar area, with zero thickener, the interface stresses equation is:

$$\eta_s \frac{\partial^2 u_s}{\partial y^2} + \left.\eta \frac{\partial u}{\partial z}\right|_{(z=0)} + f_0 \Re\{e^{i\omega t}\}\delta(y) = 0 \tag{3.4.18}$$

That in dimensionless terms became:

$$Bo \frac{\partial^2 U_s}{\partial Y^2} + \left.\frac{\partial U}{\partial Z}\right|_{(Z=0)} + \Re\{e^{i\tau}\}\delta(Y) = 0 \tag{3.4.19}$$

The $\delta(Y)$ function, has the unit of length^{-1} and has been defined at y = 0 to modelled the x-directed force per length and in Cartesian coordinates this function is defined as $\int_{-\varepsilon}^{\varepsilon} \delta(y)\, dy = 1$, where ε is some distance on either side of the delta function.

It is possible to write the dimensionless surface velocity:

$$U_s(Y,\tau) = U(Y,0,\tau) = \Re\left\{e^{i\tau}\sum_{n=1}^{\infty} a_n cos(\lambda_n Y)sinh\left[\left(\tfrac{h}{a}\right)\sqrt{\lambda_n^2 + iRe}\right]\right\} \quad (3.4.20)$$

Substituting this solution in the surface velocity equation, it is possible to obtain the a_n coefficient:

$$a_n = \left(\tfrac{a}{b}\right)\Big/\left\{Bo\lambda_n^2 sinh\left[\left(\tfrac{h}{a}\right)\sqrt{\lambda_n^2 + iRe}\right] + \sqrt{\lambda_n^2 + iRe}\,cosh\left[\left(\tfrac{h}{a}\right)\sqrt{\lambda_n^2 + iRe}\right]\right\} \quad (3.4.21)$$

It can be noted that the velocity profile in the subphase and at the interface is a function of four dimensionless parameters, where h/a and a/b, are geometrical factors and Re and Bo, are dynamic numbers. This model provides a non-linear dependence of Re on the velocity profile. More than other parameters, the high Re values involve an overestimation of the shear viscosity at low Bo, this effect is confirmed in the experimental analysis of (Verwijlen et al. 2011).

The analytical model can be extended to viscoelastic interfaces and, in linear regime, the interfacial behaviour can be expressed by a linear combination of the two contributes: elastic and viscous. So the interfacial modulus can be written as:

$$G_s^*(\omega) = G_s'(\omega) + iG_s''(\omega) = G_s^*(\omega)e^{i\delta_s(\omega)} \quad\quad (3.4.22)$$

The moduli can be combined with the Bo number:

$$Bo(\omega) = \frac{G_s''(\omega) - iG_s'(\omega)}{\omega a\eta} = \frac{\eta_s'(\omega) - i\eta_s''(\omega)}{a\eta} \quad\quad (3.4.23)$$

To obtain a numerical solution, a finite-difference approach was used, starting from Navier-Stockes equations with a cylindrical geometry:
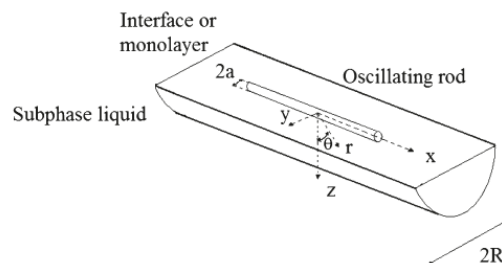
Figure 3.4.4 Needle in cylindrical channel (Verwijlen et al. 2011)

In relation to this variation, with respect to the previous discussion, the change of reference geometry can be neglected and the displacement z of each fluid element can be expressed by:

$$z = g(r,\theta)z_0^* e^{i\omega t} \tag{3.4.24}$$

Instead of r, the new coordinate p has been defined:

$$p = ln\left(\frac{r}{a}\right) \tag{3.4.25}$$

The Navier-Stockes equation can be written in the following way:

$$\frac{\partial^2 g}{\partial p^2} + \frac{\partial^2 g}{\partial \theta^2} = iRe\, e^{2p} g \tag{3.4.26}$$

And there are four boundary conditions that assume the following form:

$$g = 1 \text{ at } p = 0 \tag{3.4.27}$$

$$g = 0 \text{ at } p = ln\left(\frac{R}{a}\right) \tag{3.4.28}$$

$$\frac{\partial g}{\partial \theta} = 0 \text{ at } \theta = 0 \tag{3.4.29}$$

$$Bo\, e^{-p}\left(\frac{\partial^2 g}{\partial p^2} - \frac{\partial g}{\partial p}\right) + \frac{\partial g}{\partial \theta} = 0 \text{ at } \theta = \frac{\pi}{2} \tag{3.4.30}$$

With this information, it is possible now to evaluate the force exerted on the needle as a ratio of the total force on the needle to its displacement (Reynaert et al. 2008):

$$\frac{F_D e^{i\omega t}}{z_0^* e^{i\omega t}} = (i2L\omega\eta)Bo\left(-\frac{\partial g}{\partial p}\right)\Big|_{p=0,\theta=\frac{\pi}{2}} + (i2L\omega\eta)\int_0^{\frac{\pi}{2}}\left(-\frac{\partial g}{\partial p}\right)\Big|_{p=0} d\theta + k - \rho_{needle}\pi a^2 \omega^2 L$$

$$\tag{3.4.31}$$

Starting from the right hand side of equation 3.4.31, the first term is the drag on the needle exerted by the surface, the second term is the subphase drag contribution while the two last terms are respectively the system compliance k (derived from the restoring force created by the magnetic coils) and inertia and are independent of the resulting flow.

During the measurement, two parameters are monitored: the amplitude ratio, AR, which is the ratio of the needle amplitude displacement to the forcing amplitude, and the phase difference, δ, which is the difference between the needle response and the applied force. These were determined from the frequency spectrum obtained by taking the fast Fourier transform (FFT) of the applied force and the needle response (Brooks et al. 1999). The AR and δ factors can be expressed by:

$$AR = \frac{rod\ position\ amplitude}{force\ amplitude} = \frac{1}{\sqrt{(k-m\omega^2)^2 + (\omega d)^2}} \tag{3.4.32}$$

$$\delta = arctan\frac{-\omega d}{k-m\omega^2} \tag{3.4.33}$$

The three parameters k, d, and m are reference parameters used to describe the response of the device and are analogous to a spring constant, damping coefficient, and a needle mass, respectively.

The dynamic surface modulus, $G_s^*(\omega)$, is the parameter which correlates the stress and the strain:

$$\sigma_s e^{i\omega t} = G_s^*(\omega)\gamma_0 e^{i[\omega t - \delta(\omega)]} \tag{3.4.34}$$

σ_s is the amplitude of the applied sinusoidal stress with frequency ω and γ_0 is the amplitude (divided by the distance between the rod and the glass slide) of the resultant strain delayed with respect to the stress by a phase angle $\delta(\omega)$. Rearranging:

$$G_s^*(\omega) = \frac{\sigma_s}{\gamma_0} e^{i\delta(\omega)} = G_s'(\omega) + iG_s''(\omega) \tag{3.4.35}$$

$$tan\delta = \frac{G_s''}{G_s'} \tag{3.4.36}$$

where $G_s'(\omega)$ is the surface storage modulus and $G_s''(\omega)$ is the surface loss modulus, and δ is the phase angle evaluated as ratio of viscous part to elastic modulus. Similarly, it is possible to express the dynamic viscosity, $\mu_s^*(\omega)$, as a complex quantity and as constituted of two contributes, real and imaginary parts:

$$\mu_s^*(\omega) = \mu_s'(\omega) - i\mu_s''(\omega) = \frac{G_s^*(\omega)}{i\omega} = \frac{G_s''(\omega)}{\omega} - i\frac{G_s'(\omega)}{\omega} \tag{3.4.37}$$

The response measured with a monolayer contains the contributions from the system (water drag, surface curvature, rod inertia, etc.) as well as the interface. Assuming the additive properties of the contributes, the dynamic surface modulus can be written:

$$G_s^*(\omega) = \frac{W}{2L}\left(\frac{1}{AR_{monolayer}} e^{-i\delta_{monolayer}}\right) = \frac{W}{2L}\left(\frac{1}{AR_{measure}} e^{-i\delta_{measure}} - \frac{1}{AR_{system}} e^{-i\delta_{system}}\right) \tag{3.4.38}$$

The problem of this approach is that the stress induced at the interface can be damped by a subphase. In this case, the rate profile is not linear and the velocity is zero at the wall, where the no slip condition has been assumed. To avoid this complication, a smaller gap can be chosen to increase the stress in the film so that the surface stress dominates over the subphase stress. So a Bo number has been evaluated as ratio of the AR_{system} to $AR_{measure}$, and only if this number is greater than 100, the subtraction of the subphase effect is not necessary (Brooks et al. 1999).

3.5 Conclusions

There are many methods to evaluate the forces exhibited at interface and to evaluate the mechanical resistance of the interfacial layer. It is possible to apply several types of deformations, two in particular: shear and dilatational. In this chapter, the principal instruments were shown to measure the interfacial/surface tension and in particular two interfacial rheometers were illustrated , respectively for dilatational and shear rheology. To apply dilatational deformation it was explained, in more detail, the pendant drop rheometer and to apply shear deformation the magnetic rod interfacial rheometer was described. In the dilatational case, the advantages of pendant drop methods are numerous and, in comparison with the other techniques, only small amounts of the liquid are required. With this technique can be studied both liquid-vapor and liquid-liquid interfaces. Also, the methods have been applied to several type of materials. The continuous capture of the image, the interfacial tensions and the time-dependent properties can be studied by pendant drop analysis. On the other hand, in the shear case, the magnetic rod allows the evaluation of very low viscosity and viscoelasticity, thanks to the high sensitivity of the probe and, simply by varying the geometry (length, weight and magnetic medium) of the needle, the sensitivity of the instrument can be varied. With magnetic rod, the rheometer can be also studied the time dependent properties of the interfaces but, also, the age effect on the surface/interfacial layers can be explored and can be related to the interfacial mechanisms of the surfactant species.

Interfacial rheology is an important tool to study foam and emulsion and to correlate the interfacial effect to bulk stability.

REFERENCES

Arashiro E. Y. and Demarquette N.R. (1999) Use of the Pendant Drop Method to Measure Interfacial Tension between Molten Polymers, Materials Research, (2), 23-32

Baeza, R., A. M. R. Pilosof, C. C. Sanchez & J. M. R. Patino (2006) Adsorption and rheological properties of biopolyrners at the air-water interface. *Aiche Journal*, 52**,** 2627-2638.

Berry, J. D., M. J. Neeson, R. R. Dagastine, D. Y. C. Chan & R. F. Tabor (2015) Measurement of surface and interfacial tension using pendant drop tensiometry. *Journal of Colloid and Interface Science,* 454**,** 226-237.

Beverung, C. J., C. J. Radke & H. W. Blanch (1999) Protein adsorption at the oil/water interface: characterization of adsorption kinetics by dynamic interfacial tension measurements. *Biophysical Chemistry,* 81**,** 59-80.

Bos, M. A. & T. van Vliet (2001) Interfacial rheological properties of adsorbed protein layers and surfactants: a review. *Advances in Colloid and Interface Science,* 91**,** 437-471.

Bouyer, E., G. Mekhloufi, V. Rosilio, J. L. Grossiord & F. Agnely (2012) Proteins, polysaccharides, and their complexes used as stabilizers for emulsions: Alternatives to synthetic surfactants in the pharmaceutical field? *International Journal of Pharmaceutics,* 436**,** 359-378.

Brooks, C. F., G. G. Fuller, C. W. Frank & C. R. Robertson (1999) An interfacial stress rheometer to study rheological transitions in monolayers at the air-water interface. *Langmuir,* 15**,** 2450-2459.

Camino, N. A., O. E. Perez, C. Carrera Sanchez, J. M. Rodriguez Patino & A. M. R. Pilosof (2009) Hydroxypropylmethylcellulose surface activity at equilibrium and adsorption dynamics at the air-water and oil-water interfaces. *Food Hydrocolloids,* 23**,** 2359-2368.

Chen P., Kwok D.Y., Prokop R.M., del Rio O.I., Susnar S.S., Neumann A.W., Axisymmetric Drop Shape Analysis (ADSA) and its applications. In: M bius D. and Miller R. Editors, Drops and Bubbles in Interfacial Research, Elsevier Science (1998), 61-136.

Drelich J., Fang Ch., White C.L. (2002), Measurement of interfacial tension in fluid-fluid systems, Encyclopedia of Surface and Colloid Science

Erni, P., P. Fischer, E. J. Windhab, V. Kusnezov, H. Stettin & J. Lauger (2003) Stress- and strain-controlled measurements of interfacial shear viscosity and viscoelasticity at liquid/liquid and gas/liquid interfaces. *Review of Scientific Instruments,* 74**,** 4916-4924.

Kokelaar, J. J., A. Prins & M. Degee (1991) A NEW METHOD FOR MEASURING THE SURFACE DILATIONAL MODULUS OF A LIQUID. *Journal of Colloid and Interface Science,* 146**,** 507-511.

Masschaele K., Vandebril S., Vermant J., Madivala B., Interfacial Rheology, in RHEOLOGY - Vol. I

Miller, R., J. K. Ferri, A. Javadi, J. Kragel, N. Mucic & R. Wustneck (2010) Rheology of interfacial layers. *Colloid and Polymer Science,* 288**,** 937-950.

Ravera, F., G. Loglio & V. I. Kovalchuk (2010) Interfacial dilational rheology by oscillating bubble/drop methods. *Current Opinion in Colloid & Interface Science,* 15**,** 217-228.

Reynaert, S., C. F. Brooks, P. Moldenaers, J. Vermant & G. G. Fuller (2008) Analysis of the magnetic rod interfacial stress rheometer. *Journal of Rheology,* 52**,** 261-285.

Saad, S. M. I. & A. W. Neumann (2016) Axisymmetric Drop Shape Analysis (ADSA): An Outline. *Advances in Colloid and Interface Science,* 238**,** 62-87.

Seta, L., N. Baldino, D. Gabriele, F. R. Lupi & B. de Cindio (2012) The effect of surfactant type on the rheology of ovalbumin layers at the air/water and oil/water interfaces. *Food Hydrocolloids,* 29**,** 247-257.

Verwijlen, T., P. Moldenaers, H. A. Stone & J. Vermant (2011) Study of the Flow Field in the Magnetic Rod Interfacial Stress Rheometer. *Langmuir,* 27**,** 9345-9358.

Chapter 4

Rheology of vegetable proteins interfaces

Abstract

Many food products are multiphase systems and their structural and textural properties are determined by the interactions between the various macromolecules making up the system. They are created by homogenization of two or more immiscible phases, to form emulsions or foams. These systems are characterized by high neighbouring surfaces which are also areas of instability. Proteins are widely used to stabilize the interfaces because they are able to adsorb quickly to the interfacial layers, to decrease the interfacial tension and to improve the mechanical resistance of the interfacial layers. Recently, protein extract from vegetable seeds has been receiving much attention from the food industry, thanks to their good environmental sustainability and healthy composition, but the scientific literature is lacking about the information on the surface activity and emulsifying ability of these proteins.

Then, on the light of the above in this work, it was investigated the surface properties of three protein extracts from a vegetable source, soy, hemp and brown rice, using the pendant drop method to study the dilatational properties and a rod magnetic rheometer to study the shear properties. Static measurements of surface tension versus time were performed in the concentration range that takes to have the equilibrium isotherm. Dilatational rheological properties were studied by oscillating pendant drop method and shear rheological properties were studied by oscillating magnetic needle. The relaxation mechanisms of interfacial layers were also investigated in dilatational kinematics.

Finally a fractional and a Maxwell model were used to interpret the experimental dilatational data of stress relaxation.

Keywords: *vegetable proteins, interfacial/surface tension, soy protein, hemp protein, rice protein, pendant drop tensiometer, magnetic rod rheometer.*

4.1 Introduction

A lot of multiphase systems are food products daily used in the human diet. The stability of these systems can be due to the emulsifiers naturally present in the food, like proteins in milk, or by a suitable addition of proteins or surfactants in the system.

In the last case, the final structural and textural properties of the foodstuff are determined by the interactions between the various molecules present.

Typical examples of multiphase systems are salad dressings, mousses, whipped toppings, ice-creams, bread (Sagis and Scholten 2014; Patino and Pilosof 2011). These systems are characterized by the simultaneous presence of more than one phase, in the simplest case, they are two phases: oil and water or water and an air phase. To obtain a multiphase system it is necessary to homogenize the different phases and this process takes way with an increased energy necessary to form many interfaces.

The interfacial layers' formation takes a thermodynamic instability of the systems and may give rise to natural phase separation phenomena as coalescence, disproportion and so on. As a consequence, it is necessary to stabilize these systems by use of surface active agents that can quickly migrate to the interface layer stabilizing them. Surface active agents, the thanks to their amphiphilic nature, are able to bind the two phases one hydrophilic (water) and the second one hydrophobic (oil or air). In this way, it is possible to finely disperse the two insoluble phases in one another, to obtain a homogeneous and stable product.

The surface-active agent can be low a molecular-weight emulsifier or a macromolecule (protein and polysaccharide). In food dispersions, the proteins stabilize the fluid interface through their capacity to lower the surface (interfacial) tension of water and to form viscoelastic layers. Polysaccharides can be classified as surface active agent or not: the polysaccharides without surface activity, enhance the emulsion stability by gelling or thickening agent; the polysaccharides with surface activity can to adsorb at the interface and prevent droplet flocculation and coalescence through electrostatic and/or steric repulsive forces (Bouyer et al. 2012; Baeza et al. 2006; Dickinson 2003).

In particular, proteins are widely used to create foams or emulsions and they are widely used in the food industry due to their nutritive value and because of their potential functional properties. They are polymers of amino-acids and due to their amphiphilic structure, they can adsorb quickly to interfacial layers. Their presence leads to interfacial tension decrease

and improves the mechanical resistance of the interfacial layers. They can be used in the food industry with other components (emulsifier, polysaccharide or both) to give complex protein-polysaccharide or protein-emulsifier (Dickinson 2011; Ganzevles et al. 2006; Seta et al. 2012). Protein macromolecules have a structure with hydrophilic and hydrophobic residues randomly spread all over and that give them high surface activity. The adsorbed protein molecules and their interaction can give rise to highly viscoelastic films that stabilize the interfaces and the protein residues in the aqueous phase also providing a steric stabilization (Bouyer et al. 2012). Depending on their amino-acids sequences, proteins can be globular (folded) or random-coil (unfolded) (Mezzenga and Fischer 2013).

In the food industry, the principal source of protein is the animal source: caseins, whey proteins, gelatins, all widely examined (Seta et al. 2012; Ganzevles et al. 2006; Dickinson 2003; Bos and van Vliet 2001). Recently, protein extract from vegetable seeds have been receiving much attention from the food industry, thanks to their good environmental sustainability and healthy composition (do Carmo et al. 2016; Renzetti, Dal Bello and Arendt 2008), but also as an interesting alternative for the production of food designated as vegan and/or vegetarian, but also for consumer with lactose or gluten intolerance. The vegetable proteins could be a valid substitute as functional ingredient to use in gluten-free dough, to promote a formation of a protein network to give the overall quality and structure of bakery products (Renzetti et al. 2012; Renzetti et al. 2008; Sun and Arntfield 2012; Ramirez-Suarez and Xiong 2003). The plant's proteins are extensively studied also due to the lower cost in comparison to the animal proteins to produce cheaper food, for their low allergenicity, and for the new trend in lifestyle and environmental sensitivity. Nowadays, vegetable proteins are gaining increasing acceptance in food manufacturing for ethical problems or in preventive health care activities and because are generally well tolerated by the body. New natural nutraceuticals and functional ingredients are employed in food production and currently proteins from legumes, like soy proteins, are used in food successfully because of its beneficial effects on humans and because is rich in essential amino acids, minerals and vitamins, but also they are able to lower the glycemic index and they have good anti-tumour properties (Nishinari et al. 2014; Tang 2017).

On the light of the above, in this work, it has been investigated the surface properties of three protein extracts from a vegetable source, at the air/water interface, under dilatational and shear deformation kinematics. Soy, hemp and brown rice have been chosen as protein sources.

The protein extract from hemp seeds mainly contains edestin protein (82%) and albumin (5%) with a good nutritional profile in essential amino acids (Wang et al. 2008). The edestin molecule (the principal constitutes of hemp protein) consists of six acidic AS and basic BS subunits linked by one disulfide bond (Wang et al. 2008). The edestin molecular weight is about 300 kDa and its minor fraction, the albumin, is about 48 kDa (Wang et al. 2008). Several studies reported the structural and functional properties of hemp protein (Wang et al. 2008; Tang et al. 2006b; Tang et al. 2006a; Malomo, He and Aluko 2014), but there isn't any information about their surface/interfacial properties.

The rice is mainly consumed in the form of grains but also as a breakfast cereal or in the production of snacks or, more generally, in value-added products, is growing rapidly. Nowadays, rice protein usage is increasing in the athletic diet and thanks to its health benefits. The use of rice as a strong alternative for food products opens up the possibility for the development of gluten-free food products. The only edible part of the rice is the kernel and it is encased in the protective hull. By the elimination of hull, the brown rice is produced. Multistage milling produces white rice.
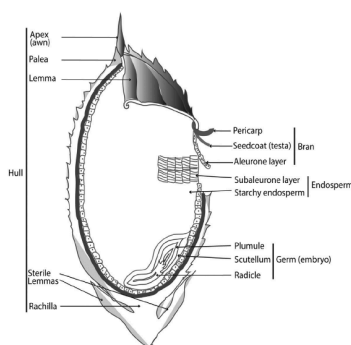
Figure 4.1.1. Scheme of rice grain composition

By a comparison between the proteins content in the white rice and the proteins content in the brown rice, the brown rice is richer in proteins. More elements which are present in the external part of the kernel are absent in the white rice because the refining processes delete these components (Cho and Lim 2016). Moreover, brown rice is richer in B vitamins (involved in different biological functions), folic acid, iron, magnesium (a mineral involved in over 300 biological functions), selenium (a mineral involved in the immune system and in the regulatory system of the thyroid glands). The protein types, according to Osborne solubility classification, are: albumin (4-22%), globulin (5-13%), and prolamin (1-5%), and glutelin (60-80% of total protein) which characterizes the main protein fraction, the rice

bran (which is the fraction contained in brown rice) contains 24-37% albumin, 15-36% globulin, 11-38% glutelin, and 2-6% prolamin (Amagliani et al. 2017a, Amagliani et al. 2017b). The rice proteins are considered hypoallergenic and their surface properties are not known in scientific literature.

For all proteins it is possible to underline that the amino acidic profile is different from animal proteins and in some cases it's more deficient, but thanks to a balance of the amino acid species present, the nutritional aspect is preserved and guaranteed (Kalman 2014).

As concern the soy proteins, better known to scientific literature, are principally constituted by glycinin (11S) that is a globular protein with hexamer structure consisted of six monomeric units of AB structure, with A= acid polypeptide and B= basic polypeptide, linked by SS bond (Martin, Bos and van Vliet 2002; Barac et al. 2004; Nishinari et al. 2014). Glycin has a low molecular flexibility and in function of physical-chemical environment, principally cause to electrostatic repulsion, it can be dissociated in other simpler forms, so, the soy proteins presented in isolate soy protein are four fraction, classified by their sedimentation coefficient (S): 3S, 7S (ß-conglycinin), 11S (glycinin) and 15S that, in general, are the 8%, 35%, 52% and 5% of the total protein content respectively (Barac et al. 2004; Martin et al. 2002; Tang 2017). The 11S/7S ratio depends on the cultivar type and this ratio affects the emulsifying properties of soy proteins (Tang 2017).

Martin et al. (2002) studied the surface effects of 3S/7S and 11S forms, reporting that also report that, at short ageing times the two proteins show different behaviour, but after long adsorption time, these difference disappear. There are other studies about soy interfacial properties that attest a good surface properties, as surface activity and as mechanical resistance, and that release a dependence of surface properties from pH and structural conformation (depending of its concentration) (Nino et al. 2005; Ortiz et al. 2003; Martin et al. 2002; Tang 2017). Wagner and Gueguen (1995) suggest that an improvement of glycinin surface behaviour can be obtained by dissociation, deamidation, and unfolding of the oligomeric structure. In particular, Martin et al. (2002) reported that the glycinin fraction 3S, 7S and 11S results present in a different quantity at different pH conditions: at pH=6,5 the percentages are 0, 3, 57% respectively, but at pH= 3 the percentages are 70, 27 and 0% respectively. This effect is related to the dissociation of glycinin in acid condition.

It is also known the effect of the soy protein in association to polysaccharides (Piazza et al. 2009) to stabilize and to improve the mechanical resistance of the interface. Patino and

coworker (Patino et al. 2003) studied in more detail the surface effect of the soy proteins in dilation cinematic.

As a result of the above, two different plant proteins were investigated in comparison with proteins from soybeans. Proteins from hemp and brown rice were selected. These are two alternative sources currently widespread as an alternative plant source to the more widespread classic ones. In this work, the interfacial rheological properties of vegetable proteins were investigated by static and dynamic measurements with the aim to evaluate their surface properties and the proteins ability to have a strong interfacial layer. Thanks to a kinetic interpretation of the static measurements it was possible to evaluate the surface activity, the diffusion velocity of the macromolecules from the bulk to the interface and the eventually interfacial layer formation and rearrangement. Moreover, by stepwise fast axial-symmetric compression or dilation of the surface area, the surface stress relaxation was monitored. The stress relaxation was analysed and the relaxation process was characterized by a main relaxation time. The data treatment then leads to a measure of homogeneity of the relaxation process. Furthermore, effective surface dilation elasticities and viscosities were calculated. The stress relaxation data were also interpreted by fractional Maxwell and Scott Blair model.

Finally, a shear interfacial characterization, able to give information about the long-term stability of the different systems, was carried out on the biopolymers interfacial films.

4.2 Materials and Methods

4.2.1 Samples preparation
In this work, three different vegetable proteins (VP), soy, hemp and brown rice, were studied. All the three proteins were purchased by Bulk Powereds® and their commercial purity are reported in Table 4.2.1.1.

Protein	Protein ID	Purity %
Hemp	H	47
Soy	S	90
Brown Rice	BR	80

Table 4.2.1.1 ID and purity percentage of the commercial proteins

Solutions were prepared by dissolving the proteins in Milli-Q ultrapure water (Millipore, USA), for at least two hours. The twicedistilled water used throughout all the experiments was obtained from a Milli-Q purification system, and it was checked for contaminants before each experiment, measuring the surface tension of the buffer solution at the air/water interface at room temperature. No aqueous solution with a surface tension other than the value commonly accepted in the literature (72 - 73 mN/m at 20 °C) was used.

Due to the high fibre content of the hemp protein sample, the solution was stirred for one hour by a magnetic stirrer (AREX Heating Magnetic Stirrer, Velp Scientifica, Italia), and then centrifuged (3000 rpm for 30 minutes) to separate the fibre part, recovered on the bottom, from the supernatant liquid. This last was analyzed.

The protein concentration was changed in the range between 10^{-7} and 10%w/w in order to obtain the interfacial tension equilibrium data at the air/water for all the investigated proteins. Then all the other measurements were carried out at the CMC (*Critical Micellar Concentration*). All the solutions were analyzed at the natural pH value, no buffer solution was used through this study and the values of each solutions were reported in Table 4.2.1.2

Protein	pH [-]
H	6.8±0.1
S	7.0±0.1
BR	5.8±0.1

Table 4.2.1.2 pH condition of protein solutions, at 1%w/w concentration

4.2.2 Total protein content in solution

In order to evaluate the quantity of solubilized protein, the Bradford assay kit (Bradford, 1976) was used. The absorbance was read at 595 nm with a spectrophotometer S-3100 (SCINKO, Korea) and bovine serum albumin was used as a standard substance (Lakemond et al. 2000; Yapo et al. 2007). Experiments were triplicated and the data were reported as their mean and the standard deviation.

4.2.3 Interfacial measurements

In order to understand the effect of the vegetable proteins on the interfacial properties, all the three different proteins were investigated under either in dilatation (static and dynamic)

and shear (dynamic) deformation field. Further, the time-dependent properties were investigated with reference to a dilatation relaxation test.

From static measurement, equilibrium data and kinetic information can be obtained together with details on adsorption an rearrangement mechanism of the the proteins at the interface.

The proteins were also characterized by harmonic drop oscillation experiments and dynamic shear experiments at the interface. Information about the ability to form emulsions and on the strength of the protein layer were obtained.

4.2.3.1 Static surface analysis

The transient interfacial tension measurements and harmonic drop oscillation experiments were performed by means of a pendant drop tensiometer (FTA200, First Ten Angstroms, USA). This apparatus is composed by a cell, where two fluids are put in contact, an illuminating device of the cell, a viewing system for the visualization of the drop and a data acquisition system. The use of the Axisymmetric Drop Shape Analysis (ADSA) allows the instrument to transform the geometric parameters, of the captured drop image, in surface/interfacial tension. In this way, it is possible to calculate the surface parameters.

Details of this apparatus are given by Biresaw, Liu, and Erhan (2008). The instrument is equipped with an automated pump that can be fitted with various sizes of syringes and needles to allow for software control of pendant drop formation and of sinusoidal variations in the drop volume or surface area. An automated image viewing and capturing system, with various image capture triggering options, was used. Image acquisition and regression of the interfacial tension were performed directly with the instrument software by fitting the Bashforth - Adams equation to the drop shape. In particular, the procedure consists in some successive steps: first, a drop is generated, then the instrument captures and digitalizes the pendant drop image, furtherly, the drop contour is extracted and the geometric parameters are determined. Finally, a software provides a smoothing of the extracted drop contour data and, by a fourth order Runge-Kutta method and a comparison with the theoretical profile based on Laplace equation, the best fitting interfacial tension value is determined (Araschiro 1999; Berry et al. 2015)

Drop-image software also controlled an automatic pipetting system that maintained constant drop volume with time period over which dynamic tensions were measured, γ. All the

experiments were carried out at room temperature (22 ±1 °C), placing the aqueous solutions in a 100 ml glass Hamilton. With this procedure it is also possible to obtain the equilibrium surface tension, γ_{eq}, determined for all the tested samples, assuming that the equilibrium is reached when the tension did not change by more than 0.5 mN/m during 30 min (Seta et al. 2012)

All experiments were carried out by making a drop of the investigated solution at the tip of a stainless-steel needle (D = 20 gauge) of a 100 ml glass Hamilton syringe (1710TLL), controlled by an automatic pump that allows the dispensing of the desired solution volume. The drop is formed in an optical quartz cuvette (5 ml), partially filled with water in order to saturate the environment with the aim to reduce evaporation phenomena. A CCD camera is connected to a computer and captures the images of the drop according to a proper test set. The surface tension measurements were performed by capturing the drop images during the experiment, beyond this time the evaporation of the sample affects the reliability of the test.

4.2.3.2 Dilatational oscillating test

To evaluate the dilatation properties of surface layers of vegetable proteins, the oscillating pendant drop method was used. According to this procedure, a drop of tested solution is subjected to periodical cycles of sinusoidal compression/expansion, obtained by decreasing/increasing the drop volume, with the desired amplitude. Thus, starting from static conditions characterized by an unperturbed initial area A_0 and a corresponding reference stress γ_0, the surface area was subjected to a sinusoidal change of a given value ΔA_0 amplitude (see eq.3.3.1.6):

$$A - A_0 = \Delta A_0 \sin(\omega t) \qquad (4.2.3.2.1)$$

Therefore, by using small oscillation amplitudes, which allow neglecting the higher frequency harmonics, the dilatation stress oscillates with a constant amplitude $\Delta \gamma_0$ and becomes (see eq.3.3.1.7):

$$\gamma - \gamma_0 = \Delta \gamma_0 \sin(\omega t + \delta) \qquad (4.2.3.2.2)$$

where δ is the phase angle between surface stress and surface area.

Eq.4.2.4.2 may be manipulated as follows:

$$\gamma - \gamma_0 = \Delta \gamma_0 \cos\delta \, \sin\omega t + \Delta \gamma_0 \sin\delta \, \cos\omega t \qquad (4.2.3.2.3)$$

Due to the deformation (expansion and/or contraction) of the interface, the surface area, A, is a function of time, t. Then the time dependence, A=A(t), is known. In fact, as the rate of

surface deformation, $\dot{\alpha}$ (t), and the surface deformation, α, are defined as (Ivanov et al. 2005):

$$\dot{\alpha}(t) \equiv \frac{1}{A}\frac{dA}{dt} = \frac{d\alpha(t)}{dt} \qquad (4.2.3.2.4)$$

$$\alpha(t) = \int_0^t \dot{\alpha}\,dt = ln\frac{A(t)}{A_0} \approx \frac{\Delta A}{A_0} \qquad (4.2.3.2.5)$$

$$\Delta A(t) = A(t) - A_0 \qquad (4.2.3.2.6)$$

Consequently, the ratio of dγ over dln A gives the interfacial dilational modulus, E_d, defined as:

$$E_d = \frac{\gamma - \gamma_0}{dlnA_0} \qquad (4.2.3.2.7)$$

If eq.4.2.4.3 is divided by the area deformation, the frequency dependent complex modulus E_d^* is found according to the development shown in paragraph 3.3.1, with reference to the basic harmonic wave:

$$E_d^*(\omega) = \frac{\gamma - \gamma_0}{\Delta A_0/A_0} = \frac{\Delta\gamma_0\cos\delta}{\Delta A_0/A_0}\,sin\omega t + \frac{\Delta\gamma_0\sin\delta}{\Delta A_0/A_0}\,cos\omega t \qquad (4.2.3.2.8)$$

Usually the two multiplying factors are indicated with E' and E'':

$$E_d{}' = \frac{\Delta\gamma_0\cos\delta}{\Delta A_0/A_0} = E_0\cos\delta \qquad (4.2.3.2.9)$$

$$E_d{}'' = \frac{\Delta\gamma_0\sin\delta}{\Delta A_0/A_0} = E_0\sin\delta \qquad (4.2.3.2.10)$$

From eq. 4.2.3.2.9 and 4.2.3.2.10 it is found:

$$tan\delta = \frac{E''}{E'} \qquad (4.2.3.2.11)$$

That gives an immediate direct view about the liquid/solid behavior trend of the surface. In general E' is linked to the solid contribution whilst E'' to the liquid one.

As harmonic function are considered, often, it is more convenient to use complex functions. Therefore, the previous equations may be written as:

$$E_d^*(i\omega) = E' + iE'' \qquad (4.2.3.2.12)$$

The complex modulus, representing the relationship between the surface modification of an interfacial layer and the related dilatational stress (Ravera, Loglio and Kovalchuk 2010); (Seta et al. 2012)) at small oscillation amplitudes. The two contributions are: the in phase storage modulus, E' (the real part of E_d^*), and the out phase loss modulus, E'' (the imaginary part E_d^*).

In such a way, as already said, storage modulus E' represents the real part coefficient, and is linked to the solid like behavior, whilst E'' is the imaginary part coefficient accounting for the liquid like one. The absolute value of the complex modulus reads:

$$|E_d^*(i\omega)| = \sqrt{E'(\omega)^2 + E''(\omega)^2}$$
(4.2.3.2.13)

If E' and E" are interpreted in terms of surface viscoelasticity, according to eq.3.3.1.4, it holds:

$$E' = E_0$$
(4.2.3.2.14)

and

$$E'' = \omega\eta$$
(4.2.3.2.15)

On the light of the above, to determine the amplitude capable to guarantee the linear response region, the complex modulus was reported versus amplitude, at an intermediate working frequency, and then the best amplitude was determined. The plot was obtained by combining several time sweep at fixed amplitude and at fixed frequency, by determining the value of the equilibrium stress realized and the equilibrium complex modulus was found. Once chosen a good amplitude, the complex modulus frequency dependence was obtained with a procedure similar to that above, i.e. time sweep test were performed to choose the amplitude at a fixed frequency. Then the equilibrium value was read and reported in a modulus/frequency diagram.

4.2.3.3 Shear oscillation test

The interfacial shear characterization has been done by means of an Interfacial Shear Rheometer (IRS400, KSV Intruments, Helsinki, Finland), where a magnetic needle is positioned at the interface and may move according to an imposed magnetic field. In this way the interface is subjected to a shear deformation.

The solution is placed in a Petri plate and the magnetic needle is gently put on the solution surface in such a way that it lies on that one. By two Helmholtz coils, an oscillating magnetic field of I_0 amplitude is generated (Brooks et al. 1999):

$$I = I_0 e^{i\omega t}$$
(4.2.3.3.1)

The magnetic field is converted into an oscillating force, F, applied to the needle along x-direction:
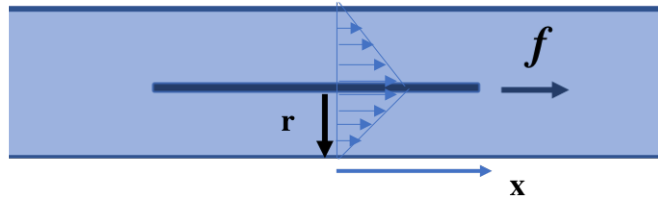
Figure 4.2.5.1 Schematic representation of rod and the force *f* applied

As already described in previous paragraph 3.4, it holds:

$$f = f_0 e^{i\omega t} \tag{4.2.3.3.2}$$

Consequently, the needle is forced to move in an oscillatory mode along the x-direction. A camera captures the position of the needle during the oscillatory movement. The shear deformation is realized between the rod and the glass slide.

Then, the shear time dependent displacement of the needle became:

$$\xi = \xi_0 e^{i(\omega t + \delta)} \tag{4.2.3.3.3}$$

The displacement ξ may be assumed as a measure of the strain.

By evaluating either the stress, from the imposed potential force, and the recorded strain, the instrument may give information about the mechanical resistance of the interface during a shear kinematic.

As already said, it is very crucial to know the rheological behaviour of the subphase liquid because the velkocity profile depends on the solution of the motion equation. Due to the expected rheological behaviour, it was considered a viscoelastic behaviour as described in paragraph 3.4. It is possible to apply small amplitude sinusoidal oscillating field, which allows neglecting higher harmonics. Thus, under these linear conditions, the shear mechanical resistance of the surfaces may be written in terms of interface complex shear modulus, G_s^*:

$$G_s^*(\omega) = \frac{\sigma_s e^{i\omega t}}{\gamma_0 e^{i[\omega t - \delta(\omega)]}} = \frac{f_0 e^{i\omega t}}{\xi_0 e^{i(\omega t + \delta)}} \tag{4.2.3.3.4}$$

Again it is useful to split the shear complex modulus $G_s^*(i\omega)$, into the storage and loss moduli, G_s' and G_s'', and according to eqs.3.4.34-35 it is found:

$$G_s^*(i\omega) = \frac{f_0}{\xi_0} e^{i\delta(\omega)} = G_s'(\omega) + iG_s''(\omega) \tag{4.2.3.3.5}$$

it holds:

$$tan\delta = \frac{G_s''}{G_s'} \tag{4.2.3.3.6}$$

That gives an immediate direct view about the liquid/solid behavior trend of the surface in shear kinematic. Generally, *G'* is linked to the solid contribution whilst *G''* to the liquid one. The complex modulus represents the relationship between the surface modification of an interfacial layer and the related shear stress. At small shear oscillation amplitudes, the in phase storage modulus *G' is* the real part of $G_d^*(i\omega)$, whilst the out phase loss modulus *G''* is the imaginary part $G_d^*(i\omega)$.

In such a way, as already said storage modulus *G'* is linked to the solid like behavior, whilst *G''* accounts for the liquid like one. The absolute value of the complex modulus reads:

$$|G_d^*(i\omega)| = \sqrt{G'(\omega)^2 + G''(\omega)^2} \qquad (4.2.3.3.7)$$

The instrument allows to verify the linearity region by comparing the shape of the resulting wave for different amplitude vales. If the amplitude is small enough, the higher harmonics are neglectable and the ξ-wave appears to be a cosine function as is the applied force, otherwise an amplitude sweep is necessary.

4.2.3.4 Surface stress-relaxation test

Because the time dependency behavior shown by the considered interfaces, the investigated interfacial layers were studied by means of a relaxation test. The surface layer response following a given perturbation was monitored, i.e. after a fast or slow compression/expansion of the drop with a given volume variation (Wustneck et al. 1997; Saulnier et al. 2001). This technique is useful only for investigation in a short time range, because, in the long time range, the evaporation effects become too great. It is worthy to note that the use of the pendant drop to carry out stress relaxation tests is advantageous because it avoids the onset of Marangoni effects (Wustneck et al. 1999).

The measurements were done by applying a square wave perturbation and the ADSA method to evaluate surface parameters. The tests were carried out by creating a protein solution drop at the air interface and by monitoring the surface tension decrease until the surface tension reaches a stationary state (see paragraph 3.3), then five different kind of square waves were imposed with different period. The basic idea of this measurement technique is to induce a perturbation of a surface starting from an equilibrium condition and to observe the re-equilibration phenomenon (Wustneck et al. 1997).

The initial volume of the drop was 9 ml and the stress relaxation was analyzed out of linearity region (ΔV>10%), for different wave periods, *T,* as indicated in Table 4.2.3.4.1. The measurements were repeated twice.

T wave period [s]	500	300	180	60

Table 4.2.3.4.1 Values of the wave periods in the relaxation test setup

In the Figure 4.2.3.4.1 a typical example of a stress relaxation test is shown.
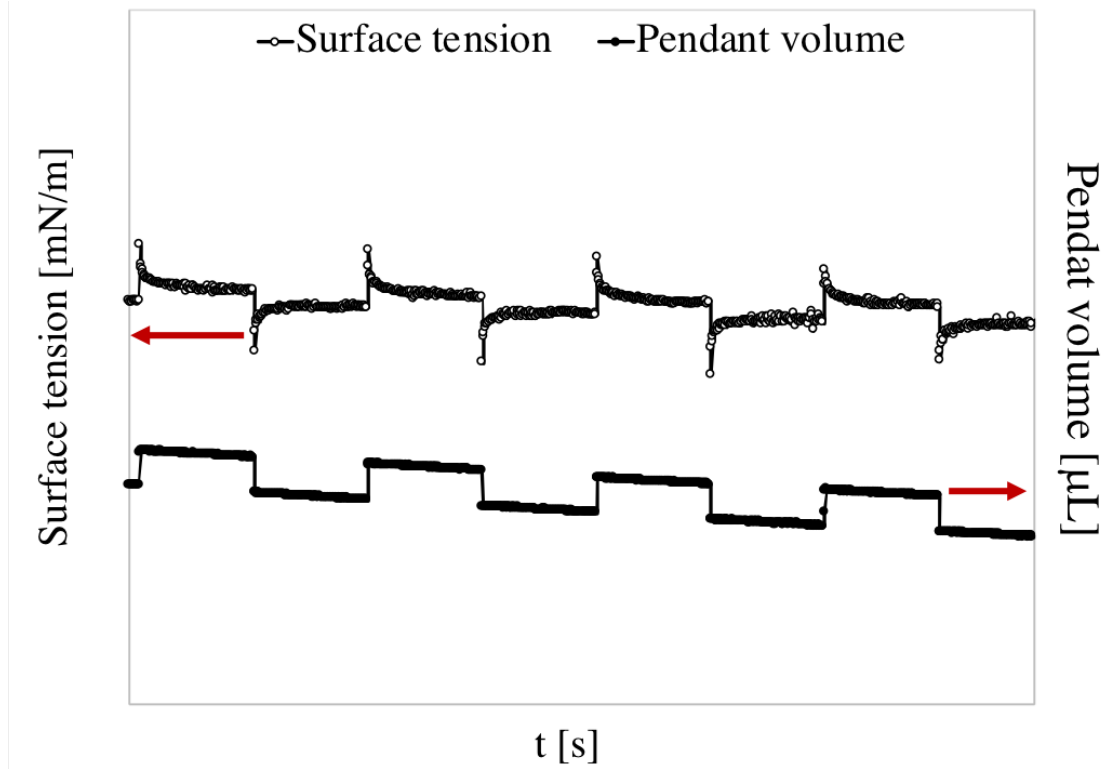
Figure 4.2.3.4.1 Typical trend in stress relaxation test

In particular, the experiments consist in generating a drop of a given volume. Then, an increase and decrease of the drop volume is realized by a fast movement of the syringe plunger in order to approximate a step variation. Repeating this different times, a square wave of volume is obtained, and, consequently, the drop area will change with an amplitude ΔA. From this variation, it results a change of the interfacial tension, $\Delta\gamma$, thus the dilatational effective surface elasticity, E_d, and the dilatational viscosity, η_d, may be written as (Wustneck et al. 1997):

$$E_d\ (t)=\Delta\gamma/(\Delta A/A_0) \qquad\qquad (4.2.3.4.1)$$

$$\eta_d\ (t)=\Delta\gamma/((dA/dt)/A_0) \qquad\qquad (4.2.3.4.2)$$

Owing to any proposed constitutive equation, these parameters will assume different forms.

4.2.4 Rheological data interpretation

Surface rheological data can be interpreted by different theoretical model based on the superposition principle with the consequence that viscous and elastic effects may be linearly assumed. Under dilatational kinematics, where both deformation and tension are isotropic, the two parameters E and η_d (see eq. 2.5.40) are obtained. Analogously, for shear deformation, G and η parameters (see eq. 2.5.41) are found.

The constitutive equation is the linear viscoelastic Maxwell model (eq.s 2.5.46-47) applied to surfaces. On the contrary, it may be proposed, as already done for the bulk behavior, that the material possess its own behavior, without assuming a sum the two contributions. In this case fractional derivatives are necessary to be introduced (see eq.s 2.6.1-2) and the Scott Blair model may be used: this was limited to the dilatational kinematics.

4.2.4.1 Dilational oscillating data

The data obtained by the oscillatory dilatation test were interpreted with a single springpot Scott Blair element. The starting point is the surface complex modulus, split into the storage and loss moduli:

$$|E_d^*(\omega)| = \sqrt{E'(\omega)^2 + E''(\omega)^2} \qquad (4.2.4.1.1)$$

The phase angle may be expressed in terms of the two shear moduli, E' and E'':

$$tan\delta = \frac{E''}{E'} \qquad (4.2.4.1.2)$$

In the case of a single Maxwell element it holds eq. 2.5.46, that for an isotropic dilatational becomes:

$$\frac{d}{dt}\Delta\gamma + \frac{E_0}{\eta_D}\Delta\gamma = 2E_0A_0\frac{dA}{dt} \qquad (4.2.4.1.3)$$

Where E_0 and η_D are the model material parameters, and the ratio between the two model parameters gives the surface relaxation time τ_D:

$$\tau_D = \frac{\eta_D}{E_0} \qquad (4.2.4.1.4)$$

The values of the storage E', and loss E'', moduli become:

$$E' = E_0\frac{\omega^2\tau_D^2}{1+\omega^2\tau_D^2} \qquad (4.2.4.1.5)$$

$$E'' = E_0\frac{\omega\tau_D}{1+\omega^2\tau_D^2} \qquad (4.2.4.1.6)$$

The loss tangent is therefore:

$$tan(\delta) = \frac{1}{\omega\tau_D} \qquad\qquad (4.2.4.1.7)$$

The value of E_0 is obtained from the experimental values of $E^*_{d,exp}$ and $\tau_{D,exp}$:

$$E_0 = E^*_{d,exp} \frac{\sqrt{1+\omega^2\tau_D{}^2}}{\omega^2\tau_D{}^2} \qquad\qquad (4.2.4.1.8)$$

From these date the figure 4.2.4.1 is obtained:
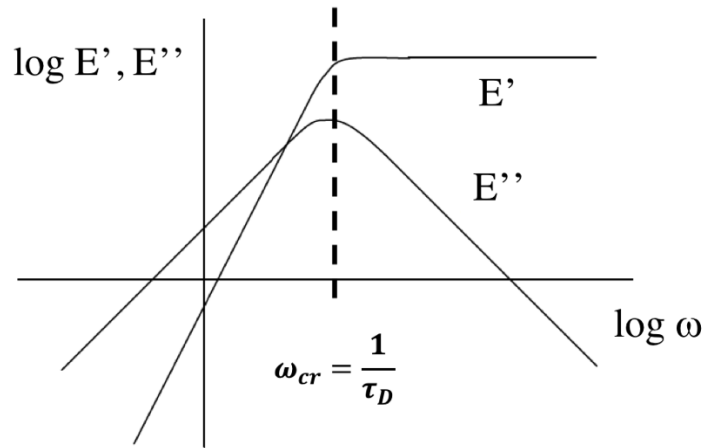
Figure 4.2.4.1 Diagram of E' and E'' for a material with viscoelastic behavior

It is worthy to note that it is evident a critical value of the frequency corresponding to:

$$\omega_{cr} = \frac{1}{\tau_D} \qquad\qquad (4.2.4.1.9)$$

At this frequency it results:

$$E' = E'' = E_0/\sqrt{2} \qquad\qquad (4.2.4.1.10)$$

And:

$$E^*_d = E_0/\sqrt{2} \qquad\qquad (4.2.4.1.11)$$

Finally, for $\omega < \omega_{cr}$ it results:

$$E' \propto \omega \qquad\qquad (4.2.4.1.12)$$

$$E'' \propto \omega^2 \qquad\qquad (4.2.4.1.13)$$

Whilst when $\omega > \omega_{cr}$, it holds:

$$E' \sim E_0/2 \qquad\qquad (4.2.4.1.14)$$

And

$$E'' \propto \omega^{-1} \qquad\qquad (4.2.4.1.15)$$

When applying Scott Blair model (eq.2.6.1) to the dilatational oscillation, it results:

$$E^*(\omega) = \mathbb{E}(i\omega)^\alpha \qquad\qquad (4.2.4.1.16)$$

That can be split into the storage and loss moduli according to:

$$E'(\omega) = \mathbb{E}\omega^\alpha cos(\pi\alpha/2) \tag{4.2.4.1.17}$$

$$E''(\omega) = \mathbb{E}\omega^\alpha sin(\pi\alpha/2) \tag{4.2.4.1.18}$$

The loss angle is then:

$$tan(\delta) = \frac{E''(\omega)}{E'(\omega)} = tan(\pi\alpha/2) \tag{4.2.4.1.19}$$

The value of the complex modulus assumes the form

$$|E_d^*(\omega)| = \sqrt{E_d'(\omega)^2 + E_d''(\omega)^2} = \mathbb{E}\omega^\alpha \tag{4.2.4.1.20}$$

A log-log plot of the complex modulus versus frequency is a straight line with a slope α, as depicted appears as in fig 4.2.4.1.2.
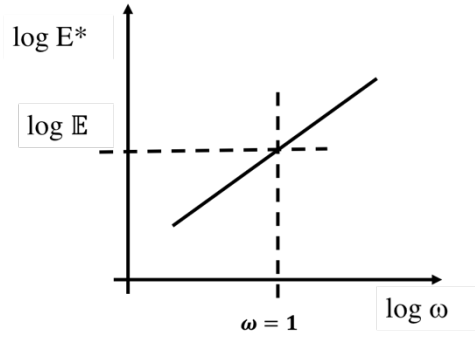
Figure 4.2.4.1.2 Diagram of E* vs frequency for Scott Blair model

The slope of the curve gives a value of the parameter α and the value of E_d^* at a frequency of 1 Hz, gives the value of the quasi-property $\mathbb{E}$.

4.2.4.2 Stress-Relaxation data interpretation

There are several relaxation models to interpret the stress-relaxation behavior (Saulnier et al. 2001), if the relaxation mechanism is assumed to be interpreted in terms of Maxwell viscoelastic model, an exponential relaxation trend is assumed.

Based on the William-Watts equation, the following equation, suggested by Saulnier, is found:

$$ln\frac{\pi(t)-\pi_\infty}{\pi_0-\pi_\infty} = -\left(\frac{t}{\tau}\right)^\beta \tag{4.2.4.2.1}$$

where τ is the average relaxation time, the exponent β varies between 0 and 1 and describes the intensity distribution or spreading of the relaxation spectrum. In particular, $\beta=1$ is referred to a single relaxation time and therefore to a Maxwell mode. Whilst $\beta < 1$ if a distribution with a long tail of short relaxation time is considered, as a consequence the named relaxation time, τ, results very close to the peak of a continuous relaxation spectrum.

Thus, from eq.4.2.4.2.1, it is possible to evaluate the dilatational time dependent surface elasticity $E_d(t)$ as:

$$E_d(t) = E_0 \exp\left(-\frac{t}{\tau}\right) \qquad (4.2.4.2.2)$$

The value of E_0 is measured as (Wustneck et al. 1997):

$$E_0 = \frac{\gamma_0 - \gamma_\infty}{\Delta A / A_0} \qquad (4.2.4.2.3)$$

Thus finally the experimental relaxation modulus reads:

$$E_d(t) = \frac{\Delta \gamma}{\Delta A / A_0} \exp\left(-\frac{t}{\tau}\right) \qquad (4.2.4.2.4)$$

The initial slope measures the value of τ experimentally.

The viscosity, η_d, may be found by the Maxwell model as:

$$\eta_d = E_d(t) \cdot \tau \qquad (4.2.4.2.5)$$

If the Scott Blair model is considered, from the $\mathbb{G}$ and α parameters evaluation, substituting the step-strain deformation in the constitutive equation for the spring-pot and making the Laplace transform, it is possible to predict the relaxation modulus (Faber, Jaishankar and McKinley 2017b, Jaishankar and McKinley 2013):

$$E_d(t) = \frac{\mathbb{G} t^{-\alpha}}{\Gamma(1-\alpha)} \qquad (4.2.4.2.6)$$

where Γ is the Gamma function. In addition, in this case the initial slope determines the value of the parameter α, and consequently at $t=1s$ the quasi property $\frac{\mathbb{G}}{\Gamma(1-\alpha)}$ is evaluated.

Furthermore, from the Scott-Blair analysis and by the experimental measurements, it is possible to evaluate the technological parameters as firmness and springiness of the interface. These two properties are classically evaluate in bulk rheology, whilst in this work, the Scott-Blair analysis will be applied to interfaces. It is found that firmness and springiness read:

$$F(t_f) = \mathbb{G}\Gamma(1+\alpha)t_f^{-\alpha} \qquad (4.2.4.2.7)$$

$$S = \frac{-\Delta t_s^{(\alpha-1)}}{\mathbb{G}\Gamma(1+\alpha)} \qquad (4.2.4.2.8)$$

The firmness is a measure of the consistency of the interface, the springiness is defined as "a rate at which a sample springs back", to give a measure of the ability to recover the deformation (Faber, Jaishankar and McKinley 2017a).

4.3 Results and discussion

4.3.1 Bradford protein concentration evaluation

On the sample solutions of the proteins, the Bradford method was performed to know the real protein solubilized in the MilliQ water. This method was carried out because the scientific literature reports poor solubility of plant proteins and solubility values strongly dependent on pH (Tang et al. 2006a). In Table 4.3.1 the real solubilized quantity of protein and the load quantity are reported .

	pH [-]	Solubilized VP w/w% [-]	Loaded VP % w/w [-]
H	6.8±0.1	0.10±0.01	0.47
S	7.0±0.1	0.40±0.02	0.90
BR	5.8±0.1	0.070±0.001	0.80

Table 4.3.1.1 pH solution values and real protein concentration by Bradford assay kit evaluation

From the Bradford evaluation, it was observed a partial solubilization of the vegetable proteins in water according with literature (Tang et al. 2006a) with only a low quantity of proteins solubilized. All the data are reported referring to the VP quantity loaded.

4.3.2 Static surface analysis

Through the interfacial analysis in static mode, the transient surface tension was evaluated for the protein samples and, from these measurements, the surface tension equilibrium values were calculated (Seta et al. 2012; Camino et al. 2009) to obtain the equilibrium adsorption isotherms. The results are reported in Figure 4.3.2.1.
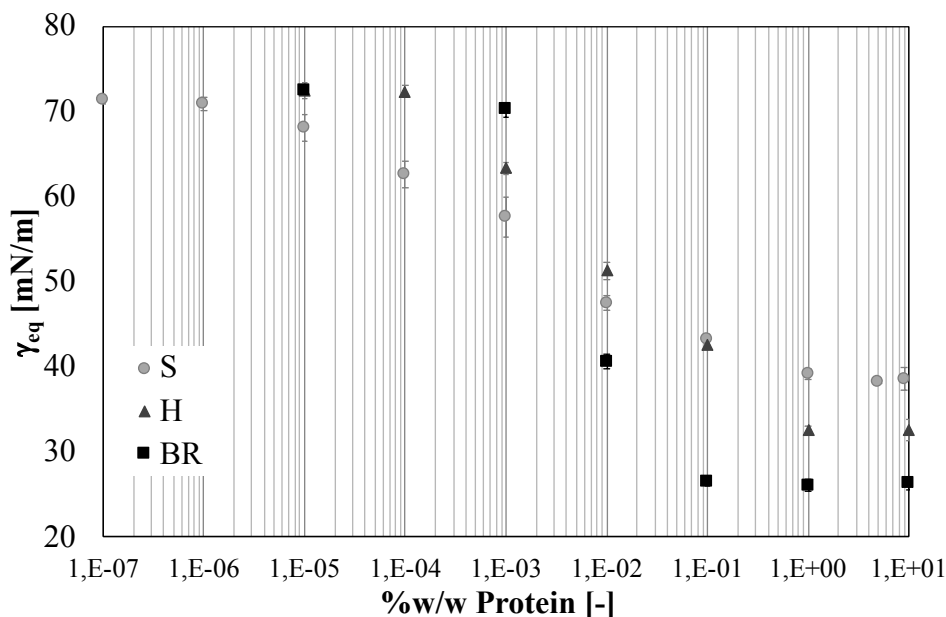
Figure 4.3.2.1 Equilibrium adsorption values for soy, hemp and brown rice protein sample

As for several protein and emulsifier (Seta et al. 2012) and as reported by Ortiz et al. (2003) and Nino et al. (2005) for soy globulins, it can be observed a sigmoidal trend of the equilibrium value, with the presence of two plateau: at low protein concentration, where the equilibrium surface tension values are constant because the surface is free of surfactant agents, and at high protein concentration, because the saturation effect of the proteins that migrate to interface and carry out to decrease the surface tension. This last plateau correspond to the CMC (Critical Micellar Concentration), namely the equilibrium surface tension values after which the interfacial tension doesn't change with the protein concentration increase, because the surfactant agents have completely covered the interface out to saturation conditions, with a consequent formation of a multilayers beneath the primary monolayer (Nino et al. 2005). For soy and hemp protein samples, the CMC is reached at 1%w/v concentration, in the brown rice protein case, this condition is already reached at 0,1%w/v. By comparison with other proteins from animal (Seta et al. 2012; Baeza et al. 2006; Nino et al. 2005) and gluten sources (glutenin and gliadin) (Li, Dobraszczyk and Wilde, 2004; Bos, Dunnewind and van Vliet 2003), the proteins tested were showed a good surface activity, comparable with that of previous proteins.

The pH value was measured at the CMC for all the proteins and the values are reported in Table 4.3.2.1.

ID sample	pH [-]
S	*8.33±0.04*
H	*6.71±0.09*
BR	*5.47± 0.02*

Table 4.3.2.1 pH values of protein solutions

The measured pH conditions are in a range of good solubility for both fraction 7S e 11S of soy proteins and in a favorite condition of surface effects (Ortiz et al. 2003). Furthermore, in this pH condition, the 11S is the glycinin form mainly present in solution (Martin et al. 2002). Also for hemp proteins the pH condition is favorite to their solubility (Malomo et al. 2014), but it is not available literature information about their surface effect as pH function. In the CMC condition, it was compared the surface tension trend for all the proteins during time and the results are reported in Figure 4.3.2.2.
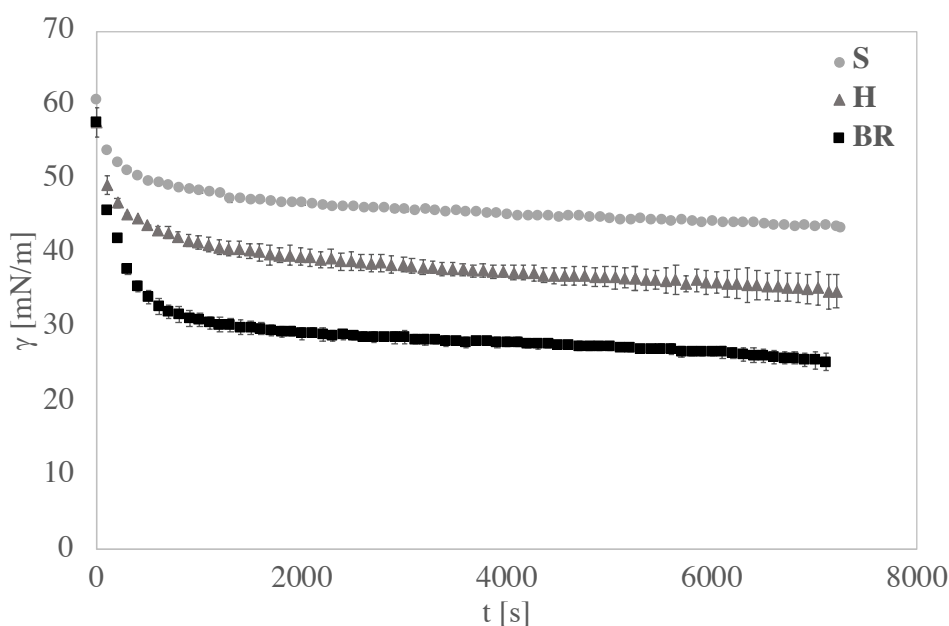
Figure 4.3.2.2 Transient surface tension in soy, hemp and brown rice samples

From samples comparison, it can be observed that soy has a lower surface activity compared to the brown rice which shows a greater surface activity. Hemp proteins shows an intermediate surface effect. From literature information (Ortiz et al. 2003), it is possible to link the soy surface effect to its β-conglycinin (7S) fraction that is its "light" fraction (MW~150 kDa (Barac et al. 2004; Martin et al. 2002) and that probably is the first to diffuse and to arrive at the interface, thanks to its poor steric size. The hemp surface activity is done from its edestin fraction that represents the 82% of the proteins sample, cause to its molecular

weight (~350 kDa (Barac et al. 2004)), it isn't able to reduce the surface tension as fast as soy proteins. To support this hypothesis, the surface tension data were analyzed using the kinetic approach, that allows to obtain kinetics parameters able to characterize several surface/interfacial mechanisms.

As reported in literature, the main features of the adsorption kinetics of proteins surfactants can include (Seta et al. 2012):

- diffusion from bulk to interface of proteins;

- molecular adsorption and rearrangement within interfacial layers;

It is possible to describe the first step using the Ward-Torday equation:

$$\pi = \gamma(t) - \gamma(t_0) = C_0 KT \frac{D_{diff}t}{\Pi} \tag{4.3.8}$$

where $\gamma(t)$ and $\gamma(t_0)$ are the surface tension at any time t and t=0, respectively, C_0 is the bulk concentration, K is the Boltzman constant, T is the absolute temperature, D_{diff} in the diffusion coefficient, Π in the pi greco value. From the plot of π versus $t^{1/2}$ it is possible to obtain the diffusion rate as the slope of the curve, that is linear if the diffusion is the controlling process (Seta et al. 2012; Camino et al. 2009). The second step can be described with the Graham and Phillips equation:

$$ln\frac{\pi_f - \pi_t}{\pi_f - \pi_0} = -k_i t \tag{4.3.9}$$

where π_f, π_0 and π_t are the surface pressure at the last time of the adsorption, at the first time and at any time. k_i is the first order constant. From the data plot, it is possible to differentiate two slopes, the first slope can be related to the adsorption constant, k_{ads}, and the second to the rearrangement constant, k_r(Seta et al. 2012; Camino et al. 2009).

	Soy Protein		*Hemp Protein*		*Brown Rice Protein*	
C	LAG time		LAG time		LAG time	
%w/w	[s]	[min]	[s]	[min]	[s]	[min]
10	-	-	-	-	-	-
1	-	-	-	-	-	-
0.1	-	-	-	-	5.1	
0.01	5	0.1	100	1.7	223	0.1

| 0.001 | 2207 | 36.8 | 1940 | 32.3 | | |
| 0.00001 | 5843 | 97.4 | | | | |

Table 4.3.2.2 LAG phase of the three sample investigated

From Table 4.3.2.2 it is worth noticing that samples with higher molecular weight are characterised by an initial period where no change in γ is observed (called induction or lag time). All the investigated samples show the presence of a LAG phase for low concentrations. For soy proteins, the data is confirmed by (Martin et al. 2002). In particular, at the decreasing of the protein concentration, also the LAG time decreases. The soy sample shows a wider range of concentrations in which LAG phase's kinetics are assessable. This effect could be related to the two fraction present in the soy proteins, the 7S and the 11S. So many effects could be present at the interface and a retardation in the migration effect could be related to the competitive effect given by the two species present.

	k_{diff} [mN·m^{-1}*s$^{-0.5}$]		
C %w/w	*Soy Protein*	*Hemp Protein*	*Brown Rice Protein*
10	*too fast*	*too fast*	
1	*too fast*	*too fast*	*too fast*
0.1	*too fast*	0.78 ± 0.007	1.88 ± 0.01
0.01	0.76 ± 0.017	0.24 ± 0.002	0.47 ± 0.02
0.001	0.31 ± 0.012	0.18 ± 0.001	
0.00001	0.40 ± 0.044		

Table 4.3.2.3 Diffusion rate for the three samples analysed obtaine with the *Ward*-Torday equation.

From Ward-Torday equation, it was possible to evaluate diffusion rate for the three proteins, as reported in Table 4.3.2.3. From the kinetic analysis, the diffusion rate is too fast to be detected by experimental method used in this work, because the initial π value is greater than 10 mN/m (Seta et al. 2012; Camino et al. 2009). As the protein concentration decreases, the rate of diffusion decreases, as generally for surfactant species. From Graham and Philips fitting, the adsorption and the diffusion rates were evaluated and they are reported in Table 4.3.2.3 and Table 4.3.2.4 respectively.

	$k_{ads} \cdot 10^{\wedge 4}$

C	[s^{-1}]		
%w/w	*Soy Protein*	*Hemp Protein*	*Brown Rice Protein*
10	3.65 ± 0.05	2.34 ± 0.05	
1	3.50 ± 0.02	3.34 ± 0.02	2.5 ± 0.7
0.1	3.30 ± 0.02	5.95 ± 0.6	4.0 ± 0.1
0.01	2.40 ± 0.01	6.84 ± 0.8	5.0 ± 0.1

Table 4.2.2.3 Adsorption rate of the three vegetable proteins at A/W interface

From Table 4.3.2.3 it is possible to see the trend of the adsorption rates for the three proteins and it is possible observe the dependence with the concentration, which is different in the three cases. In fact, the soy proteins show an increase of the adsorption rate with the concentration increase in agreement with (Nino et al. 2005). While, for hemp and brown rice proteins, the trend is opposite and in particular, as the concentration increases the adsorption rate decreases. The different behavior of the three samples could be attributed to their different protein components from which they are composed. For soy sample, two different species are present in conspicuous parts, the 7S and the 11S, so probably the increasing trend which is possible to observe, is related to the possibility for the protein to adsorb more quickly thanks to its greater presence in bulk and consequently at the interface. For hemp and brown rice protein, the trend is opposite probably because of the steric hindrance of the two predominant fractions that characterize the two proteins, edestin and glutenine, respectively. In fact, these two proteins are more encumbered respect to 7S of the soy proteins, so probably as the amount of protein present increases, the difficulty of adsorption increases and consequently the adsorption rate decreases.

C	$k_{rearr} \cdot 10^{\wedge 3}$ [s^{-1}]		
%w/w	*Soy Protein*	*Hemp Protein*	*Brown Rice Protein*
10	1.03 ± 0.09	5.6 ± 0.3	
1	1.5 ± 0.5	5.5 ± 0.2	2.65 ± 0.78
0.1	1.3 ± 0.02	4.0 ± 0.3	2.95 ± 0.64
0.01	1.59 ± 0.05	3.2 ± 0.8	2.55 ± 0.21

Table 4.3.2.3 Rearrangement rate of the three vegetable proteins at A/W interface

The last step of the interfacial kinetics is the rearrangement and in the Table 4.3.2.3 the rearrangement rate was reported. There isn't an important dependence from the concentration for soy and brown rice proteins. The soy proteins show a rearrangement rate increment with the protein concentration increase, above the CMC, the rate remains constant.

Known the values of the three speed steps it is possible to observe the differences in the kinetics of the interfacial phenomena between the three proteins. For the diffusion step, it is possible to observe how the highest diffusion speed is that of the soy proteins, followed by the black rice proteins and, lastly, of the hemp. This result is in accordance with the molecular size of the proteins characterizing the three studies and leads us to think that in the case of soy sample, the interfacial phenomena are linked to the 7S fraction, smaller and more quick.

The adsorption step is the one that follows the diffusive step. Soy is the fastest to reach the interface, but it is not the fastest to adsorb. The trends in the three cases are different and therefore it is difficult to compare them. From the data analysis it appears as if the soy, once arrived at the interface, is slower to settle at the interface. This could be due to the fact that its hydrophobic sites are not well exposed and then it takes more time for them to adsorb. In the case of hemp proteins, the effect is certainly due to the high steric encumbrance of edestin, which, when present at the interface at high concentrations, has more difficulty in exposing the sites that will adsorb to the interface. Although less pronounced, this same effect is visible in the proteins of brown rice.

The last kinetic step is the rearrangement. Soy and brown rice rearrangement rates don't have an important dependence from concentration. Hemp protein rearrangement rate decrease with the concentration decrease, lower is the protein at the interface, lower is the rate at which the molecules are rearranged.

4.3.3 Small amplitude oscillating measurements

Through measurements in oscillating mode, it has been evaluated the dynamic dilatational modulus and loss angle as frequency function for the soy, hemp and brown rice samples in CMC condition. The preliminary amplitude sweep test was carried out to explore the linearity region.

Thus it is possible to evaluate the surface dilatational modulus E_d (Camino et al. 2009; Ravera et al. 2010; Seta et al. 2012) by using the following definition:

$$E_d = \frac{d\gamma}{\Delta A / A_0}$$ (4.3.3.1)

For small amplitude oscillations, E_d is referred as complex modulus that represents the relationship between the surface modification of an interfacial layer and the corresponding dilatational stress (Ravera et al. 2010; Seta et al. 2012). It is possible to calculate the storage modulus E' and loss modulus E'', being the phase and out phase moduli:

$$E_d = E' + iE'' = \frac{\Delta\gamma}{\Delta A / A_0} cos\delta + i \frac{\Delta\gamma}{\Delta A / A_0} sin\delta$$ (4.3.3.2)

The frequency sweep test has been obtained by evaluation of equilibrium values from the time sweep tests carried out at single frequencies (in twice).
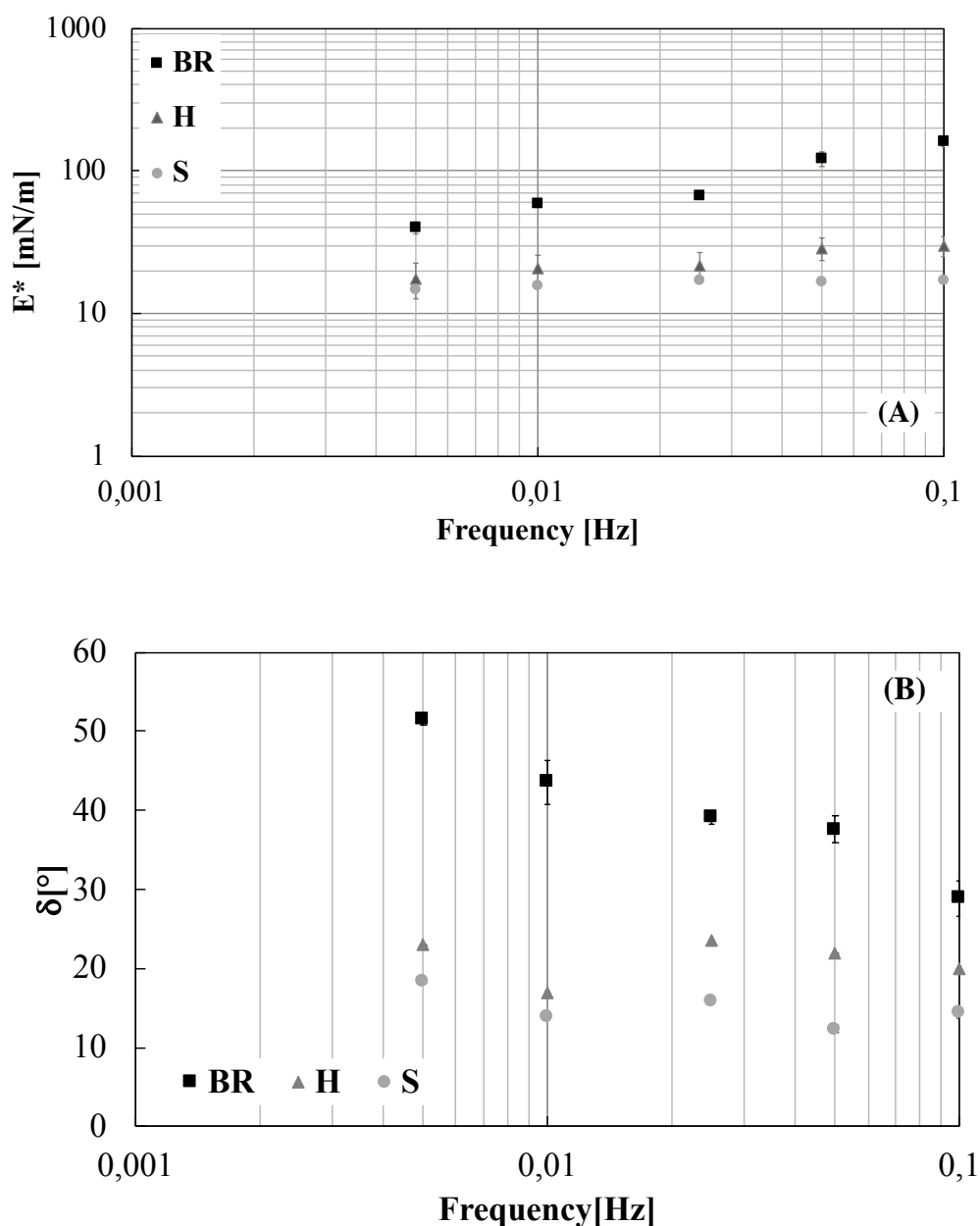
Figure 4.3.3.1 Surface dilatational moduli (A) and loss angle (B) as frequency function of the three samples analyzed

It is possible to observe a viscoelastic behavior and a solid-like behavior for all surface layers. From the slope of the dynamic modulus, it is possible to have a measure of the structuration of the interfacial film. So, from Figure 4.3.3.1 (A), the modulus slopes of the three proteins suggest that soy and hemp proteins, at the interface, give a more structured film and the frequency dependence of the interfacial film formed is low. The brown rice protein, instead of the previous, shows moduli more dependents from the frequency, so, less

structured and more flexible. From the loss angle analysis, as shown in Figure 4.3.3.1 (B), the soy gives a more hard interfacial structure, followed by hemp protein. The brown rice does an interface less solid-like with delta values, strongly depend from the frequency, and in all frequency range greater than the other two proteins investigated.

Respect to the classical animal proteins, as the casein (Bos, Dunnewind and van Vliet 2003), the vegetable proteins show good mechanical resistance, good structuration, so their use as substitute of the animal proteins, could be suggested.

4.3.4 Stress Relaxation test

The stress relaxation tests were carried out to investigate the time dependence of the interface in the three cases, when it is structured by the three different proteins. In order to see the whole process of relaxation it is necessary to wait for some time, between the measurements carried out, therefore, it was reported the measurements with longer times in which it is possible to observe the complete relaxation of the interface. For the soy sample this time is 250 s, while for the others two proteins is 500 s. In these times, the interface shows all the relaxation phenomena necessary to reach a new equilibrium status.
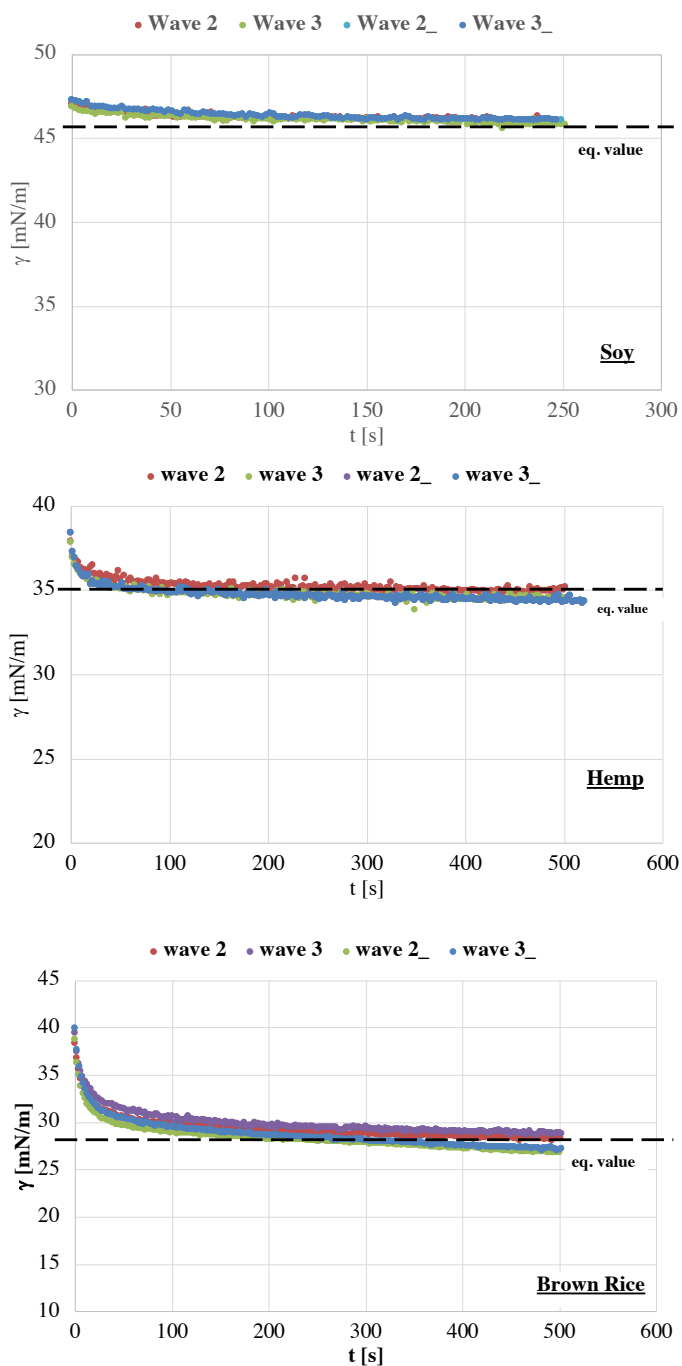
Figure 4.1.4.1 Surface tension of soy hemp and brown rice interfaces during expansion phase by square wave

From Figure 4.1.4.1 it is possible to observe the relaxation phenomena of the surface tension for the three interfaces analyzed. All samples reach the equilibrium value after the perturbation, but following different mechanisms. In particular, it is possible to note as the greater difference between the three interfaces is the elasticity shown during the perturbation. In particular, brown rice shows a good ability to change the actual state because the imposed disturb, but also a big ability to recovery their original state. This behavior could

113

be suggest greater value in elasticity and viscosity. Hemp shows a similar behavior, but less pronounced. Finally, soy interface is less influenced by the perturbation.

From compression wave analysis, in Figure 4.3.2.2 there are reported the trend of the surface tension in the three cases, when the drop is perturbed by a square wave with a quickly compression of the interface.
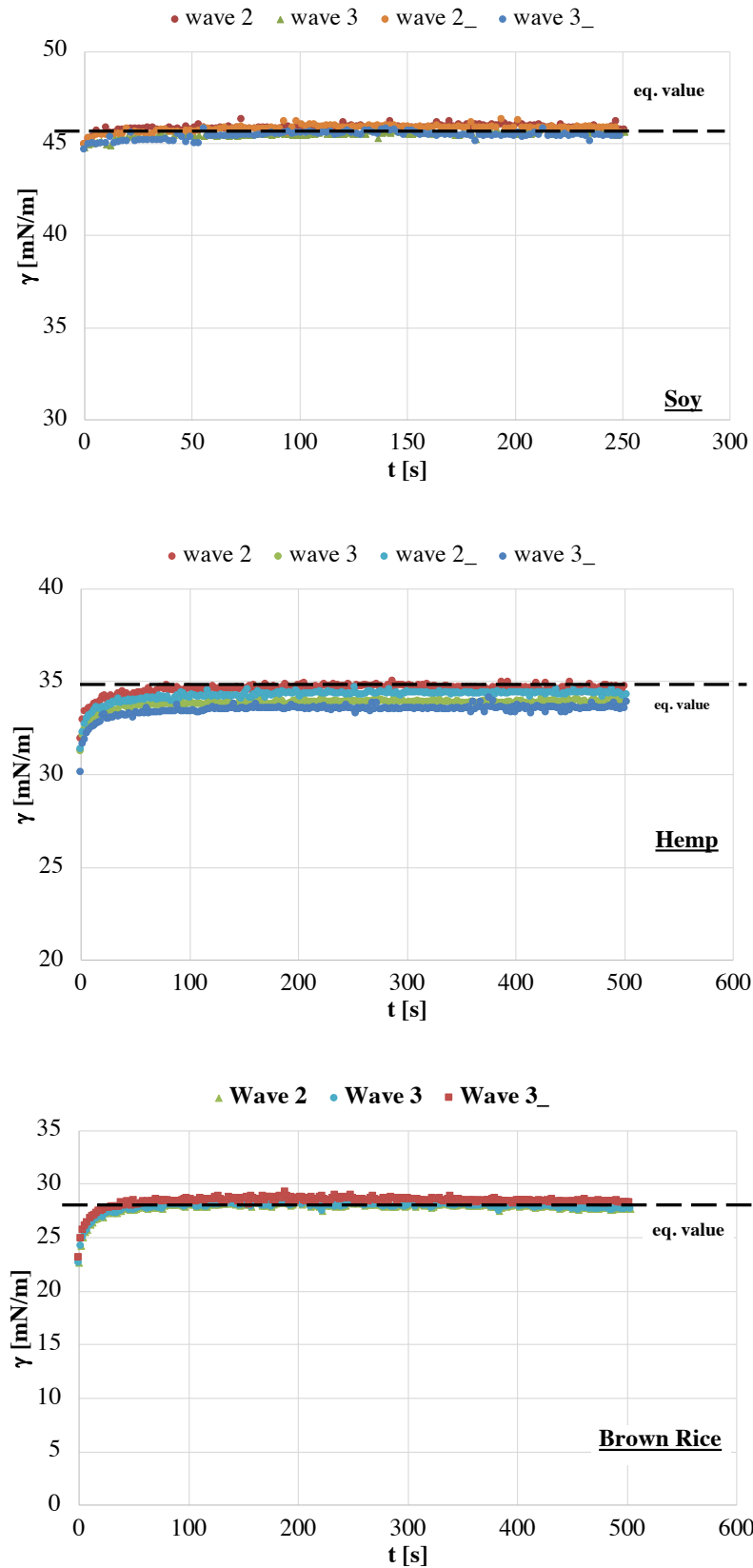
Figure 4.3.2.2 Surface tension of soy hemp and brown rice interfaces during compression phase by square waves

By a comparison between the expansion and compression plots, it is possible observe that the compression phase gives a faster recovery of the equilibrium condition than the expansion phase. Only hemp shows some differences. It is possible observe as the waves subsequent to the first aren't able to recover completely the equilibrium condition. It is probably caused by the big steric hindrance of the edestin.

4.3.5 Oscillating shear results

From shear surface analysis in oscillating mode, under small amplitude oscillations and in linearity, the surface moduli (G' and G'') were evaluated as frequency functions. The plot in Figure 4.5 shows the samples behavior.
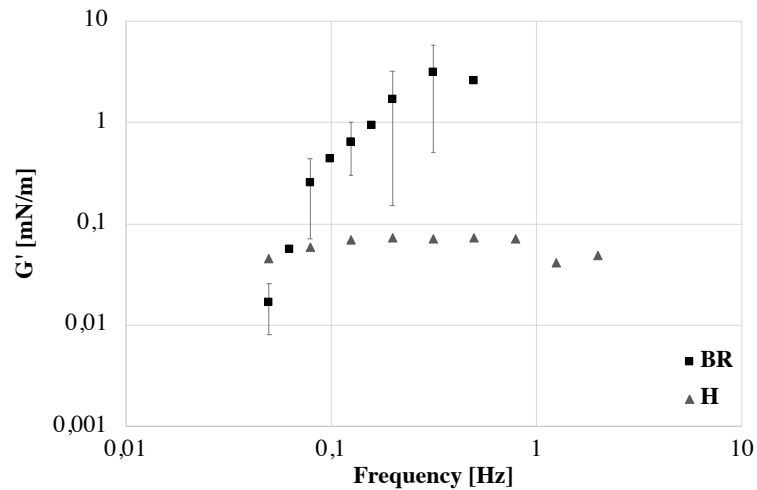

Figure 4.3 Frequency sweep test for the samples investigated
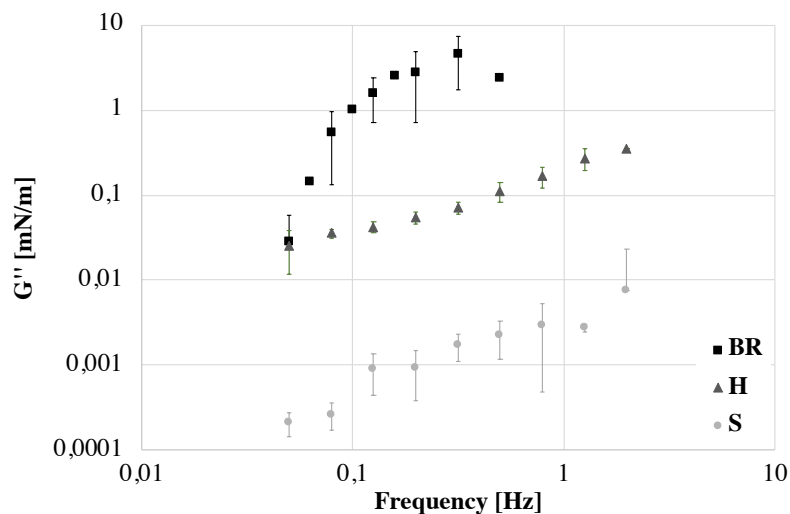

Figure 4.3.5.1 Frequency sweep test for the samples investigated

The Figure 4.3 Frequency sweep test for the samples investigated reports the G' values only for brown rice and hemp. The soy proteins give at the surface only a viscous effect and the surface solid contribute isn't evaluable. The brown rice gives rise to more consistent surface structure, but the slope of G' suggests a weak structuring degree. Hemp proteins at the surface give G' values low, but the slope suggests a greater structuration. These results are in agreement with the dilational analysis: brown rice increase the consistency of the surface but hemp protein is more structuring. From G'' evaluation it is possible to observe that brown rice shows greater viscosity than other proteins, hemp is intermediate and soy gives only a low viscosity at the surface. Brown rice and hemp, at low frequency shows a solid behavior but at high frequency the behavior is liquid-like. In the range between 0.1-1 Hz, for both proteins it is possible observe a cross of the moduli.

From a comparison between dilational and shear values, it is possible to note that the mechanical resistance in shear is lower than dilational kinematics, as classically found in literature.

4.3.6 Experimental data interpretation

4.3.6.1 Stress relaxation data interpretation

The stress relaxation data were interpreted to evaluate viscosity, relaxing time and elasticity of the interface covered by the three vegetable proteins analyzed. These parameters are reported in Table 4.3.6.1 for the first three wave of the relaxation process.

	τ [s]		
	Soy	*Hemp*	*Brown Rice*
I expansion	96.6 ± 3.0	37±1	74 ± 10
II expansion	160.5 ± 9.9	30±5	28.4 ± 0.6
III expansion	221.1 ± 11.2	27±1	20 ± 0.2
	β [-]		
	Soy	***Hemp***	***Brown Rice***
I expansion	0.369 ± 0.043	0.360±0.057	0.51 ± 0.09

II expansion	0.572 ± 0.098	0.360±0.007	0.39 ± 0.01
III expansion	0.538 ± 0.007	0.340±0.001	0.34 ± 0.14
	η_d [mN·s·m^{-1}]		
	Soy	*Hemp*	*Brown Rice*
I expansion	2.43 ± 0.11	4.48±0.11	5.1 ± 0.5
II expansion	2.38 ± 0.24	4.34±0.83	9.1 ± 0.5
III expansion	2.49 ± 0.07	4.09±0.45	10.0 ± 0.8
	E [mN/m]		
	Soy	*Hemp*	*Brown Rice*
I expansion	19 ± 2	33 ± 3	91 ± 9
II expansion	22 ± 2	33 ± 2	87 ± 5
III expansion	22 ± 4	43 ± 4	97 ± 8

Table 4.3.6.1.1 Viscosity, relaxing time and beta parameter, for the three samples, from expansion waves

From the fitting analysis with William Watts equation (Khare, Greenberg and Krantz 2003), the relaxing time is decreasing from soy sample to brown rice. The soy is slower to reach its initial equilibrium condition despite the fact that its deviation from its initial value is small. This behavior suggests a rigid interfacial structure and as the waves disturb the interface, the relaxing times increase and this effect becomes more pronounced. The hemp sample shows homogeneity in the relaxing time evaluated in the three expansions and relaxation happens more quickly than with soy sample. Finally, the brown rice interface is the faster to reach the initial equilibrium condition. The first time of the relaxation is greater than other two, probably because, being the first break of the interface, it requires more time for its reform. In Table 4.3.4.1.2, the relaxation parameters, in compression phase, has been reported.

	τ [s]		
	Soy	*Hemp*	*Brown Rice*
I compression	2.1 ± 1	$3 \cdot 10^{-7} \pm 1 \cdot 10^{-7}$	$2 \cdot 10^{-10} \pm 1 \cdot 10^{-10}$

II compression	17.8 ± 0.1	$4 \cdot 10^{-7} \pm 5 \cdot 10^{-7}$	$2 \cdot 10^{-11} \pm 2 \cdot 10^{-11}$
III compression	20 ± 3	$4 \cdot 10^{-7} \pm 6 \cdot 10^{-7}$	660 ± 100
	β [-]		
	Soy	*Hemp*	*Brown Rice*
I compression	0.09 ± 0.02	0.041 ± 0.002	0.04 ± 0.01
II compression	0.11 ± 0.02	0.038 ± 0.005	0.03 ± 0.01
III compression	0.130 ± 0.002	0.05 ± 0.01	0.48 ± 0.14
	η_d **[mN·s·m^{-1}]**		
	Soy	*Hemp*	*Brown Rice*
I compression	2.8 ± 0.3	5.0 ± 0.2	7.6 ± 0.3
II compression	2.9 ± 0.2	5.10 ± 0.06	6 ± 1
III compression	2.5 ± 0.08	2.3 ± 0.3	6.1 ± 0.5
	E **[mN/m^{-1}]**		
	Soy	*Hemp*	*Brown Rice*
I compression	21 ± 2	38 ± 2	56 ± 2
II compression	22 ± 1	38.4 ± 0.7	51 ± 3
III compression	19.3 ± 0.6	35 ± 5	94 ± 8

Table 4.3.4.1.2 Viscosity, relaxing time and beta parameter, for the three samples, from compression waves

From compression waves, it is possible to observe as viscosity and elasticity values are similar to expansion phase, but the great difference is with the relaxing time and beta factor. The time to recovery the equilibrium state, in compression phase, is much lower and also β coefficient decrease, indicating that the relaxation time that characterizes the compression phase is one. For the soy sample this effect is less evident, in fact although there is a decrease in the value of relaxation time changes of one the magnitude order. For hemp and brown rice

proteins the differences are very marked and the relaxation time changes of more the magnitude orders. Probably, this discrepancy is related to an unsuitable interpretation of the data and the William-Watts equation could deviate from experimental trend.

By comparison with oscillating measurements, it is possible to note that elastic modulus measured in oscillating mode is comparable with the same calculated in relaxation mode, as already verified by Saulnier with other materials (Saulnier et al. 2001).

Furthermore, it is interesting to compare the surface effect of the vegetable proteins investigated with the proteins that you want to replace. In static conditions, the surface activity of the proteins examined both is comparable with which of gluten protein. Li (Li, Dobraszczyk and Wilde 2004) studied the surface active part of gluten, gliadin, that has equilibrium surface tension about 48 mN/m, comparable with soy and hemp protein surface tension. Furthermore, the elastic modulus of gliadin is around a 30 mN/m, a value comparable with hemp protein modulus. The results were compared also with dairy proteins, as β-lactoglobulin, but in literature, the results are discordant among themselves and in some studies (Ulaganathan et al. 2017) the moduli values are greater than proteins investigated here, in other studies (Torcello-Gomez et al. 2011) the vegetable proteins studied seem to be greater. The last comparison is with casein, that is widely used in food products. It is possible to note that both the surface activity and the surface moduli of vegetable proteins are comparable with casein effect and, in particular, in the hemp case, it is greater (Bos et al. 2003).

4.3.6.2 Rheological Modelling

The rheological data, obtained in oscillating dynamic mode are fitted using the fractional constitutive model of the spring pot (Jaishankar and McKinley 2013, Faber et al. 2017b). From this interpretation, the quasi properties and the alfa exponent have been evaluated and they are reported in Table 4.3.6.2.1.

ID	$\mathbb{E}$	α
S	19±1	0,05±0,01
H	46±5	0,18±0,03
BR	508±91	0,49±0,06

Table 4.3.6.2.1 Spring-pot parameters for oscillating dilational data

$\mathbb{E}$ is a quasi property that measures of the consistency of the interface and α indicates how much the interface behaves as liquid or solid. From spring-pot parameters it possible to observe that the interface covered by brown rice shows the greater consistency, followed by hemp and finally by the soy protein. From the comparison of the alfa exponent, it is found that the interface with brown rice shows a more behavior, compared to the hemp and soy interfaces showing a more rigid structure, because the α exponents of these latter are lower. These results suggest that brown rice that shows a greater consistency to the interface, contemporary creates a flexible structure with a mobility that is markedly liquid. On the contrary, soya proteins cerate interfaces less consistent, but with a more rigid structures with the consequence of a solid-like behavior.

From the $\mathbb{E}$ e α parameters it is possible to model the relaxation modulus that is a fundamental rheological property, allowing to distinguish between solid and liquid behaviors. In the Figure 4.3.6.2.2 the relaxation moduli, $E\ (t) = \frac{\Delta\gamma(t)}{\Delta A(t)/A(t)}$, are reported for the three investigated interfaces:
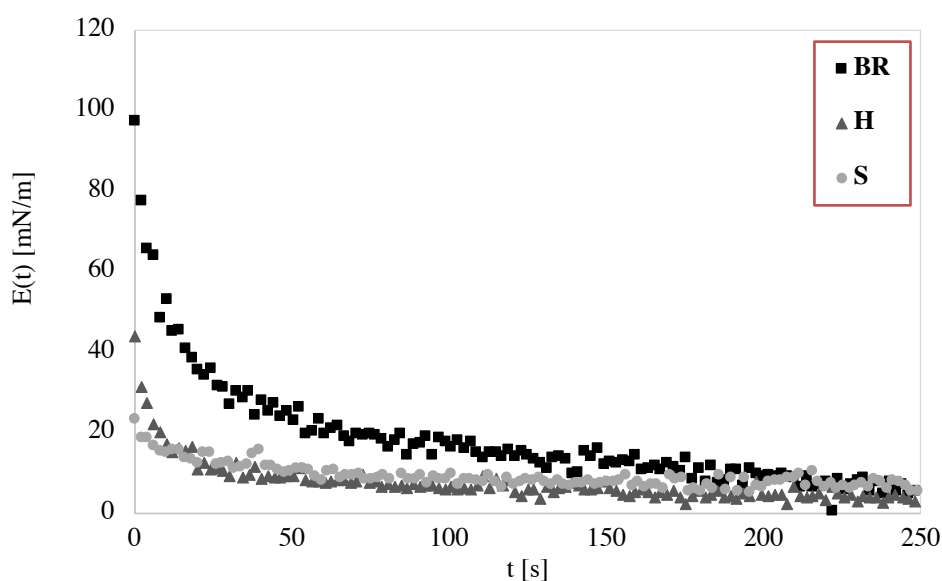

Figure 4.3.6.2.2 Relaxation modulus for the indicated interfaces

The relaxation moduli following compression and expansion waves have been interpreted with Scott-Blair model and the comparison between the experimental data and the model predictions is shown in Fig. 4.3.6.2.3, in which it is also reported the prevision with a simple one element viscoelastic Maxwell model ($E(t) = Ee^{-t/t_{relax}}$).
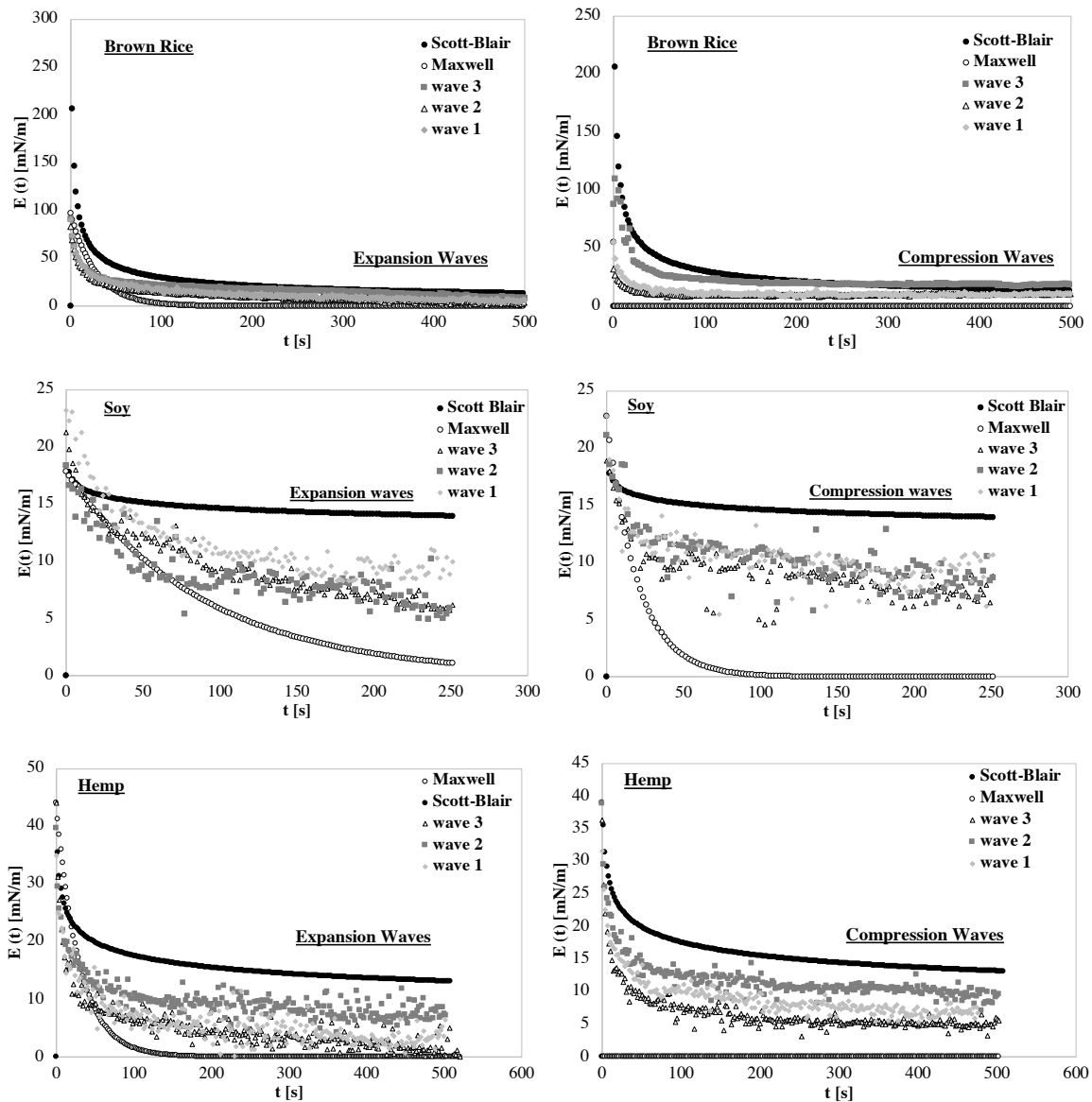
Figure 4.3.6.2.3 Comparison between the experimental relaxation modulus and prediction by Scott-Blair model and Maxwell model.

From the comparison between the two curves, the Scott-Blair model interprets the relaxation trend well but does not correctly predict the relaxation value. The best interpretation has been obtained for interface covered by brown rice proteins, although the initial estimated elasticity values are high compared to the experimental ones. The corresponding model of Maxwell does not match the data well because of the exponential that quickly brings to zero the value of E(t) which, in reality, although it decreases, does not lead to null values.

From the general comparison, Maxwell deviates greatly from the experimental data in the compression phase, where, due to the estimated low relaxation times, the estimated E(t) instantly collapses to zero.

Scott-Blair model interprets well the trend of the data even if it differs in the forecast of the correct value. this leads to think that probably an improvement of the prediction could be obtained by increasing the number of Scott-Blair elements to describe the behaviour of the interface. Indeed, literature has reported the use of 4 Scott Blair elements to predict the behaviour of a thicken up clear (TUC) solutions, demonstrating that the use of multiple elements of Scott Blair can provide an accurate prediction of the data comparable to that achievable with 50 elements of Maxwell (Wagner et al. 2017).

From Scott-Blair parameters, the technological parameters typically evaluated in bulk, firmness (F) and springiness (S) were evaluated and they are reported in Figure and Figure .
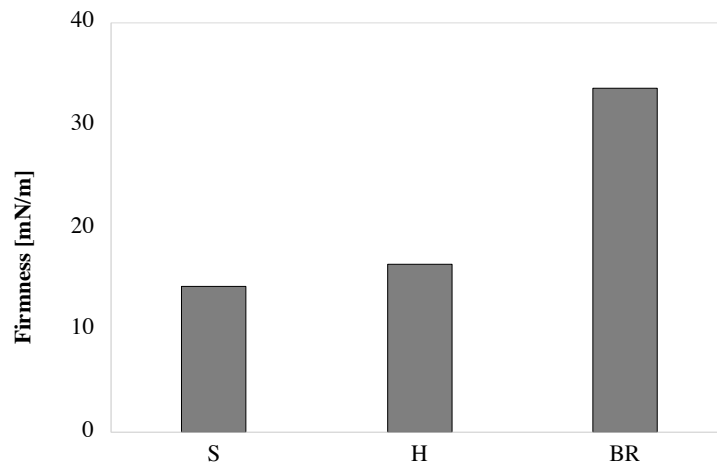

Figure 4.3.6.2.5 Firmness values for the three interfaces

The firmness is a direct measure of the consistency of the interface evaluated by Scott-Blair analysis. Also in firmness evaluation, the interface covered by brown rice shows the consistency greater. The soy and hemp proteins give lower consistency at the interface. The results are in agreement with the surface analysis effectuated.
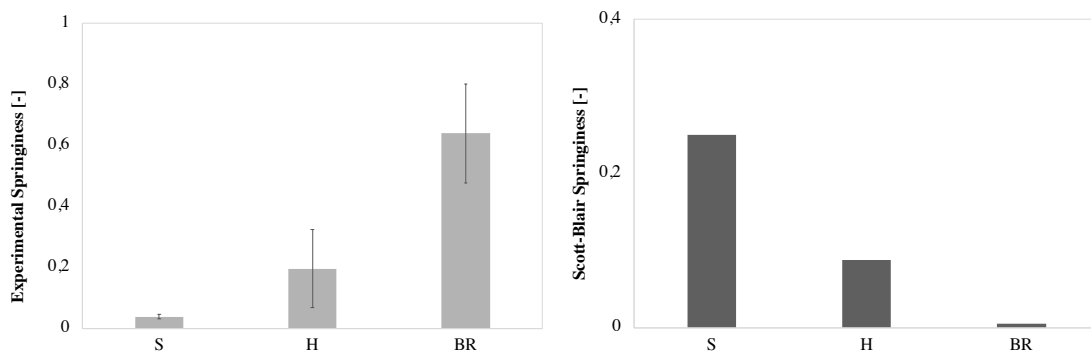

Figure 4.3.6.2.5 Springiness evaluation for the three interfaces

The springiness measure has been effectuated evaluating the slop of the relaxation phenomenon and it was also evaluated using the model of Scott Blair. The two plots show a big differences, in the values but also in the trend which is opposite in the two cases. Because the springiness is a direct measure of the elasticity of the interface and because the brown rice is the protein which gives the greater elasticity to the interface, the experimental evaluation is more plausible than the evaluation obtained by the analysis of Scott Blair. Also in this case, the use of a single element representing the behavior of the interface could have been penalizing and, in the case of springiness, disabling with respect to the result obtained.

4.4 Conclusions

There exists an increasing interest for the use of the vegetable protein for the formation and stabilization of emulsions and foams. The demand for high-safe, quality and health foods with good nutritional value has increased the interest for these proteins. In particular, vegetable source proteins could be used to produce the soft food, the sport drinks rich in proteins, the vegetable milk alternative to classical bovine milk, but also as an alternative to gluten to impart the necessary viscoelastic properties in gluten-free mixtures. In all these cases, the surface activity and the rheological properties of surface layers are   important factors, for the formation, stabilization and optimization of the input of energy involved in the emulsification or foaming process and for the stabilization of food products.

So, in this work, it was investigated the surface properties of soy, hemp and brown rice proteins, in static and dynamic conditions, in dilatational cinematic, with oscillating and square wave mode, using the pendant drop tensiometer and ASDA method and in shear cinematic using the magnetic rod rheometer.

From a comparison with the other proteins usually employed as foaming/emulsion elements of food products, it was observed that the three proteins have a comparable surface activity and mechanical surface properties, such as to make them excellent substitutes for animal proteins classically used in the food industry.

In small amplitude analysis, all samples show a solid like behavior and the dynamic moduli are comparable with which of other proteins usually used. In shear kinematic the mechanical resistance is lower than dilational case. As in shear as in dilational, the brown rice is the protein able to give the greater force to the interface. The rheological and surface kinetic properties evaluated are the best of the three proteins tested. Allows rapid formation of the

interfacing layer using fewer amounts of protein in solution, from place to more elastic and less rigid interfacing layers.

From the spring pot interpretation, the Scott Blair model used was interesting because it was able to predict the trend of the relaxation module, but it imposes an improvement because it is not able to predict correctly the values. In this work was made the first attempt to use the Scott Blair model at the interface and in dilation kinematic, to have a direct evaluation of technological parameters directly used to characterize a food.

4.5 References

Arashiro E.Y., Demarquette N. R., (1999) Use of the Pendant Drop Method to Measure Interfacial Tension between Molten Polymers. Materials Research, Vol. 2, No. 1, 23-32.

Amagliani, L., J. O'Regan, A. L. Kelly & J. A. O'Mahony (2017a) The composition, extraction, functionality and applications of rice proteins: A review. *Trends in Food Science & Technology*, 64**,** 1-12.

Amagliani, L., J. O'Regan, A. L. Keny & J. A. O'Mahony (2017b) Composition and protein profile analysis of rice protein ingredients. *Journal of Food Composition and Analysis*, 59**,** 18-26.

Barac, M. B., Stanojevic, S., P., Jonanovic, S., T., & Pesic, M., P. (2004) - Soy protein modification: A review. APTEFF, 35, 1-280.

Baeza, R., A. M. R. Pilosof, C. C. Sanchez & J. M. R. Patino (2006) Adsorption and rheological properties of biopolyrners at the air-water interface. *Aiche Journal*, 52**,** 2627-2638.

Berry, J. D., M. J. Neeson, R. R. Dagastine, D. Y. C. Chan & R. F. Tabor (2015) Measurement of surface and interfacial tension using pendant drop tensiometry. *Journal of Colloid and Interface Science*, 454**,** 226-237.

Biresaw, G., Liu, Z. S. & Erhan, S. Z. (2008) Investigation of the surface properties of polymeric soaps obtained by ring-opening polymerization of epoxidized soybean oil. Journal of Applied Polymer Science, 108(3), 1976-1985.

Bos, M. A., B. Dunnewind & T. van Vliet (2003) Foams and surface rheological properties of beta-casein, gliadin and glycinin. *Colloids and Surfaces B-Biointerfaces*, 31**,** 95-105.

Bos, M. A. & T. van Vliet (2001) Interfacial rheological properties of adsorbed protein layers and surfactants: a review. *Advances in Colloid and Interface Science*, 91**,** 437-471.

Bouyer, E., G. Mekhloufi, V. Rosilio, J. L. Grossiord & F. Agnely (2012) Proteins, polysaccharides, and their complexes used as stabilizers for emulsions: Alternatives to synthetic surfactants in the pharmaceutical field? *International Journal of Pharmaceutics,* 436**,** 359-378.

Brooks, C. F., G. G. Fuller, C. W. Frank & C. R. Robertson (1999) An interfacial stress rheometer to study rheological transitions in monolayers at the air-water interface. *Langmuir,* 15**,** 2450-2459.

Camino, N. A., O. E. Perez, C. Carrera Sanchez, J. M. Rodriguez Patino & A. M. R. Pilosof (2009) Hydroxypropylmethylcellulose surface activity at equilibrium and adsorption dynamics at the air-water and oil-water interfaces. *Food Hydrocolloids,* 23**,** 2359-2368.

Cho, D. H. & S. T. Lim (2016) Germinated brown rice and its bio-functional compounds. *Food Chemistry,* 196**,** 259-271.

Dickinson, E. (2003) Hydrocolloids at interfaces and the influence on the properties of dispersed systems. *Food Hydrocolloids,* 17**,** 25-39.

Dickinson, E. (2011) Mixed biopolymers at interfaces: Competitive adsorption and multilayer structures. *Food Hydrocolloids,* 25**,** 1966-1983.

do Carmo, C. S., A. N. Nunes, I. Silva, C. Maia, J. Poejo, S. Ferreira-Dias, I. Nogueira, R. Bronze & C. M. M. Duarte (2016) Formulation of pea protein for increased satiety and improved foaming properties. *Rsc Advances,* 6**,** 6048-6057.

Faber, T. J., A. Jaishankar & G. H. McKinley (2017a) Describing the firmness, springiness and rubberiness of food gels using fractional calculus. Part I: Theoretical framework. *Food Hydrocolloids,* 62**,** 311-324.

Faber, T. J., A. Jaishankar & G. H. McKinley (2017b) Describing the firmness, springiness and rubberiness of food gels using fractional calculus. Part II: Measurements on semi-hard cheese. *Food Hydrocolloids,* 62**,** 325-339.

Ganzevles, R. A., M. A. C. Stuart, T. van Vliet & H. H. J. de Jongh (2006) Use of polysaccharides to control protein adsorption to the air-water interface. *Food Hydrocolloids,* 20**,** 872-878.

Ivanov, I. B., K. D. Danov, K. P. Ananthapadmanabhan & A. Lips (2005) Interfacial rheology of adsorbed layers with surface reaction: On the origin of the dilatational surface viscosity. *Advances in Colloid and Interface Science,* 114**,** 61-92.

Jaishankar, A. & G. H. McKinley (2013) Power-law rheology in the bulk and at the interface: quasi-properties and fractional constitutive equations. *Proceedings of the Royal Society a-Mathematical Physical and Engineering Sciences*, 469.

Kalman D. S. (2014), Amino Acid Composition of an Organic Brown Rice Protein Concentrate and Isolate Compared to Soy and Whey Concentrates and Isolates, *Foods*, 3, 394-402.

Khare, V. P., A. R. Greenberg & W. B. Krantz (2003) Development of pendant drop mechanical analysis as a technique for determining the stress-relaxation and water-permeation properties of interfacially polymerized barrier layers. *Journal of Applied Polymer Science*, 90, 2618-2628.

Lakemond, C. M. M., H. H. J. de Jongh, M. Hessing, H. Gruppen & A. G. J. Voragen (2000) Soy glycinin: Influence of pH and ionic strength on solubility and molecular structure at ambient temperatures. *Journal of Agricultural and Food Chemistry*, 48, 1985-1990.

Li, W., B. J. Dobraszczyk & P. J. Wilde (2004) Surface properties and locations of gluten proteins and lipids revealed using confocal scanning laser microscopy in bread dough

Malomo, S. A., R. He & R. E. Aluko (2014) Structural and Functional Properties of Hemp Seed Protein Products. *Journal of Food Science*, 79, C1512-C1521.

Martin, A. H., M. A. Bos & T. van Vliet (2002) Interfacial rheological properties and conformational aspects of soy glycinin at the air/water interface. *Food Hydrocolloids*, 16, 63-71.

Mezzenga, R. & P. Fischer (2013) The self-assembly, aggregation and phase transitions of food protein systems in one, two and three dimensions. *Reports on Progress in Physics*, 76, 43.

Nino, M. R. R., C. C. Sanchez, V. P. Ruiz-Henestrosa & J. M. R. Patino (2005) Milk and soy protein films at the air-water interface. *Food Hydrocolloids*, 19, 417-428.

Nishinari, K., Y. Fang, S. Guo & G. O. Phillips (2014) Soy proteins: A review on composition, aggregation and emulsification. *Food Hydrocolloids*, 39, 301-318.

Ortiz, S. E. M., C. C. Sanchez, M. R. R. Nino, M. C. Anon & J. M. R. Patino (2003) Structural characterization and surface activity of spread and adsorbed soy globulin films at equilibrium. *Colloids and Surfaces B-Biointerfaces*, 32, 57-67.

Patino, J. M. R., S. E. M. Ortiz, C. C. Sanchez, M. R. R. Nino & M. C. Anon (2003) Dynamic properties of soy globulin adsorbed films at the air-water interface. *Journal of Colloid and Interface Science,* 268**,** 50-57.

Patino, J. M. R. & A. M. R. Pilosof (2011) Protein-polysaccharide interactions at fluid interfaces. *Food Hydrocolloids,* 25**,** 1925-1937.

Piazza, L., N. Durr-Auster, J. Gigli, E. J. Windhab & P. Fischer (2009) Interfacial rheology of soy proteins - High methoxyl pectin films. *Food Hydrocolloids,* 23**,** 2125-2131.

Ramirez-Suarez, J. C. & Y. L. Xiong (2003) Effect of transglutaminase-induced cross-linking on gelation of myofibrillar/soy protein mixtures. *Meat Science,* 65**,** 899-907.

Ravera, F., G. Loglio & V. I. Kovalchuk (2010) Interfacial dilational rheology by oscillating bubble/drop methods. *Current Opinion in Colloid & Interface Science,* 15**,** 217-228.

Renzetti, S., J. Behr, R. F. Vogel, A. Barbiroli, S. Iametti, F. Bonomi & E. K. Arendt (2012) Transglutaminase treatment of brown rice flour: A chromatographic, electrophoretic and spectroscopic study of protein modifications. *Food Chemistry,* 131**,** 1076-1085.

Renzetti, S., F. Dal Bello & E. K. Arendt (2008) Microstructure, fundamental rheology and baking characteristics of batters and breads from different gluten-free flours treated with a microbial transglutaminase. *Journal of Cereal Science,* 48**,** 33-45.

Sagis, L. M. C. & E. Scholten (2014) Complex interfaces in food: Structure and mechanical properties. *Trends in Food Science & Technology,* 37**,** 59-71.

Saulnier, P., F. Boury, A. Malzert, B. Heurtault, T. Ivanova, A. Cagna, I. Panaiotov & J. E. Proust (2001) Rheological model for the study of dilational properties of monolayers. Comportment of dipalmitoylphosphatidylcholine (DPPC) at the dichloromethane (DCM)/water interface under ramp type or sinusoidal perturbations. *Langmuir,* 17**,** 8104-8111.

Seta, L., N. Baldino, D. Gabriele, F. R. Lupi & B. de Cindio (2012) The effect of surfactant type on the rheology of ovalbumin layers at the air/water and oil/water interfaces. *Food Hydrocolloids,* 29**,** 247-257.

Sun, X. D. & S. D. Arntfield (2012) Gelation properties of myofibrillar/pea protein mixtures induced by transglutaminase crosslinking. *Food Hydrocolloids,* 27**,** 394-400.

Tang, C. H. (2017) Emulsifying properties of soy proteins: A critical review with emphasis on the role of conformational flexibility. *Critical Reviews in Food Science and Nutrition,* 57**,** 2636-2679.

Tang, C. H., Z. Ten, X. S. Wang & X. Q. Yang (2006a) Physicochemical and functional properties of hemp (Cannabis sativa L.) protein isolate. *Journal of Agricultural and Food Chemistry,* 54**,** 8945-8950.

Tang, C. H., H. Wu, H. P. Yu, L. Li, Z. Chen & X. Q. Yang (2006b) Coagulation and gelation of soy protein isolates induced by microbial transglutaminase. *Journal of Food Biochemistry,* 30**,** 35-55.

Torcello-Gomez, A., J. Maldonado-Valderrama, M. J. Galvez-Ruiz, A. Martin-Rodriguez, M. A. Cabrerizo-Vilchez & J. de Vicente (2011) Surface rheology of sorbitan tristearate and beta-lactoglobulin: Shear and dilatational behavior. *Journal of Non-Newtonian Fluid Mechanics,* 166**,** 713-722.

Ulaganathan, V., I. Retzlaff, J. Y. Won, G. Gochev, D. Z. Gunes, C. Gehin-Delval, M. Leser, B. A. Noskov & R. Miller (2017) beta-Lactoglobulin adsorption layers at the water/air surface: 2. Dilational rheology: Effect of pH and ionic strength. *Colloids and Surfaces a-Physicochemical and Engineering Aspects,* 521**,** 167-176.

Wagner, C. E., A. C. Barbati, J. Engmann, A. S. Burbidge & G. H. McKinley (2017) Quantifying the consistency and rheology of liquid foods using fractional calculus. *Food Hydrocolloids,* 69**,** 242-254.

Wagner, J. R. & J. Gueguen (1995) EFFECTS OF DISSOCIATION, DEAMIDATION, AND REDUCING TREATMENT ON STRUCTURAL AND SURFACE-ACTIVE PROPERTIES OF SOY GLYCININ. *Journal of Agricultural and Food Chemistry,* 43**,** 1993-2000.

Wang, X. S., C. H. Tang, X. Q. Yang & W. R. Gao (2008) Characterization, amino acid composition and in vitro digestibility of hemp (Cannabis sativa L.) proteins. *Food Chemistry,* 107**,** 11-18.

Wustneck, R., J. Reiche & S. Foster (1997) Surface dilational behavior of docosanic acid monolayers spread on the surface of drops of polymer solutions. *Thin Solid Films,* 307**,** 100-105.

Wustneck, R., N. Wustneck, D. O. Grigoriev, U. Pison & R. Miller (1999) Stress relaxation behaviour of dipalmitoyl phosphatidylcholine monolayers spread on the surface of a pendant drop. *Colloids and Surfaces B-Biointerfaces,* 15**,** 275-288.

Yapo, B. M., C. Robert, I. Etienne, B. Wathelet & M. Paquot (2007) Effect of extraction conditions on the yield, purity and surface properties of sugar beet pulp pectin extracts. *Food Chemistry,* 100**,** 1356-1364.

Chapter 5

Vegetable proteins as emulsifiers in vegetable drinks: preparation and short-time stability

Abstract

Many food products used in the food industry, such as milk, sauces, beverages, dressing, desserts and so on are diluted emulsions. The stabilization of these products is very difficult because of the important difference between the two phases and the low viscosity of these systems. In the food industry, dairy proteins are classically used as stabilizing agents, thanks to their ability to lower the interfacial tension and to give a good viscoelasticity at the interface, forming resistant layer against separation phenomena. Despite the good stabilizing properties of these proteins, their consumption is a problem for those people who are intolerant or who, for ethical reasons, do not want to consume them. Vegetable proteins could be a valid alternative to animal proteins as stabilizing agents for many productions such as proteinaceous beverages. The aim of this work is the stabilization of emulsions in which three vegetable proteins, hemp, soy and brown rice were used as emulsifiers agents. Stabilizers such as pectin, starch, xanthan gum, guar, tara gum and gellan gum were also added to stabilize the continuous phase and then to improve the stability. The difficulty of stabilizing these dilute systems has led to the preparation of multiple stable and unstable samples. A microscopy investigation, the rheological characterization and zeta potential measurements were performed on the stable samples. A preliminary study was conducted on a benchmark milk to identify the properties with which to compare the prepared samples. From the experimental investigation, the gellan gum appears to be the polysaccharide able to stabilize all three emulsions, already at low concentration, and to give a low viscosity to the emulsions even though it is still higher than the studied benchmark milk.

Keywords: vegetable proteins, diluted emulsions, polysaccharides, stability

5.1   Introduction

Many food systems, such as creams, milk, sauces, beverages, dressing, desserts, margarine or butter are systems that can be classified as emulsions. An emulsion is a system consisting of two immiscible liquids (usually oil and water), in which one liquid phase (dispersed or discontinuous phase) is dispersed as small spherical droplets in the second liquid phase (dispersing or continuous phase) (McClements, 2007). If the continuous phase is the oily phase, the resulting emulsion is oil in water (O/W), typically margarine and butter, while if the continuous phase is the aqueous phase, the resulting emulsion is water in oil (W/O), typically milk beverages and dressing (McClements, 2007). In order to obtain a homogeneous and well-distributed system, it is necessary to finely disperse one phase within another and this operation is known as emulsification (or homogenization) and consists in breaking a continuous phase into small drops. The immiscibility of the two phases means that this operation is thermodynamically disadvantaged and requires energy. At the end of the emulsification operation, the natural separation phenomena can occur and give in a short time stratification and separation of the product. Therefore, to stabilize these systems against creaming, sedimentation and other phenomena, it is necessary to add components, an emulsifier, able to act at the interfacial level in different ways, lowering the interface tension and facilitating the breakage of the phase in small droplets, and creating a viscoelastic interfacial layer able to prevent breakage phenomena. In this way it is possible to stabilize an emulsion or to make it stable for a defined period of time during which to resist changes in its properties with time (McClements, 2007).

Proteins are typically used to control interface properties. They are able to lower the interface tension rapidly, migrating rapidly to the interface, and creating a resistant interfacial layer with good viscoelastic properties (Bos and van Vliet, 2001). Usually polysaccharides are also used in emulsions for gelling, thickening or, more generally, to control the rheology and structure of the dispersing phase and then to improve the stability of oil droplets against phase separation (Patino and Pilosof 2011,; Dickinson et al. 1998). In fact, an increase in the continuous phase viscosity is one of the reasons for the enhancement of emulsion stability. Several polysaccharides can be present as thickening and gelling agents. Attractive or repulsive interactions between polysaccharides and proteins can be and can have a key role on stabilizing properties and for aggregation and creaming behaviour of the emulsions (Bouyer et al. 2012; Lam and Nickerson, 2013). The use of both proteins and polysaccharides can be really important to stabilize emulsions, but an important aspect is a compatibility between these two biopolymers. The compatibility is important in determining the structure and the mechanical properties of products. Moreover, the environmental conditions, such as pH, ionic strength, co-solute, temperature, can result in specific protein-polysaccharide interaction of

an attractive or repulsive nature, which leads to the establishment of phenomena of stability or instability.

Animal proteins from the dairy industry, such as caseins and lactoglobulins, are widely used in the food industry (Dickinson, 1999). If the stabilizing properties of animal proteins are well known, it is also well known that in the food industry there is currently a strong focus on the formulation of products that contain ethically correct components and that are also consumed by people who cannot consume dairy products because of food intolerances like cow milk allergy or lactose intolerance. This trend is growing and has led the food industry to work on products prepared with vegetable sources. So, in the light of this, vegetable proteins can be considered as an alternative protein source to the classical animal one. These proteins are rich in essential amino acids and thanks to the excess of some of these, the amino acidic profile is balanced. The vegetable proteins are suitable to reduce the glycemic index, they are recognized as anti-tumour and able to lower cholesterol (Wang, Jiang and Xiong, 2018; Wanezaki et al. 2015). Vegetable proteins have various health benefits and because of this many efforts have been made to develop food based on vegetable proteins.

In particular, in this work proteins extracted by soy, hemp and brown rice plants will be used. All of these are globular proteins of different nature. Soy proteins are mainly globulins (Tang, 2017), hemp proteins are mainly edestin (Tang et al. 2006) and brown rice proteins are mainly glutenins (Cao et al. 2009). There are many works in the scientific literature about vegetable drink produced with vegetable proteins, especially with soy proteins and, about their utilization with polysaccharides to form functional complexes (by covalent or non-covalent bonds) with good stabilizing properties (Lin et al. 2017). Several methods are suggested in the literature to create emulsions suitable for vegetable drinks like those used to create hemp drink (Wang et al. 2018). With this method, the hemp oil is dispersed mechanically into fine droplets and it is available for the next homogenization phases. No other methods for obtaining hemp drink are reported in the literature.

On the contrary, many studies are present in the literature about emulsions prepared with soy protein. Kong et al. (2017) used a high-pressure homogenizer to obtain a stable emulsion with soy protein. Another process used to form emulsions for vegetable drinks is a layer-by-layer (LBL) electrostatic deposition technique (Noshad et al. 2016; Xiang, Lyu and Narsimhan, 2016; Zhao et al. 2015). This technique involves the formation of multiple interfacial layers. To have this effect the emulsification process passes through multiple emulsification steps which give, finally, a stable emulsion (Noshad et al. 2016; Burgos-Diaz et al. 2016). Vegetable milk alternatives are prepared to start directly from the plant or seeds, mixing in water and obtaining products similar in consistency and appearance to milk (Sethi, Tyagi and Anurag, 2016). The literature shows that several polysaccharides have been studied in added to vegetable proteins to stabilize the systems and in particular have been used pectin

(Zhao et al. 2015), carboxymethyl cellulose (Diftis and Kiosseoglou, 2003), starch, and chitosan (Noshad et al. 2016).

In this work, several polysaccharides were also used to stabilize the emulsions, in particular, starch, pectin, xanthan gum, guar gum, tara gum and gellan gum.

The aim of this work is to obtain a stable and homogeneous emulsion, with a milk like texture, using the vegetable proteins as emulsifiers and for this purpose, a benchmark vegetable drink was studied to compare its texture with the experimental samples. Three vegetable proteins were used, soy, hemp and brown rice in combination with several polysaccharides to enhance the stability. In particular, LM pectin, starch, xanthan gum, guard, tara gum and gellan gum were tested. The stability was investigated first by an optical observation of the product and for the stable samples the investigation under microscopy, the rheological characterization and the zeta potential measurements were performed.

5.2 Material and Methods

5.2.1 *Materials*

In order to evaluate the properties of a commercial benchmark product, a classic cow milk (Parmalat S.p.A., Italy), a whole rice drink (Isola Bio, Abafoods S.r.l., Italy) and a soy drink (Valsoia S.p.A., Italy) were evaluated. The commercial vegetable proteins used for the emulsion tests are hemp (H), soy (S) and brown rice (BR) and were purchased from Bulk Power. Vegetable proteins solutions were prepared by dissolving the proteins in Milli-Q ultrapure water for at least two hours. Owing to the high fibre percentage in the hemp protein sample, after stirring for one hour by a magnetic stirrer (AREX Heating Magnetic Stirrer, Velp Scientifica, Italia), a next purification was employed, by subjecting the premixed sample to centrifugation (3000 rpm for 30 minutes). At the end of the centrifugation, the fiber part of the sample is spread on the bottom and the supernatant liquid used as an aqueous protein solution to make emulsions.

Some polysaccharide species were used as follows:

- Potato starch(S) (GIAS, Italy)
- LM Pectin (Silvateam Food Ingredients S.r.l., Italy)
- Guar (G) (Sigma Aldrich, Germany)
- Xanthan gum (X) (Farmalabor, Italy)
- Tara Gum (Silvateam Food Ingredients S.r.l., Italy)
- Gellan Gum powder (Alfa Aesar, Germany)

For the oily phase of the emulsions, commercial sunflower oil (Fabiano S.r.l., Italy) was used. The oil was used without preliminary purification, to investigate the behaviour of a commercial product that could be commonly adopted for industrial applications.

5.2.2   *Emulsion with the only VP*

To test the emulsifying effect of vegetable proteins, O/W emulsions were prepared at different concentration levels: 0.5, 1, 1.5, 2 and 3%w/w. After a preliminary solubilization of vegetable protein in MilliQ water, the 5%w/w of sunflower oil was dispersed in the 95%w/w of vegetable protein solution, using a rotor-stator system (Ultra Turrax T-25, IKA Instruments, Germany), at 10500 rpm for 260 s, following the procedure suggested by Seta et al. (2013). After the preparation, the emulsions were monitored within 24 hours of preparation.

5.2.3   *Emulsion with VP and polysaccharide*

The samples prepared with soy proteins are reported in Table 5.2.3.1 where the soy is present always at 4%w/w and are indicated by the first ID letter (Soy Protein, SP), while the last ID letter indicates the polysaccharide used and the number indicates its concentration.

	SPS0.5	SPS1	SPS1.5	SPG1	SPX1
Component	%w/w	%w/w	%w/w	%w/w	%w/w
MilliQ water	**90.4**	**89.9**	**89.4**	**89.9**	**89.9**
SOY protein	**4**	**4**	**4**	**4**	**4**
NaCl	**0.1**	**0.1**	**0.1**	**0.1**	**0.1**
Polysaccharide	**0.5**	**1**	**1.5**	**1**	**1**
Oil	**5**	**5**	**5**	**5**	**5**

Table 5.2.3.1 Soy emulsion formulations

The starch solution was prepared by stirring aqueous solution of starch at 85°C for 30 min, and after solution cooling, the protein and the other component were added and stirred for few minutes and subsequently the solution was emulsified with the oil phase with T50 (Ultra Turrax T-50, IKA Instruments, Germany) at 8000 rpm for 260 s.

Guar (G) and xanthan gum (X) solutions were prepared by stirring the dispersions vigorously for 30 min at room temperature, followed by heating at 50 °C until the solution became clear following the procedure suggested by Ercelebi and Ibanoglu (2009). Afterwards the soy proteins were added and subsequently the solution was emulsified with the oil phase with Ultra Turrax T-50 at 8000 rpm for 260 s.

Different pectin emulsions were also prepared and the composition of the emulsions is reported in Table 5.2.3.2 **Composition of pectin emulsion tested**

	*vp*2P1	*vp*2P0.5	*vp*P0.5
Component	%w/w	%w/w	
Buffer solution	**83.6**	**88.25**	**86.25**
BR	**2**	**2**	**4**
NaCl	**0.1**	**0.1**	**0.1**
PEC	**1**	**0.5**	**0.5**
CaCl$_2$ (2.2%w/w) solution	**8.3**	**4.15**	**4.15**
Oil	**5**	**5**	**5**

Table 5.2.3.2 Composition of pectin emulsion tested

The buffer solution with citric acid and tribasic sodium citrate, supplied by Sigma Aldrich (Italy), was used to keep the sample pH at 4.2 ± 0.1. The pectin emulsions were prepared by homogenizing by 5% w/w of the oil phase (sunflower oil by Fabiano) and 95% w/w aqueous solution of several vegetable proteins. Before the emulsification step, the aqueous phase was prepared, dispersing the protein in a buffer solution, in the presence of NaCl, and kept under agitation on a thermostated plate at 40 °C for 2 hours. Then, the pectin was solubilized with ethanol (ratio pectin: ethanol = 1:2) and the protein solution was added and stirred for another 15 minutes. Finally, the oil and aqueous phase were blended with a rotor-stator system (Ultra-Turrax T 50, IKA-Werke, Germany) at 6000 rpm for a mixing time of 120 s. The emulsions were stored at 4°C. Only for *vp*2P1 emulsions, the procedure provided the addition of the calcium solution in the last 15 seconds of the emulsification phase .

Other three samples, for each protein, were prepared with Tara Gum polysaccharide and the composition is reported in Table 5.2.3.3. A citrate buffer solution was used to dissolve the components.

	*vp*T0.1	*vp*T0.2	*vp*T0.4
Component	%w/w		
Vegetable Protein solution (*2%w/w Protein*)	**94.79**	**94.69**	**94.49**
NaCl	0.1	0.1	0.1
CaCl2	0.01	0.01	0.01
Tara Gum	**0.1**	**0.2**	**0.4**
Oil	5	5	5

Table 5.2.3.3 Tara gum emulsions composition

The tara gum solution was prepared to solubilize the polysaccharide in a buffer solution at room temperature under magnetic stirring for 2 h and left to rest all night at 4°C before using it, as suggested by Wu et al. (2015). After this period, all the other components were added and mixed for about one hour to then emulsified, adding the oily phase.

Gellan Gum emulsions were prepared and their composition is reported in Table 5.2.3.4.

	*vp*G0.1	*vp*G0.05	*vp*G0.02	*vp*G0.01
Component	*%w/w*			
VP solution (*2%w/w Protein*)	94.79	95.84	94.87	94.88
NaCl	0.1	0.1	0.1	0.1
CaCl2	0.01	0.01	0.01	0.01
Gellan Gum	0.1	0.05	0.02	0.01
Oil	5	5	5	5

Table 5.2.3.4 Gellan gum emulsions composition

The protein solution was prepared with the addition of $CaCl_2$ and NaCl. Gellan solutions were prepared by dissolving the powder in the buffer at room temperature under magnetic stirring and heating the dispersions at 90°C for 10 min. Solutions were weighed and citrate buffer was added to make up any weight lost in evaporation (Sosa-Herrera et al. 2008). Blends of protein–polysaccharide were made by mixing equal parts of aqueous solutions of individual components. The oil and aqueous phase were blended with a rotor stator system (Ultra-Turrax T 50, IKA-Werke, Germany) at 6000 rpm for a mixing time of 120 s and, after one hour's rest at 4°C, a new step of emulsification at 500 rpm for 30 s was effectuated, and after another one hour's rest at 4°C a light mixing was carried out manually, whereupon the emulsions were stored at 4°C (3STEP-EMU).

5.2.4   *Methods*

5.2.4.1 *Surface tension measurements*

The vegetable proteins were characterized by transient surface tension measurements. Axisymmetric Drop Shape Analysis (ADSA) was used to calculate the drop volume, area and interfacial tension by using an automated pendant drop tensiometer (FTA200, First Ten Angstroms, USA) equipped with fta32 v2.0 software and able to evaluate the surface tension in static conditions. The measures were performed on the VP solution. The measures were extensively discussed in a previous chapter therefore only the most significant data will be reported to the CMC condition in order to compare these results with those useful for emulsions.

5.2.4.2 *Microscopy and drop diameter distribution*

The morphology of the emulsion droplets was observed with contrast phase microscope (MX5000, Meiji, Japan), equipped with phase contrast 40x and 20x lens (according to the samples analyzed). In order have a good visualization of the images, some samples were diluted in distilled water with a weight ratio 1:20 and manually mixed in a non-vigorous way to not modify emulsion droplet dimensions (Seta et al. 2013; Lupi et al. 2017). The measures were performed placing a drop of diluted emulsion on a microscope slide and observed. The images of the emulsions were acquired using specific software (dhs image database, Germany), which, by greyscale detection, gives the number-based surface equivalent diameters. The drop size distribution can be well described by a lognormal model:

$$f(d) = \frac{1}{d \cdot \sigma_{ln} \cdot \sqrt{2\pi}} exp \left[\frac{-(\ln(d) - d_{ln})^2}{2\sigma_{ln}^2} \right]$$

(5.2.4.2.1)

where d_{ln} and σ_{ln} are, respectively, the mean and the standard deviation of the normal model (Lupi et al. 2017, Seta et al. 2013), which allow the evaluation of the mean diameter, d_s, and the variance σ_s^2:

$$d_s = e^{d_{ln} + \sigma_{ln}^2/2}$$

(5.2.4.2.2)

$$\sigma_s^2 = e^{2d_{ln} + \sigma_{ln}^2}(e^{\sigma_{ln}^2} - 1)$$

(5.2.4.2.3)

σ_s, is the standard deviation and it is commonly considered as an index of polydispersity (Lupi et al. 2017, Seta et al. 2013). This technique is potentially available to investigate droplet coalescence (McClements 2007) even if data have to be carefully analyzed to exclude potentially different phenomena such as flocculation or Ostwald ripening.

5.2.4.3 ζ-*potential analysis*

The ζ-potential measurement was conducted using an electrophoretic dynamic light scattering instrument (ZPS - Zetasizer NANO, Malvern Instrument Limited, UK). A static electrical field was applied via a pair of electrodes to the emulsion in a cell, in order to move charged oil drops towards the oppositely charged electrode. The electrophoretic mobility was estimated by means of laser-Doppler velocimetry and the ζ-potential was calculated from the Smoluchowski equation. It is known in the literature that high zeta potential absolute values are an index of emulsion stability, in particular, for zeta potential absolute values greater than 30 mV, the emulsion can be considered stable. The measure has been effected on the strongly diluted (0.1%w/w) emulsion sample as suggested by the literature (Kong et al. 2017) to facilitate the optical conditions.

5.2.4.4 *Rheological characterization*

The stable emulsions were characterized by the rheological investigation with a rotational rheometer DSR 200 (Rheometric Scientific, USA) adopting a parallel plates geometry (diameter = 40 mm) and ARES-RFS (TA Instruments, USA) adopting a parallel plates geometry (diameter = 50 mm), both thermostated with a Peltier system (± 0.1 °C) acting under the lower plate. Flow curves are performed at 25°C and preliminary step rate tests were performed to evaluate the delay before measurement. The frequency sweep tests were performed only for the BR2P1 sample at 25 °C (from 0.1 up to 10 Hz), in the linear regime, previously identified with stress sweep tests.

5.3 Results and discussion

5.3.1 Surface tension analysis

An extensive evaluation of the surface tensions of vegetable proteins mixtures were made in the previous chapter, and then only the trend of the surface tensions of vegetable proteins studied, with the aim to compare their surfactant properties, are reported in Figure 5.3.1.1.
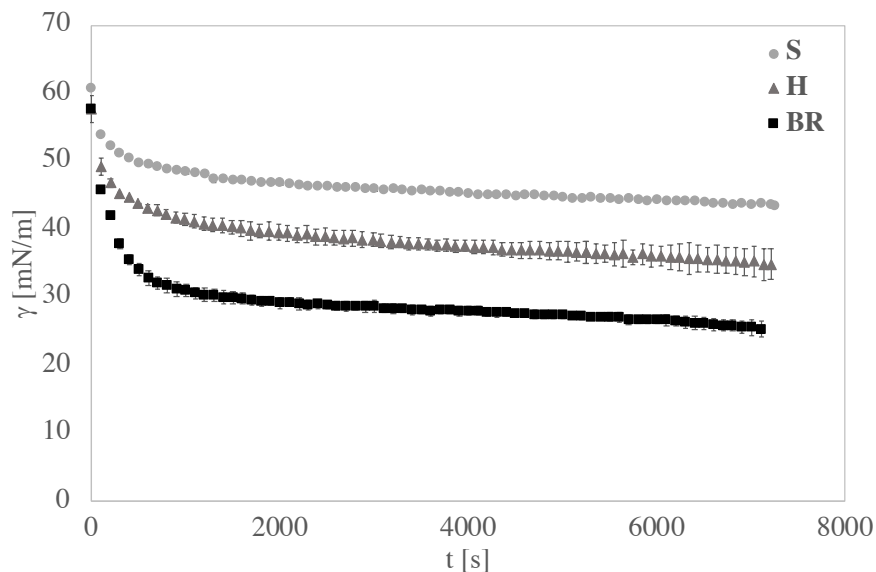
Figure 5.3.1.1 Surface tension of the soy (S), hemp (H) and brown rice (BR) proteins at A/W interface by pendant drop technique

All the three vegetable proteins have a good surface activity, comparable with the dairy proteins (Bos, Dunnewind and van Vliet 2003). The brown rice protein is the more surface active, followed by hemp and soy proteins. Then, from a kinetic evaluation, the brown rice protein is also the faster to migrate at the interface, followed by soy and finally hemp, which is the slower probably due to the higher molecular weight. The good surface activity found on the vegetable protein samples has suggested the possibility of using them as emulsifying agents.

5.3.2 Emulsions with only vegetable proteins (VP)

In the early stage of this work, the emulsifying properties of the vegetable proteins were investigated, varying the protein concentration in the emulsions in the range between 0.5 and 3% w/w.

The procedure of the preparation was reported in the previous section. As an example of the microphotographs of the emulsions after 3 hours of storage time, three pictures for soy and for hemp emulsions were reported in Figure 5.3.2.1.
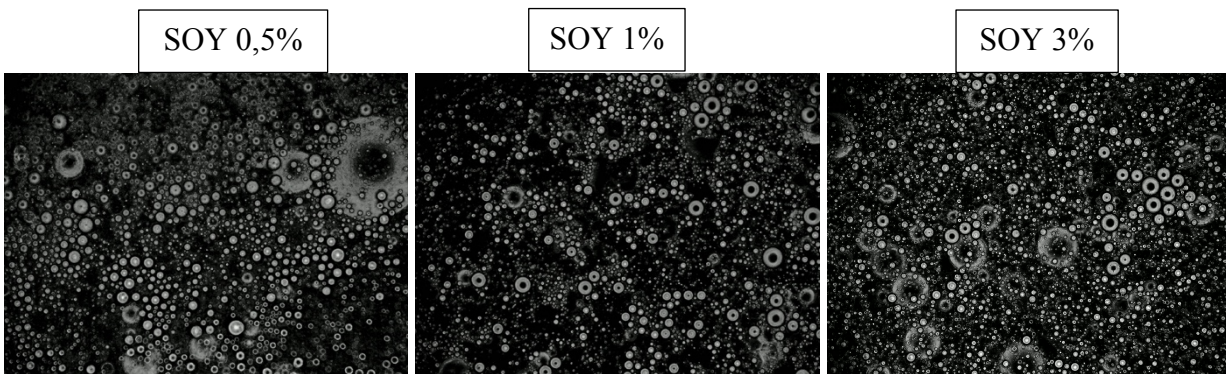

| SOY 0,5% | SOY 1% | SOY 3% |

Figure 5.3.2.1 Microphotographs of the emulsions for three different concentrations (magnification 20X)

| S 1% | S 1.5% | S 2% | BR 1% | BR 1.5% | BR 2% |
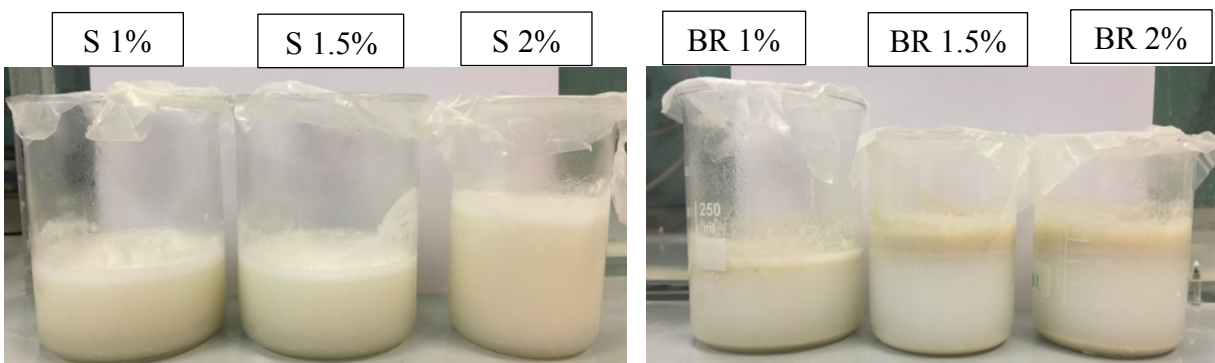
Figure 5.3.2.2 Emulsions after 3 hr from preparation

The emulsions are all highly unstable, showing the formation of multiple layers of separation, as can be seen from the samples in Figure 5.3.2.2 given as an example. The figures show the images of some emulsions a few hours after the formation of the emulsion. The strong instability did not allow its characterization. The emulsions formed, however, all showed a surface layer of foam, induced by the known surfactant properties of proteins. This surfactant power allows the system to incorporate air during the emulsification process. In this regard, an evaluation of the foam layer that the proteins create in the emulsification process was carried out and the results are reported in Figure 5.3.2.3.
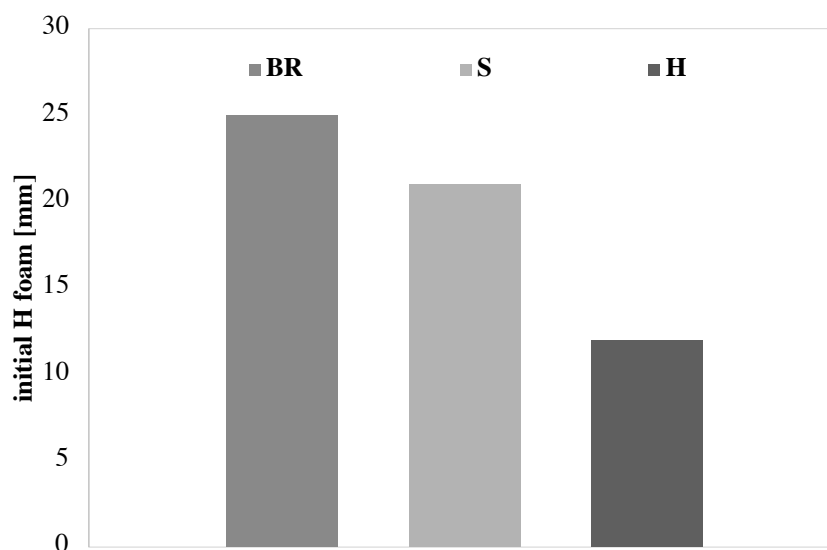
Figure 5.3.2.3 Initial foam layer for the emulsion in 1.5%w/w proteins concentration

The brown rice proteins in the emulsification phase are the most able to incorporate air and consequently lead to the formation of a higher initial foam layer. This is in line with the results of surface activity obtained from a preliminary surface analysis of the proteins under study.

The hemp proteins, on the contrary, do not reflect the trend of surface tensions and create foam layers lower than those created in the presence of the soy protein. This is true when the comparison is made with equilibrium tensions, but in the phenomena of emulsification, more than the equilibrium tensions value, the rate at which the protein (or more generally, the emulsifying species) is brought to the interface is a key parameter.

From the complete profile of the surface tensions, it is, in fact, possible to obtain an evaluation of the kinetic parameters, in terms of diffusion rate at the interface, adsorption rate and molecular rearrangement rate. From the evaluation, previously carried out, of the diffusion rate of vegetable proteins, it results that the trend is $r_{diff}^{BR} > r_{diff}^{S} > r_{diff}^{H}$. The height of the foam layer follows the same trend as the rate of diffusion of plant proteins at the air/water interface, as evaluated with the pendant drop tensiometer.

5.3.3   Benchmark milk study

In order to obtain a product as similar in sensory characteristics to what the market offers, a bulk rheological analysis was conducted on some protein drinks to be used as a reference for the future development of our vegetable drink.
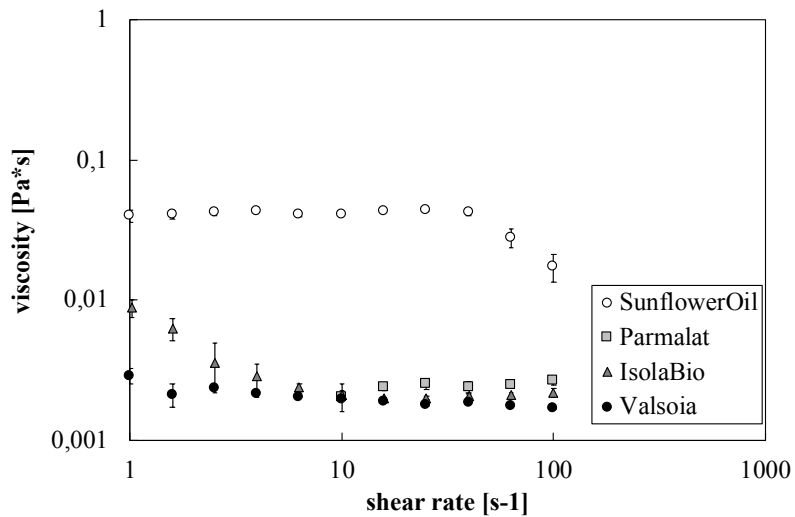

Figure 5.3.3.1 Benchmark drinks studied

Figure 5.3.3.2 Flow curves of three benchmark drinks.

From Figure 5.3.3.2 it can be observed that the dependence of viscosity from shear rate is almost Newtonian for the samples analyzed except for IsolaBio drink, which shows a slight shear-thinning behaviour at low shear rate.
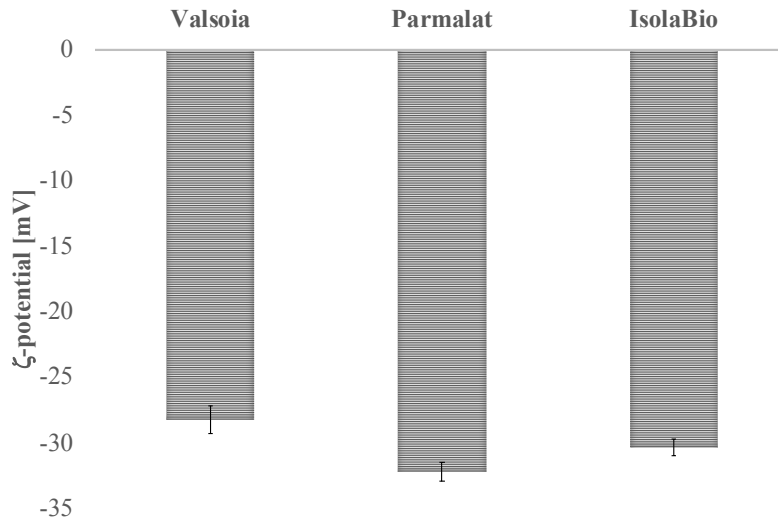
Figure 5.3.3.3 ζ-potential of benchmark milk

From the ζ-potential evaluation on commercial drinks (Figure 5.3.3.3) it can be seen that the zeta values are around 30 mV in absolute value only for Parmalat and Whole Rice, while for soy drink the zeta potential lower, then less stable and confirming the necessity to shack the package before the use. In order to have a complete characterization of the benchmark samples, pH and °Brix values were obtained and are reported in Table 5..

	pH	°Brix
Valsoia	6.82±0.03	11.9±0.1
Parmalat	6.75±0.05	17.3±0.1
Isola Bio	6.7±0.1	18.2±0.5

Table 5.3.3.4 pH and °Brix values for the three commercial drinks

Visual monitoring was also carried out to verify the formation of any layers and it can be observed that for Isola Bio drink, the stratification occurs and it is still visible after a few hours. In particular, it is possible to observe both a sediment at the bottom and a layer of depleted serum at the top (see Figure5.11). This is the main problem of the vegetable drinks present on the market today. This can be seen from the inscription on all commercial vegetable milk labels, "shake before use", index of the formation of sediment and inhomogeneity of these products.

t=0   **t= 12 h**   **t= 4 h**

| T=25°C | T=4°C | T=25°C | T=4°C |
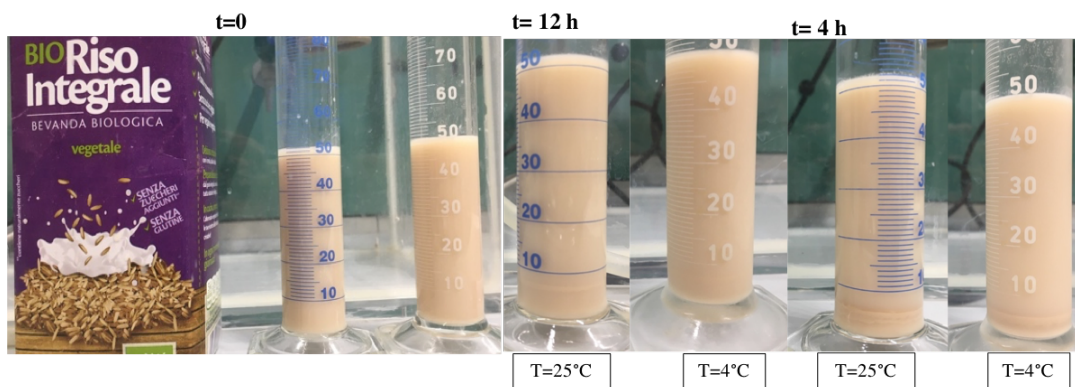
Figure 5.3.3.5 visual monitoring of benchmark milk of whole rice

The same monitoring was carried out on the Valsoia sample and also in this case a slight residue was found, lower than that of Isola Bio.

5.3.4   Emulsion with polysaccharide addition

The emulsions prepared using only vegetable proteins as stabilizing agents were all unstable, indicating that the interfacial properties, controlled by vegetable proteins, are not sufficient to stabilize the whole system. The instability phenomena are not only due to the interface, which in this case is stable, but is mainly due to the difference in density between the mixed phases (oily and aqueous), which leads to obvious phenomena of phase separation, such as the creaming of large drops, or the sedimentation of fibrous particles. In particular, thickening and gelling agents were added to give a light structuration to the emulsion.

5.3.4.1 Guar, xanthan gum, starch

To stabilize the emulsions, some polysaccharides, guar, xanthan gum (X) and potato starch (S), were added to the aqueous phase, at 1%w/w (SPX1, SPG1 and SPS1) as detailed in Table 5.2.3.1. The emulsions prepared with these formulations and methodologies showed good stability but a high consistency comparable to a pudding product.
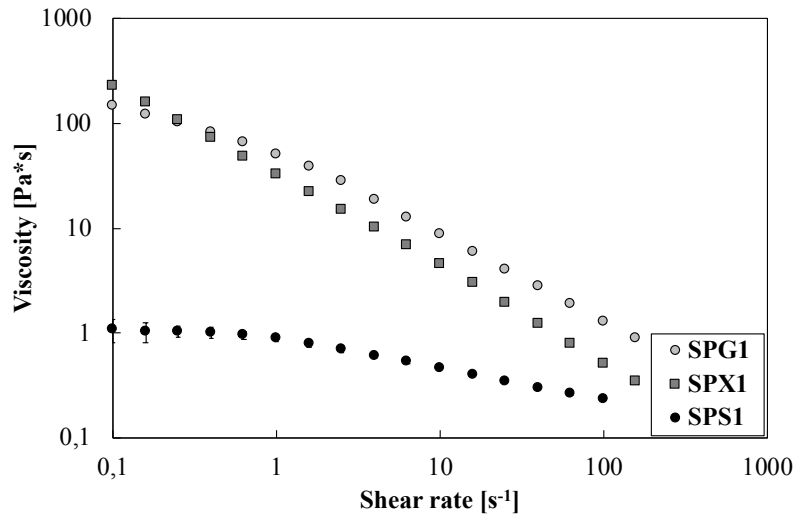
Figure 5.3.4.1.1 Flow curves of the soy emulsion with xantan gum (SPX), guar (SPG) and potato starch (SPS)

The flow curves of the three samples show that the viscosity of these products is so high that it differs significantly from that of milk or the other two vegetable drinks. Xanthan gum and guar have shown themselves to be strong thickening agents, so it was decided to continue the evaluation of emulsions using the starch whose contribution to the viscosity of the emulsion is lower but still stabilizing. Then three different starch compositions, as detailed in Table 5.2.3.1, SPS0.5- SPS1- SPS1.5 were studied and the resulting emulsions are shown in Figure 5.3.4.1.2.
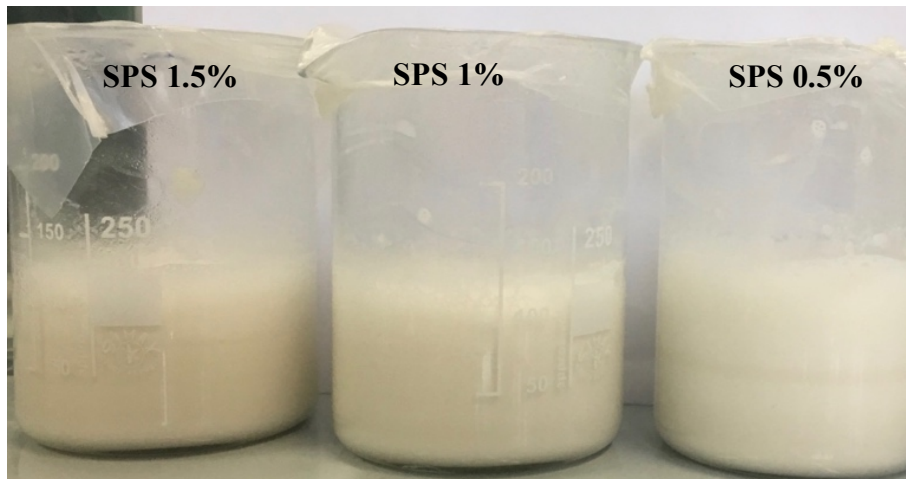
Figure 5.3.4.1.2 Emulsion stabilized by 4%w/w of VP and starch in the range of 0.5 to 1.5%w/w

From a first purely sensory analysis, the samples prepared, while showing a good homogeneity and the absence of stratification phenomena, show also a quite structured consistency quite different from a vegetable drink as shown in Figure 5.3.4.1.2.
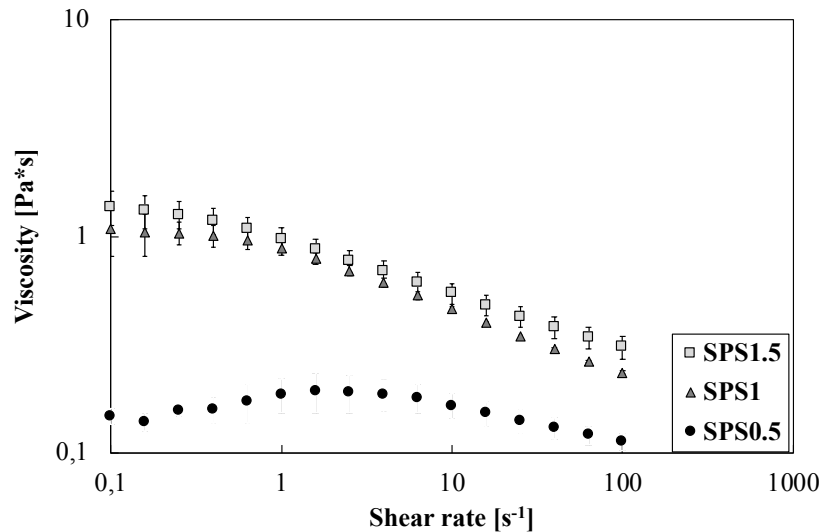

Figure 5.3.4.1.3 Flow curve of soy sample emulsions prepared with starch at three different concentrations

The hydrocolloid-protein complex has a marked influence on the vegetable systems. In fact, it can be observed that the hydrocolloids act on the bulk of the aqueous phase thickening and structuring it and slowing down the migration kinetics of the surfactant on the oil/water interface and, owing to the synergistic action of the two compounds, they modify the interfacial properties of the two phases, changing the DSD and the viscosity accordingly (Seta et al. 2013; Seta et al. 2012).

The samples with a high hydrocolloids concentration show shear thinning behaviour, while at 0.5%w/w the system shows an almost Newtonian behaviour. To evaluate the long-term stability, the ζ-potential measurements were carried out and the results were reported in Figure 5..
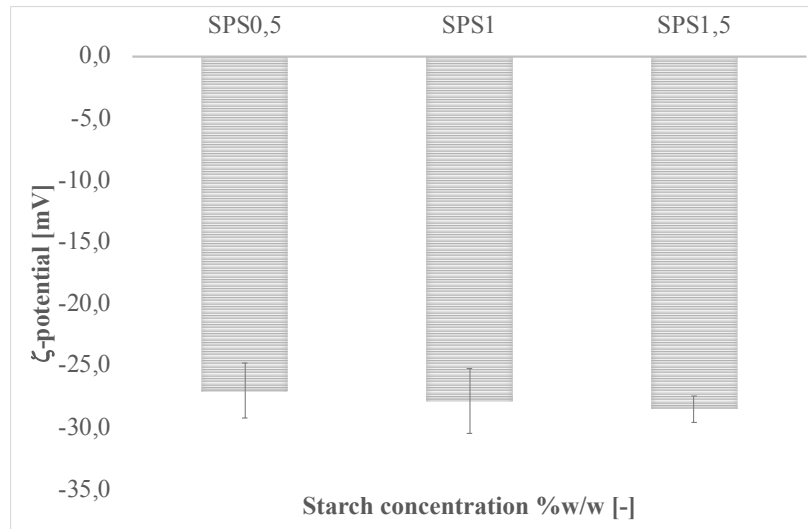
Figure 5.3.4.1.4 ζ-potential of the SPS emulsion at the three starch concentration investigated.

From the ζ -potential results, it seems that the addition of starch in the aqueous phase, even if it modifies the rheology of the samples, does not strongly influence their stability. In fact, as can be seen from the values of the ζ-potential, increasing the starch concentration the ζ-potential remain unchanged. In addition to not being a well stable system, we cannot go further down with the concentration of starch since the starch is a polysaccharide and to gel requires minimum conditions of concentrations, below which it does not gelatinize and does not give the desired viscous effect.
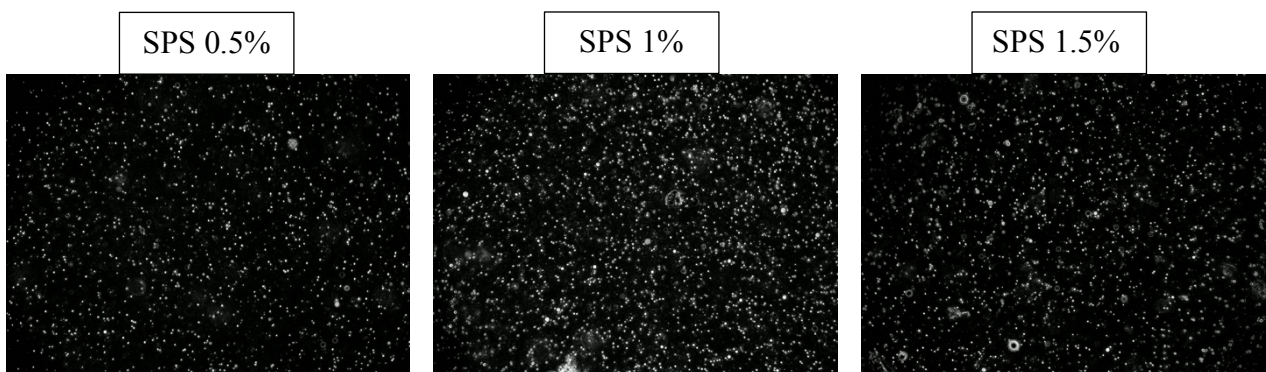
Figure 5.2 Emulsions microphotographs of prepared samples at different starch concentration with soy proteins
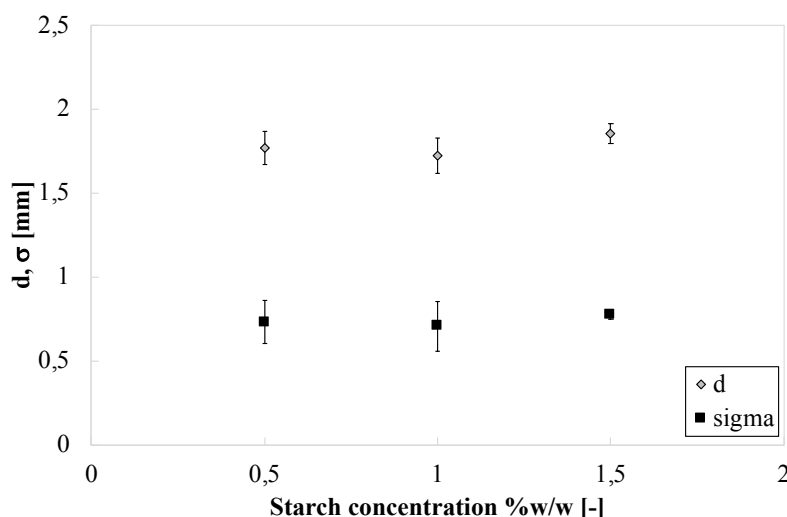
Figure 5.3.4.1.6 Effect of starch concentration on average droplets diameter and standard deviation

From microscopy analysis, reported in Figure 5.2 and Figure 5.3.4.1.6, the average droplets diameter and standard deviation of the emulsions do not seem to be dependent on the starch concentration adopted, and this information could be an indication that the interface is controlled by the vegetable protein. To validate this hypothesis, a comparison was made between the values of the average diameter of the drops of the SPS samples and those of the emulsions prepared with soy only. In the latter, it is seen that as the concentration of protein presents increases (from 3%w/w onwards) the average diameter of the drops decreases to values of about 2. If for soy proteins, the starch in this formulation, while giving high values of viscosity, could stabilize the system, with hemp proteins, the effect was highly unstable and the emulsions prepared, just after the emulsification, were stratified. Therefore, given the instability that starch causes in the presence of hemp proteins and the high viscosity obtained with the best-prepared sample, it was decided to change polysaccharide.

5.3.4.2 Pectin

Trying to improve the emulsion stability, a different polysaccharide was added. A low methoxyl grade pectin (LM) was chosen for all the investigated vegetable emulsions. LM pectin gives a gelation process in an acidic environment and in the presence of bivalent co-solutes which leads to the formation of connections between pectin molecules of the egg-box type by creating bridges between the carboxyl groups ends (Baldino et al. 2018; Thakur et al. 1997). So it was decided to use a buffer solution in our formulations to control the pH environment. Moreover, calcium solution was added

to favourite the gelation process and the optimized concentration was obtained from a previous investigation (data not shown) (Baldino et al. 2018; Thakur et al. 1997). In addition, since the presence of salt in this phase can help the interface stabilization, the use of MilliQ water was replaced by using distilled water. The pictures of the obtained emulsions are reported in Figure 5.3.4.2.1.
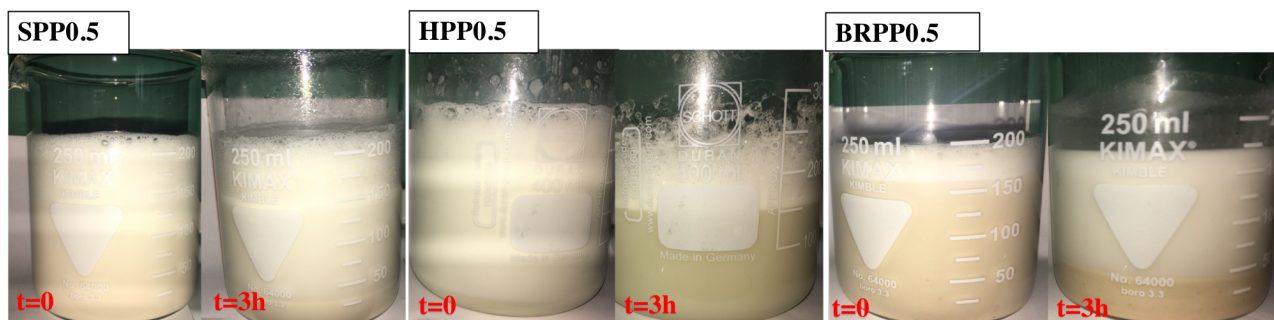

Figure 5.3.4.2.1 Emulsions prepared with three different vegetable proteins (4%w/w) and with pectin LM at 0.5%w/w concentration.

Although the consistency seems to be lower than that of the samples produced with starch, the phenomena of instability are evident by visually comparing the products after 3 hours of preparation. The emulsions were prepared first at 4%w/w of protein and at the lower amount of hydrocolloid (0.5%w/w), preventing increasing the system consistency.

The vegetable emulsions were also prepared keeping constant the hydrocolloid and lowering the protein amount (2%w/w) to improve the stability (see Figure 5.3.4.2.2).

To obtain the emulsions the same emulsification process was always used, only changing the last step to have the gelation at the end of the emulsification. Specifically speaking, the calcium solution was added at the last 15 seconds of the process.
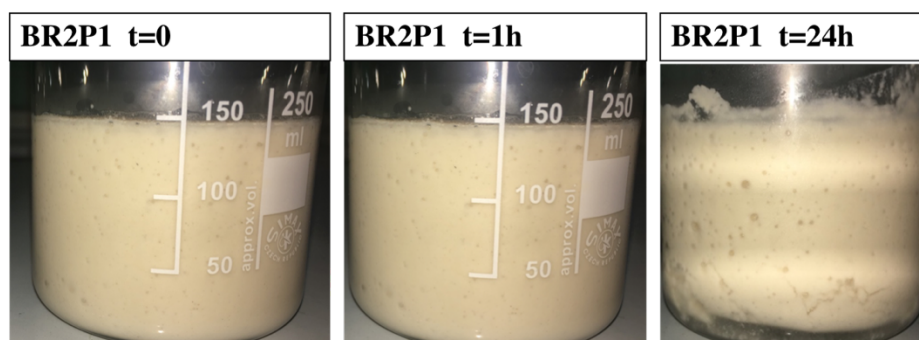

Figure 5.3.4.2.2 Emulsion with brown rice at 2%w/w and pectin at 1%w/w at several time

Even if the protein quantity was lowered to 2%w/w, the consistency of the product resulted too high when compared to one of the benchmarks. The emulsions prepared showed syneresis after 24h and a high complex modulus (G*) and a very low angle phase at 14 h of preparation, as shown in the frequency sweep test reported in Figure 5.3.4.2.3.
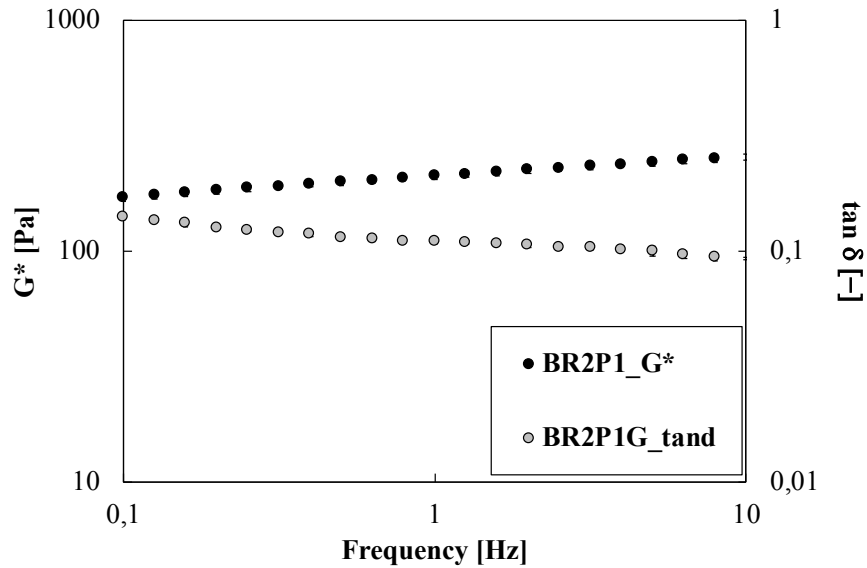

Figure 5.3.4.2.3   G* and tanδ for the BR2P1 emulsion

The obtained results suggested the possibility of adding another step to the emulsification process trying to improve the time stability, which increased although not for a much longer time.

5.3.4.3 Tara Gum

The other polysaccharide tested to stabilize the emulsions was Tara Gum. In the Figures below it is reported, as an example, brown rice emulsion at 2%w/w of protein and with tara gum in the range of 0.1 to 0.4 %w/w. The investigated systems showed a really low stability with all the investigated proteins.
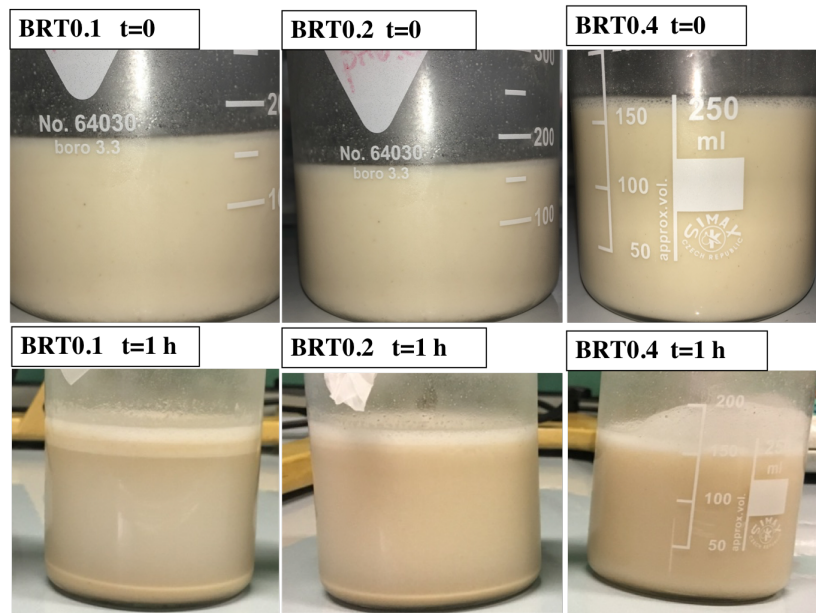
Figure 5.3.4.3.1 BRT emulsions at different tara concentration and observation time.

Specifically speaking, the increase of tara gum concentration has a significant effect on the structuring of the bulk system and the emulsion at 0.4 %w/w shows the best result no matter that the consistency of this is not adequate for a vegetable drink. The emulsions were prepared with and without the additional emulsification step mentioned in the previous paragraph.

5.3.4.4 Gellan Gum

The last hydrocolloid tested is Gellan Gum. The concentration tested for this was set at 0.01%w/w, 0.02%, 0.05%, 0.1%w/w. All the prepared emulsions were obtained with the additional emulsification step (named 3STEP-EMU), because the first method of emulsification did not give good results.

The gellan emulsion shows a good stability for a whole week. Only the samples prepared by lowering the amount of gellan to 0.01 and 0.02%w/w showed full instability. As an example the BRG0.05 was depicted in Figure 5.3.4.4.1.
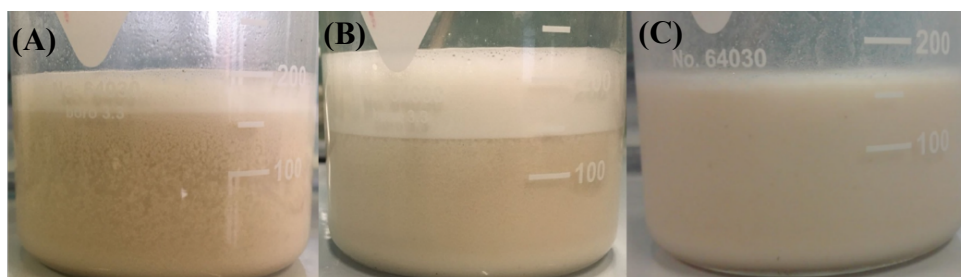

Figure 5.3.4.4.1 Gellan gum (0.05%w/w) emulsion (BRG), after the first emulsification step (A), after the second emulsification step (B) and after the last step (C)

Consequently, the systems with all the three proteins were optimized considering not only the time stability but also the viscosity. After viscosity measurements performed on all the prepared emulsions, because of the high viscosity at 0.1%w/w of gellan gum (as an example see the BRG system), the final good formulation resulted that with 0.05%w/w of hydrocolloid.
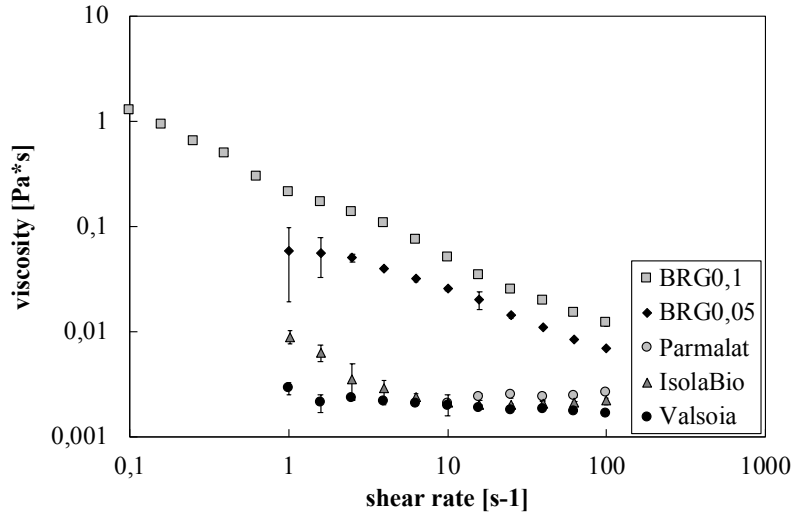

Figure 5.3.4.4.2 Flow curve of BRG0.1 and BRG0.05 systems vs benchmarks.

From the flow curves trend, it can be observed that the two samples prepared still have a higher viscosity when compared with the benchmark. The same trend was found for the other emulsifiers as can be observed in Figure 5.3.4.4.3.
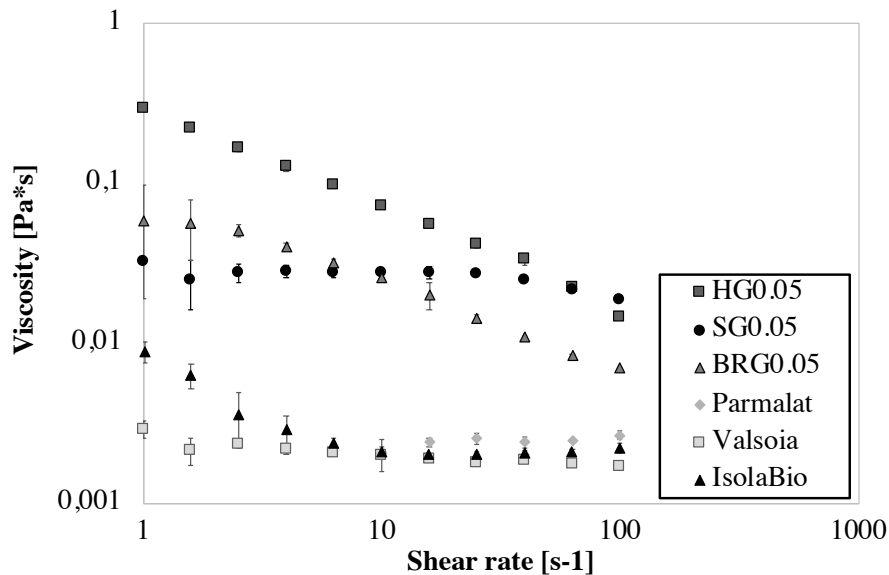

Figure 5.3.4.4.3 Flow curves of the optimized samples in comparison with the benchmark drink

The resulted emulsions are reported in Figure 5.3.4.4.4.

Figure 5.3.4.4.4 Stabilized emulsion with 0.05%w/w of gellan gum and hemp (HG0.05), brown rice (BR0.05) and soy (SG0.05)

From the viscosity measurements, reported in Figure 5.3.4.4.3, it can be seen that all three samples have higher viscosity than the benchmarks. In particular, emulsions with hemp and brown rice proteins differ from Newtonian behaviour and show shear-thinning behaviour, while the sample prepared with soy shows an almost Newtonian trend. It is worth noting that the viscosity values obtained in this work are lower than those obtained in the scientific literature (Noshad et al. 2016).

The non-Newtonian and Newtonian behaviour of our systems can be in agreement with the results obtained from shear surface analysis shown in the previous chapter. In fact, from the frequency sweep tests, the soy system showed a purely viscous behaviour differently from the other two proteins, which were able to give a 3D-network.

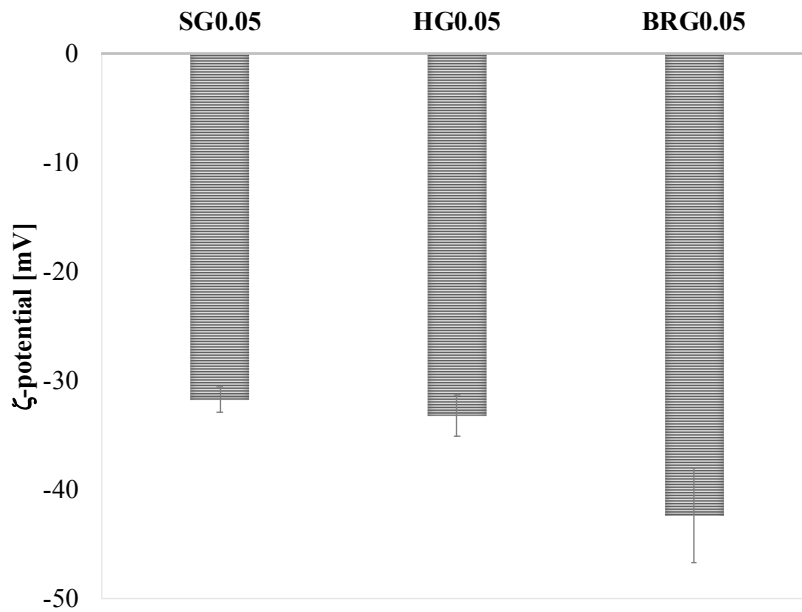For these systems, the ζ-potential measurements were performed and the results put in Figure 5.3.4.4.5.

Figure 5.3.4.4.5 ζ**-potential values for the optimized emulsions**

From the zeta-potential evaluation, all the samples prepared show good zeta values, always higher than |30| mV. In particular, the values are perfectly in line with those of the benchmarks studied. The emulsion obtained with black rice proteins shows the highest zeta value to which is imputable the higher stability.

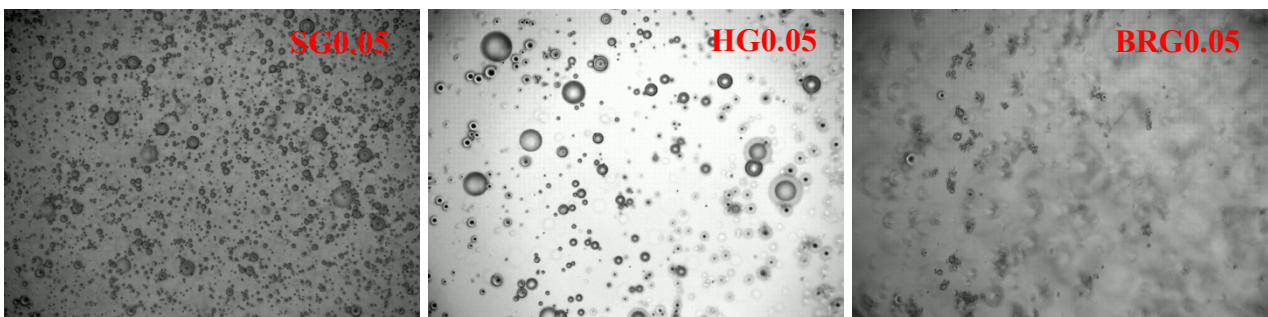**Figure 5.3.4.4.6 Microphotographs of emulsions prepared with gellan gum at 0.05%w/w and soy, hemp and brown rice proteins (magnification 40x).**
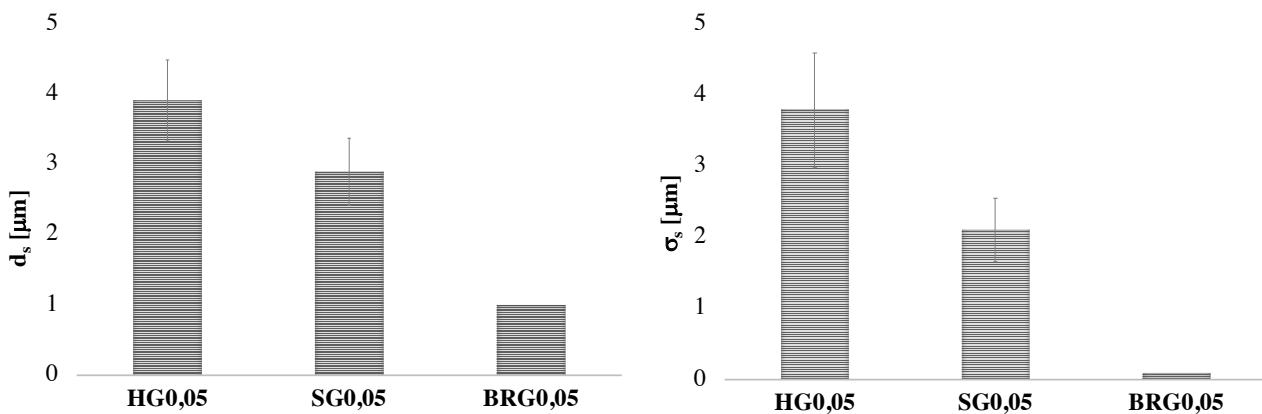

Figure 5.3.4.4.7 Average droplets diameter and standard deviation of HG0.05, SG0.05 and BRG0.05.

From the microscope results, it is possible to observe how the black rice is the protein capable of creating smaller and more homogeneous drops. In fact, the values of diameter and standard deviation are the lowest with respect to the other proteins. Once again, it was verified that the hemp, probably because of its lower speed of diffusion at the interface (see chapter 4), gives larger and more polydisperse drops than those formed in the presence of the soy protein.

5.4 Conclusions

The use of vegetable protein is a good and nutrient alternative to the animal source, suitable for consumers with milk allergy, lactose intolerance or for people who prefer to follow vegan diets. The preparation of emulsions, with consistency and appearance similar to milk, is very complicated because of the instability phenomena typical of very diluted O/W emulsions.

In fact, nowadays, the vegetable drinks present on the market are products characterized by the formation of sediments that lower the attractiveness of the product.

In this work, three different vegetable proteins were tested thanks to their potential surface activity together with the use of polysaccharides as thickening and stabilizing agents. In fact, the use of protein alone does not give any result, because the system results unstable over three hours. It was found that not all the hydrocolloids used (starch, pectin, xanthan gum, guar, tara gum) are compatible with the protein used, only the gellan gum gave the best results in terms of time stability, rheological properties, microscopy analysis and technological parameter (ζ-potential).

Finally, in order to stabilize the emulsion, it was necessary to use a three-step emulsification process.

REFERENCES

Bajaj, I. B., S. A. Survase, P. S. Saudagar & R. S. Singhal (2007) Gellan gum: Fermentative production, downstream processing and applications. *Food Technology and Biotechnology,* 45**,** 341-354.

Baldino, N., O. Mileti, F. R. Lupi & D. Gabriele (2018) Rheological surface properties of commercial citrus pectins at different pH and concentration. *Lwt-Food Science and Technology,* 93**,** 124-130.

Bos, M. A., B. Dunnewind & T. van Vliet (2003) Foams and surface rheological properties of beta-casein, gliadin and glycinin. *Colloids and Surfaces B-Biointerfaces,* 31**,** 95-105.

Bos, M. A. & T. van Vliet (2001) Interfacial rheological properties of adsorbed protein layers and surfactants: a review. *Advances in Colloid and Interface Science,* 91**,** 437-471.

Bouyer, E., G. Mekhloufi, V. Rosilio, J. L. Grossiord & F. Agnely (2012) Proteins, polysaccharides, and their complexes used as stabilizers for emulsions: Alternatives to synthetic surfactants in the pharmaceutical field? *International Journal of Pharmaceutics,* 436**,** 359-378.

Burgos-Diaz, C., T. Wandersleben, A. M. Marques & M. Rubilar (2016) Multilayer emulsions stabilized by vegetable proteins and polysaccharides. *Current Opinion in Colloid & Interface Science,* 25**,** 51-57.

Cao, X. H., H. B. Wen, C. J. Li & Z. X. Gu (2009) Differences in functional properties and biochemical characteristics of congenetic rice proteins. *Journal of Cereal Science,* 50**,** 184-189.

da Silva, M. V. & J. Delgado (2009) The Effect of Mg2+ and Tara Gum Concentrations on the Rheological Properties of WPI Solutions. *Diffusion in Solids and Liquids Iv,* 283-286**,** 571-+.

Dickinson, E. (1999) Adsorbed protein layers at fluid interfaces: interactions, structure and surface rheology. *Colloids and Surfaces B-Biointerfaces,* 15**,** 161-176.

Dickinson, E., M. G. Semenova, A. S. Antipova & E. G. Pelan (1998) Effect of high-methoxy pectin on properties of casein-stabilized emulsions. *Food Hydrocolloids,* 12**,** 425-432.

Diftis, N. & V. Kiosseoglou (2003) Improvement of emulsifying properties of soybean protein isolate by conjugation with carboxymethyl cellulose. *Food Chemistry,* 81**,** 1-6.

Ercelebi, E. A. & E. Ibanoglu (2009) Rheological properties of whey protein isolate stabilized emulsions with pectin and guar gum. *European Food Research and Technology,* 229**,** 281-286.

Horinaka, J., K. Kani, Y. Hori & S. Maeda (2004) Effect of pH on the conformation of gellan chains in aqueous systems. *Biophysical Chemistry,* 111**,** 223-227.

Kong, X. Z., C. Jia, C. M. Zhang, Y. F. Hua & Y. M. Chen (2017) Characteristics of soy protein isolate/gum arabic-stabilized oil-in-water emulsions: influence of different preparation routes and pH. *Rsc Advances,* 7**,** 31875-31885.

Lam, R. S. H. & M. T. Nickerson (2013) Food proteins: A review on their emulsifying properties using a structure-function approach. *Food Chemistry,* 141**,** 975-984.

Lin, D. Q., W. Lu, A. L. Kelly, L. T. Zhang, B. D. Zheng & S. Miao (2017) Interactions of vegetable proteins with other polymers: Structure-function relationships and applications in the food industry. *Trends in Food Science & Technology,* 68**,** 130-144.

Lupi, F. R., M. P. De Santo, F. Ciuchi, N. Baldino & D. Gabriele (2017) A rheological modelling and microscopic analysis of bigels. *Rheologica Acta,* 56**,** 753-763.

McClements, D. J. (2007) Critical review of techniques and methodologies for characterization of emulsion stability. *Critical Reviews in Food Science and Nutrition,* 47**,** 611-649.

Noshad, M., M. Mohebbi, A. Koocheki & F. Shahidi (2016) Influence of Interfacial Engineering on Stability of Emulsions Stabilized with Soy Protein Isolate. *Journal of Dispersion Science and Technology,* 37**,** 56-65.

Patino, J. M. R. & A. M. R. Pilosof (2011) Protein-polysaccharide interactions at fluid interfaces. *Food Hydrocolloids,* 25**,** 1925-1937.

Sandolo, C., P. Matricardi, F. Alhaique & T. Coviello (2009) Effect of temperature and cross-linking density on rheology of chemical cross-linked guar gum at the gel point. *Food Hydrocolloids,* 23**,** 210-220.

Seta, L., N. Baldino, D. Gabriele, F. R. Lupi & B. de Cindio (2012) The effect of surfactant type on the rheology of ovalbumin layers at the air/water and oil/water interfaces. *Food Hydrocolloids,* 29**,** 247-257.

Seta, L., N. Baldino, D. Gabriele, F. R. Lupi & B. de Cindio (2013) The influence of carrageenan on interfacial properties and short-term stability of milk whey proteins emulsions. *Food Hydrocolloids,* 32**,** 373-382.

Sethi, S., S. K. Tyagi & R. K. Anurag (2016) Plant-based milk alternatives an emerging segment of functional beverages: a review. *Journal of Food Science and Technology-Mysore,* 53**,** 3408-3423.

Sosa-Herrera, M. G., C. L. A. Berli & L. P. Martinez-Padilla (2008) Physicochemical and rheological properties of oil-in-water emulsions prepared with sodium caseinate/gellan gum mixtures. *Food Hydrocolloids,* 22**,** 934-942.

Tako, M., T. Teruya, Y. Tamaki & T. Konishi (2009) Molecular origin for rheological characteristics of native gellan gum. *Colloid and Polymer Science,* 287**,** 1445-1454.

Tang, C. H. (2017) Emulsifying properties of soy proteins: A critical review with emphasis on the role of conformational flexibility. *Critical Reviews in Food Science and Nutrition,* 57**,** 2636-2679.

Tang, C. H., Z. Ten, X. S. Wang & X. Q. Yang (2006) Physicochemical and functional properties of hemp (Cannabis sativa L.) protein isolate. *Journal of Agricultural and Food Chemistry,* 54**,** 8945-8950.

Thakur, B. R., R. K. Singh & A. K. Handa (1997) Chemistry and uses of pectin - A review. *Critical Reviews in Food Science and Nutrition,* 37**,** 47-73.

Trujillo-Cayado, L. A., J. Santos, M. C. Alfaro, N. Calero & J. Munoz (2016) A Further Step in the Development of Oil-in-Water Emulsions Formulated with a Mixture of Green Solvents. *Industrial & Engineering Chemistry Research,* 55**,** 7259-7266.

Wanezaki, S., N. Tachibana, M. Nagata, S. Saito, K. Nagao, T. Yanagita & M. Kohno (2015) Soy beta-conglycinin improves obesity-induced metabolic abnormalities in a rat model of nonalcoholic fatty liver disease. *Obesity Research & Clinical Practice,* 9**,** 168-174.

Wang, Q. L., J. Jiang & Y. L. L. Xiong (2018) High pressure homogenization combined with pH shift treatment: A process to produce physically and oxidatively stable hemp milk. *Food Research International,* 106**,** 487-494.

Wu, Y. B., W. Ding, L. R. Jia & Q. He (2015) The rheological properties of tara gum (Caesalpinia spinosa). *Food Chemistry,* 168**,** 366-371.

Xiang, N., Y. Lyu & G. Narsimhan (2016) Characterization of fish oil in water emulsion produced by layer by layer deposition of soy beta-conglycinin and high methoxyl pectin. *Food Hydrocolloids,* 52**,** 678-689.

Zhao, J. J., T. Wei, Z. H. Wei, F. Yuan & Y. X. Gao (2015) Influence of soybean soluble polysaccharides and beet pectin on the physicochemical properties of lactoferrin-coated orange oil emulsion. *Food Hydrocolloids,* 44**,** 443-452.

Zhong, L., M. Oostrom, M. J. Truex, V. R. Vermeul & J. E. Szecsody (2013) Rheological behavior of xanthan gum solution related to shear thinning fluid delivery for subsurface remediation. *Journal of Hazardous Materials,* 244**,** 160-170.

Conclusions

In this PhD work the properties of the interfacial layers covered by vegetable proteins were investigated in dilatational and shear kinematics at the air/water (A/W) interface, respectively by pendant drop method and interfacial rod magnetic field rheometer.

The investigated vegetable proteins were soy, hemp and brown rice, at several ranges of concentration in static condition and at CMC condition of oscillating (for shear and dilatational case) and stress relaxation measurements. The kinetic models were used to study the diffusion, the adsorption and the rearrangement steps which characterize the covering of the interface. The fractional Scott Blair and Maxwell models were used to interpret the rheological behaviour of the relaxation phenomena. By Scott-Blair model, the technological parameters of firmness and springiness were evaluated. An optimized emulsion, using the vegetable proteins as emulsifier agents and several polysaccharides as stabilizing agents, was conducted.

From a comparison with animal proteins (such as casein or lactoglobulin) classically used as foaming/emulsifier agents of food products, the three proteins have comparable surface properties, such as to make them excellent substitutes for animal proteins classically used in the food industry, in terms of surface activity but also of the rheological behavior. In particular, in oscillating dilatational analysis a solid-like behavior was observed for all interfaces investigated. In oscillating shear analysis the mechanical resistance is lower than dilatational case. As in shear as in dilatational, brown rice protein is more surface active and has the greater mechanical resistance. The Scott Blair interpretation does not predict well the experimental data, suggesting future improvement by adding more elements.

The use of the vegetable proteins as only stabilizing agent is not effective to preserve the homogeneity of the product. The use of some polysaccharides, in several concentrations, gives products with high consistency and the use of low polysaccharide concentration gives instability phenomena. The use of gellan gum has proved favourable in stabilising the emulsion, giving emulsions with low viscosities close to those of a vegetable milk. A three-step emulsification process with a decreasing rate of homogenization was used to stabilize the optimized formulation.

List of publication

International Journal

Baldino N., **Mileti O.**, Lupi F. R., Gabriele D., *Rheological surface properties of commercial citrus pectins at different pH and concentration*, LWT - Food Science and Technology, 93, 124–130 (2018)

Caputo P., Miriello D., Bloise A., Baldino N., **Mileti O.**, and Ranieri G. A., Correlation for assessing agreement between two methods of adhesion bitumen measurement: Boiling Tests and Contact Angle Tests, Advances in Materials Science and Engineering. Submitted for pubblication

Proceeding in International Conferences

Baldino N., **Mileti O.**, Lupi F. R., Gabriele D., de Cindio B., Surface behavior of vegetable proteins with pendant drop method, Atti del convegno, THE ANNUAL EUROPEAN RHEOLOGY CONFERENCE, AERC - SORRENTO, 2018

Baldino N., **Mileti O.**, Lupi F. R., Gabriele D., de Cindio B., Surface rheological analysis of vegetable proteins with pendant drop method, Atti del convegno, THE ANNUAL EUROPEAN RHEOLOGY CONFERENCE, AERC - COPENHAGEN, 2017

Mileti O., Lupi F. R., Baldino N., Gabriele D., de Cindio B., Rheological investigation of starch based edible coatings for ready-to-eat potato production, ABSTRACT BOOK OF THE 7th INTERNATIONAL SYMPOSIUM ON FOOD RHEOLOGY AND STRUCTURE, ZURICH SWITZERLAND, JUNE 7 – 11, EDITORS PETER FISCHER ERICH J. WINDHAB, 2015, pp. 242

Proceeding in Italian Conferences

Mileti O., Lupi F. R., Baldino N., Gabriele D., de Cindio B., Caratterizzazione reologica di sistemi a base di amido per la realizzazione di rivestimenti edibili, Atti di convegno, XIV Convegno Nazionale di Reologia - Montepaone Lido (CZ) 2016

Mileti O., Seta L., Gabriele D., Baldino N., Lupi F. R., de Cindio B, Studio delle proprietà reologiche interfacciali di pectine a basso ed alto grado di metossilazione in sistemi bifasici A/W ed O/W, Atti del convegno "XIII Convegno della Società Italiana di Reologia", Brescia, 7-10 Settembre 2014, A cura di Agnelli S., Baldi F., Pandini S., Ragnoli J. Riccò T., 2014, pp. 129-134.

Activities

Partecipation to XIII European annual Conference of Rheology – 17-20/04/2018 - Sorrento (NA)
Partecipation to XIV Italian Conference of Rheology – 1-4/06/2016 - Montepaone Lido (CZ)